UNIVERSITY OF CALIFORNIA,
IRVINE

RNA Regulation and Cocaine: Novel Links to the Circadian Clock

DISSERTATION

submitted in partial satisfaction of the requirements
for the degree of

DOCTOR OF PHILOSOPHY

in Biomedical Sciences

by

Marlene Cervantes

Dissertation Committee:
Donald Bren Professor Paolo Sassone-Corsi, Chair
Professor Peter Kaiser
Professor Xing Dai
Professor Yongsheng Shi
Assistant Professor Kai Kessenbrock

2020

DEDICATION

In loving memory of

my scientific father, Paolo Sassone-Corsi,

we shared this journey, you were so proud.

&

To my beloved family,

my mom and dad, the original Dreamers

my sisters and brother, the other five Musketeers.

All for one, one for all

- Alexandre Dumas

TABLE OF CONTENTS

LIST OF FIGURES

LIST OF TABLES

ACKNOWLEDGMENTS

It has been an absolute honor and privilege to call Paolo my mentor. He saw in me something he had not seen in someone in over 15 years and gave me the opportunity to be the only Ph.D. student in his lab. Boss, thank you for believing in me even when I found it difficult to believe in myself. I thank you for your unwavering support and all the big dreams you had for me, you were always my biggest cheerleader. You looked after me like a second dad, in and out of the lab. I will forever take with me the many scientific discussions we had, the life lessons you so carefully instilled upon me, our affectionate teasing of one another, and the many stories you always seemed to have to tell. I will always remember you for your heart of gold and inspirational wisdom. I will miss you forever.

I would like to thank my committee Xing Dai, Peter Kaiser, Yongsheng Shi and Kai Kessenbrock. Thank you for the insightful questions and discussions that helped me see my science through different lenses. A very special thank you to Peter, you became my surrogate PI and have provided me with continuous support in Paolo's absence.

To Emiliana, thank you for having given me that first chance we all need as an undergrad, my experience in your lab piqued my curiosity for research. Thank you for convincing your husband to hire me as a technician, that alone has changed my life in so many ways. Thank you for double checking that Boss and I were completing all the grad student/mentor milestones, since neither of us really knew what we were doing.

I am eternally indebted to Selma, thank you for letting me learn by ruining your gels. I thank you for being tough on me and never allowing me to give anything less than my best; making me a decent scientist but more importantly a better person. I will cherish all the Starbucks walks we had, the shenanigans we got into, the many memories we have with Boss. You became like a sister to me and have let me learn through your experiences just like a big sister would. Thank you, Nick for always being the voice of reason, sharing your advice over dinners and beers. You have become a role model I look up to, especially your quick, witty comments, they are always spot on.

Thank you to all the past and present members of the Sassone-Corsi lab for your constant companionship, making walking in to the lab at 10pm, 12am, 2am, 6am or anytime in between seem like a perfectly normal time to be in the lab. To the 2020 PSC lab, Carolina, Shogo, Tomoki, Kohei, Kevin, Jacob, Paul, Shoko, Will, and Lauren, we experienced the worst-case scenario together, but it has only made our bond stronger. I look forward to reuniting in the future reminiscing of all the great times and many laughs we had with Boss.

I also want to thank the Borrelli and Masri lab members for helping make the third floor of Sprague Hall my home away from home. A warm thank you to Robert and Maggie, I would not have been able to survive the ending of this long journey without you guys, thank you for all the laughs, cries, and lunches.

I thank everyone that collaborated with me throughout the years including Marina, Selma, Ken (Dyar), Kristen, Ken (Kinouchi), Luciana, Carolina, Paul, Karen, and Robert. As well as Ignasi Forné, Axel Imhof, Suman Ranjit, and Enrico Gratton. You all gave me an opportunity to learn and explore completely different angles of the circadian clock.

To my friends outside the science world, Abby, Yesi, Megan, and Carmin, thank you for keeping me in touch with the real world and reminding me that there is life outside the lab.

Most importantly, to my family, thank you for your unconditional love and unflinching support, because even when I was late to family gatherings due to experiments that ran late you always waited without complaint. *Amá, gracias por enseñarme que nunca debes decir "no puedo," tu ejemplo a nunca rendirte y luchar por lo que quieres me dio la fuerza para seguir adelante. Apá, gracias por inculcar en mí tu pasión por el aprendizaje. Los quiero mucho.* Roci, you have always been the leader of the pack, thanks for always being the first to lend me a helping hand. Ise, you never let me go hungry, thank for making me bean and cheese burritos and giving me snacks for my long days in the lab. Mares, you have always encouraged the boys to enjoy science, thank you for trusting me to be a role model for them. Brother, thanks for always being my competitor, bringing the best out of me and inspiring me to pursue a Ph.D. Abs, my partner in crime, thanks for always listening to my endless stories about the lab. To my siblings-in-law, Cuñis, Joe, Matt, Mel, and Stevie, thank you for putting up with the Cervantes clan, but especially with me. Thank you to my nephews, Beto, Diego, Milo, Antho, Mike, Pete, Nans, and Zeke, without you even realizing, your smiling faces helped me get through the toughest of times.

And finally, I would like to acknowledge the funding that supported my Ph.D. studies which included individual predoctoral fellowships from the American Heart Association (17PRE33410952) and the National Institute of General Medical Sciences (F31GM117942). Thank you also to Stanley Behrens and family for the UCI School of Medicine Stanley Behrens Research Excellence Award.

Curriculum Vitae

Marlene Cervantes

EDUCATION:

September 2014 – October 2020.	*Ph.D., Biomedical Sciences* University of California, Irvine, California **Advisor: Paolo Sassone-Corsi, Ph.D.**
September 2009 – June 2011.	*B.S., Health Sciences* University of California, Santa Cruz, California

RESEARCH EXPERIENCE:

September 2014 – October 2020.
Graduate Student Researcher.
Laboratory of Paolo Sassone-Corsi, Ph.D.
Center for Epigenetics and Metabolism, Department of Biological Chemistry
University of California, Irvine

- Revealed a non-canonical role for the circadian clock machinery in the nucleolus.
- Co-performed and analyzed two studies to investigate the consequences of drugs of abuse on the circadian clock in the nucleus accumbens and liver metabolome.
- Multiple collaborations including studying the role of the methionine metabolic enzyme, AHCY, in circadian transcription, identifying how lung adenocarcinoma-induces circadian rewiring of the liver, and investigating the rhythmic changes on the peripheral circadian clock under nutritional challenge.

August 2011 – August 2014.
Laboratory Assistant.
Laboratory of Paolo Sassone-Corsi, Ph.D.
Center for Epigenetics and Metabolism, Department of Biological Chemistry
University of California, Irvine

- Maintained up to 20 different mouse colonies at once, tasks included but was not limited to: daily monitoring of mouse lines, genotyping, setting of breeder pairs to regulate colony expansion/reduction.
- Two collaborations with post-doctoral fellows to carry out behavioral experiments detecting the effects of a pharmacological activator of SIRT1 on mouse locomotor activity, as well as identifying the distinct circadian functions of SIRT1 and SIRT6.

September 2009 – June 2011.
Undergraduate Student Researcher.
Laboratory of Yi Zuo, Ph.D.
Department of Molecular, Cell and Developmental Biology
University of California, Santa Cruz

- Contributed to a study aimed to differentiate the astrocyte and neuronal effects of the Fragile X mutation using immunohistochemistry and Western blot analyses.

June 2009 – September 2009, June 2010 – September 2010.
Undergraduate Student Researcher.
Laboratory of Emiliana Borrelli, Ph.D.
Department of Microbiology and Molecular Genetics
University of California, Irvine
– Performed immunohistochemical staining on mouse pituitary gland tissue to identify the selective effect of each dopamine D2 receptor isoform on intracellular signaling.

FELLOWSHIPS AND AWARDS:

2020 2019-2020 UC Irvine School of Medicine Ph.D. Student Travel Award
2019 UC Irvine School of Medicine Stanley Behrens Research Excellence Award
2019 2018-2019 UC Irvine School of Medicine Ph.D. Student Travel Award
2018 UC Irvine School of Medicine Excellence in Research and Health for the Latino Community Award, Latino Excellence and Achievement in Graduate Education
2018 NIH F31, Ruth L. Kirschstein National Research Service Award Individual Predoctoral Fellowship to Promote Diversity in Health-Related Research (F31GM117942)
2017 American Heart Association Predoctoral Fellowship (17PRE33410952)
2016 French-American Doctoral Exchange (FADEx) Program (Declined)
2016 UC Irvine Faculty Mentor Program- Honorable Mention
2016 Ford Foundation Fellowship Program- Honorable Mention
2015 Ford Foundation Fellowship Program- Honorable Mention
2009 UC Santa Cruz Workshops for Engineering and Science Transfers Program Fellow
2009 NIH R25, Bridges to the Baccalaureate Research Training Program Fellow (R25GM056647)

PUBLICATIONS:

1. Greco CM, **Cervantes M**, Fustin JM, Kakeru I, Ceglia N, Samad M, Shi J, Forne I, Ranjit S, Gaucher J, Kinouchi K, Kojima R, Gratton E, Li W, Baldi P, Imhof A, Okamura H, Sassone-Corsi P. S-adenosyl-L-homocysteine hydrolase links methionine metabolism to the circadian clock and chromatin remodeling. ***Submitted***.
2. Brami-Cherrier K*, Lewis RG*, **Cervantes M***, Liu Y, Tognini P, Baldi P, Sassone-Corsi P**, Borrelli E**. Cocaine-mediated circadian reprogramming in the striatum through dopamine-driven PPARγ activation. ***Nat Commun.*** 2020 Sep 7;11(1):4448.
*Equal contribution, **Co-corresponding
3. **Cervantes M**, Forné I, Ranjit S, Gratton E, Imhof A, Sassone-Corsi P. BMAL1 associates with NOP58 in the nucleolus and contributes to pre-rRNA processing. ***iScience***. 2020 Jun 26;23(6):101151.
4. Ferreira LL, **Cervantes M**, Froufe HJC, Egas C, Cunha-Oliveira T, Sassone-Corsi P, Oliveira PJ. Doxorubicin persistently rewires cardiac circadian homeostasis in mice. ***Arch Toxicol***. 2020 Jan;94(1): 257-271.
5. **Cervantes M**, Sassone-Corsi P. Modification of histone proteins by serotonin in the nucleus. ***Nature***. 2019 Mar;567(7749):464-465.
6. Kinouchi K, Magnan C, Ceglia N, Liu Y, **Cervantes M**, Pastore N, Huynh T, Ballabio A, Baldi

P, Masri S, Sassone-Corsi P. Fasting imparts a switch to alternative daily pathways in liver and muscle. ***Cell Reports***. 2018, 25(12):3299-3314.

7. Dyar KA, Lutter D, Artati A, Ceglia NJ, Liu Y, Armenta D, Jastroch M, Schneider S, de Mateo S, **Cervantes M**, Abbondante S, Tognini P, Orozco-Solis R, Kinouchi K, Wang C, Swerdloff R, Nadeef S, Masri S, Magistretti P, Orlando V, Borrelli E, Uhlenhaut NH, Baldi P, Adamski J, Tschop MH, Eckel-Mahan K, Sassone-Corsi P. Atlas of circadian metabolism reveals system-wide coordination and communication between clocks. ***Cell***. 2018, 174(6):1571-1585.
8. Masri S, Papagiannakopoulos T, Kinouchi K, Liu Y, **Cervantes M**, Baldi P, Jacks T, Sassone-Corsi P. Lung adenocarcinoma distally rewires hepatic circadian homeostasis. ***Cell***. 2016, 165(4):896-909.
9. Masri S, Orozco-Solis R, Aguilar-Arnal L, **Cervantes M**, Sassone-Corsi P. Coupling circadian rhythms of metabolism and chromatin remodeling. ***Diabetes Obes Metab***. 2015, 17 Suppl 1:17-22.
10. Masri S, Rigor P, **Cervantes M**, Ceglia N, Sebastian C, Xiao C, Roqueta-Rivera M, Deng C, Osborne TF, Mostoslavsky R, Baldi P, Sassone-Corsi P. Partitioning circadian transcription by SIRT6 leads to segregated control of cellular metabolism. ***Cell***. 2014, 158(3):659-672.
11. Masri S, **Cervantes M**, Sassone-Corsi P. The circadian clock and cell cycle: interconnected biological circuits. ***Curr Opin Cell Biol***. 2013, 25:730-734.
12. Bellet MM, Nakahata Y, Boudjelal M, Watts E, Mossakowska DE, Edwards KA, **Cervantes M**, Astarita G, Loh C, Ellis JL, Vlasuk GP, Sassone-Corsi P. Pharmacological modulation of circadian rhythms by synthetic activators of the deacetylase SIRT1. ***Proc Nat Acad Sci U.S.A***. 2013, 110(9):3333–3338.

PRESENTATIONS:

1. **Cervantes M**. Epigenetic and metabolic architecture of the circadian clock. Charla Científica, UCI-Mexico Graduate Research and Education Program. Virtual oral presentation. International (2020)
2. **Cervantes M**, Forné I, Ranjit S, Gratton E, Imhof A, Sassone-Corsi P. Nucleolar BMAL1 interacts with Box C/D small nucleolar RNA protein NOP58 to regulate pre-ribosomal RNA processing. 2nd Epigenetics Conference: From Mechanisms to Disease. Poster presentation. Nassau, Bahamas (2020)
3. **Cervantes M**, Forné I, Ranjit S, Gratton E, Imhof A, Sassone-Corsi P. Nucleolar BMAL1 interacts with Box C/D small nucleolar RNA protein NOP58 to regulate pre-ribosomal RNA processing. 84th Cold Spring Harbor Laboratory Symposium on Quantitative Biology: RNA Control & Regulation. Poster presentation. Cold Spring Harbor, NY (2019)
4. **Cervantes M**, Forné I, Imhof A, Sassone-Corsi P. BMAL1 interacts with nucleolar protein NOP58 and regulates the maturation of pre-ribosomal RNA. UC Irvine School of Medicine GRAD Day. Poster presentation. Irvine, CA (2017)
5. **Cervantes M** and Sassone-Corsi P. Regulation of ribosomal RNA by the circadian clock. Biological Chemistry Second Year Symposium. Oral presentation. Irvine, CA (2016)
6. **Cervantes M**, De Mei C, Borrelli E. Effects of Dopamine D2L Receptor on Pituitary Gland Function. Minority Science Program Bridges Research Symposium. Oral presentation. Irvine, CA (2009)

TEACHING EXPERIENCE:

September 2016 – December 2016.
Teaching Assistant.
BIO SCI D111L - Developmental and Cell Biology Laboratory
Department of Developmental and Cell Biology
University of California, Irvine
- Wrote and graded weekly pre-lab quizzes and final examination questions.
- Graded laboratory notebooks and laboratory reports.
- Led in-class laboratory demonstrations.
- Maintained and monitored online class discussion forums.

September 2015 – December 2015.
Teaching Assistant.
BIO SCI D103 - Cell Biology
Department of Developmental and Cell Biology
University of California, Irvine
- Created Active Learning Assignments to provide students with an alternative method of learning.
- Assisted in-class Active Learning Activities designed by the instructor.
- Planned and led weekly discussion sections for 20-80 students.
- Organized and led midterm and final examination review sessions.
- Proctored and graded midterm and final examinations.

ABSTRACT OF THE DISSERTATION

RNA Regulation and Cocaine: Novel Links to the Circadian Clock

by

Marlene Cervantes
Doctor of Philosophy in Biomedical Sciences
University of California, Irvine, 2020
Donald Bren Professor Paolo Sassone-Corsi, Chair

Circadian rhythms regulate our physiological, metabolic, and behavioral activity in a 24-hour cycle to maintain organismal homeostasis. In virtually all tissues, the intrinsic circadian clock is governed by a canonical molecular transcriptional-translational feedback mechanism that is self-sustained. Whether additional functions for the molecular circadian clock exist remains largely unexplored. Here we investigate an unprecedented role for the circadian clock protein, BMAL1, in the nucleolus. We identified novel BMAL1 interactions with resident nucleolar proteins using biochemical fractionation and pull-down assays. Moreover, through use of molecular assays we reveal a critical role in pre-ribosomal RNA processing and maturation. Instead, environmental-mediated synchronization of peripheral tissues is regulated in part by external cues including light-dark, sleep-wake, and feed-fasting cycles. The degree to which non-photic environmental factors perturb the circadian clock in the brain continues to be a major point of interest. We studied an *in vivo* model to elucidate the effects of drugs of abuse as stressors on the striatal circadian clock. Mice treated with an acute dose of cocaine were sampled throughout a full circadian cycle. Using high-throughput RNA sequencing, our findings show cocaine drastically reprograms the circadian

transcriptional clock in the nucleus accumbens. Furthermore, we reveal dopamine signaling is required for the cocaine-mediated PPARγ activation that leads to *de novo* circadian transcriptional rhythmicity. Taken together, in the studies presented, we implement two discrete approaches to further our knowledge on the versatility and reprogrammability of the molecular clock. Our novel findings provide previously unexplored connections between RNA regulation or drugs of abuse and the circadian clock, and uncover new possible therapeutic targets for treatment development for disorders such as addiction.

Chapter 1

Introduction

PART I

The circadian clock

Circadian rhythmicity of biological processes is controlled by a complex clock system that establishes a constant ~24-hour cycle (Asher and Sassone-Corsi, 2015). The circadian clock network consists of biological pacemakers found in all tissues that direct and maintain proper rhythms required for organism homeostasis (Green et al., 2008; Schibler and Sassone-Corsi, 2002). A central circadian clock or "master clock" housed in the suprachiasmatic nucleus (SCN), a cluster of neurons in the hypothalamus, is synchronized by light, the most potent external time giver or *zeitgeber*, via signals from the eye through the retino-hypothalamic tract (Buttgereit et al., 2015). Subsequently, the central clock

synchronizes rhythms in all peripheral tissues through secreted humoral signals (Welsh et al., 2010). Other external cues such as sleep-wake, food-fasting cycles and physical activity also have a direct impact on peripheral tissues and can uncouple the peripheral clocks from the central clock.

In mammals the molecular circadian clock tightly regulates cellular function through transcriptional regulation (Gallego and Virshup, 2007; Ripperger and Schibler, 2006). Two beta helix-loop-helix (bHLH) transcription factors, Circadian Locomotor Output Cycles Kaput (CLOCK) and Brain and Muscle ARNT-Like 1 (BMAL1), heterodimerize and bind to conserved E-box sequences in target clock-controlled gene (CCG) promoters initiating the transcriptional-translational feedback that includes clock repressors *Period* (*Per1*, *Per2*, and *Per3*) and *Cryptochrome* (*Cry1* and *Cry2*) which negatively regulate transcription and trigger the rhythmic expression of CCGs (Green et al., 2008; Lamia et al., 2009; Stratmann and Schibler, 2006).

In addition to regulation of circadian transcription, other roles performed by the core clock proteins involve post-translational modifications including acetylation, SUMOylation, ubiquitination, and phosphorylation (Masri et al., 2013b; Robles et al., 2017). Clock-dependent post-translational modifications have been reported to either directly modify the circadian machinery or control enzymatic activity, protein interactions, intracellular localization and stability (Dallmann et al., 2012; Gallego and Virshup, 2007; Sahar and Sassone-Corsi, 2009). CLOCK has been characterized as having intrinsic acetyltransferase activity on histone H3 (H3) (Doi et al., 2006), its own binding partner BMAL1 (Hirayama et al., 2007), as well as the glucocorticoid receptor (GR) (Akashi et al., 2002). These post-translational modifications have an important role in circadian gene regulation and are

linked with modulation of enzymatic activity (Lamia et al., 2009; Shim et al., 2007). Acetylation of BMAL1 and GR has an inhibitory affect, while H3 acetylation has a role in facilitating gene expression. Moreover, cytoplasmic BMAL1 functions as a shuttling protein and is required for the nuclear import of CLOCK, critically affecting the transcriptional activation of CCGs (Kondratov et al., 2003). It is evident that the core clock proteins have multifunctional roles that deviate from their canonical transcriptional factor function; however, our understanding of their roles in sub- nuclear compartments remains incomplete.

The nucleolus

The nucleolus is the largest nuclear sub-compartment and is the site of ribosomal RNA (rRNA) and ribosome production (Boisvert et al., 2007). rRNAs are the central component of the ribosome subunits and have an active role as ribozymes during protein translation (Dahlberg, 1989). Unique to the nucleolus is the presence of RNA Polymerase I (Pol I) whose sole function is the transcription of ribosomal DNA (rDNA) (Grummt, 2003), a gene containing the polycistronic precursor (pre-rRNA) for three rRNAs; 18S, 5.8S, and 28S (Grozdanov et al., 2003). Although pre-rRNA is the only transcript produced by Pol I-driven transcription, rRNAs account for over 80% of the total RNA produced in the cell (Grummt and Ladurner, 2008). Mature rRNAs are derived from the pre-rRNA transcript that undergoes a series of post-transcriptional modifications including: methylation, pseudouridylation, and cleavage (Grozdanov et al., 2003; Henras et al., 2015). pre-rRNA processing small nucleolar ribonucleoprotein (snoRNP) complexes are comprised of specific nucleolar proteins and small nucleolar RNAs (snoRNAs) that mediate the post-

transcriptional modifications (Dieci et al., 2009). The snoRNAs guide snoRNP complexes to the specific rRNA sequence and sites of activity (Boisvert et al., 2007). Bioinformatic analysis of nascent and mature RNA sequencing datasets discovered a time-of-day dependent expression of snoRNAs (Aitken and Semple, 2017). Interestingly, 63% of total snoRNAs display rhythmic expression but only 4% are unique snoRNAs demonstrating that the circadian snoRNAs are very specific and highly expressed (Aitken and Semple, 2017). The rhythmicity of these key factors, involved in the processing and maturation of rRNA, reveals a strong potential for a novel functional role of the circadian clock in the nucleolus.

Typically, the circadian clock is associated with genes transcribed by RNA Polymerase II (Pol II) and not with Pol I or RNA Polymerase III (Pol III)-mediated transcription (Takahashi, 2015). Noteworthy, however, found within the rDNA sequence are E-boxes (Poortinga et al., 2011), the conserved motif recognized by the basic helix-loop-helix Per-Arnt-Sim (bHLH-PAS) domain of CLOCK and BMAL1 (Huang et al., 2012), and thus hints at the possible involvement of the clock in rDNA transcription. In fact, a circadian study on ribosome biogenesis reported the circadian rhythmic expression of rRNA (Jouffe et al., 2013), but did not provide a mechanism for the circadian regulation. Nevertheless, a circadian nuclear proteomic study identified the temporal nuclear availability of several Pol I subunits and proteins associated with the rRNA post-transcriptional modifications (Wang et al., 2017). These studies raise the questions, is the circadian clock required for proper transcription and/or processing of rRNAs and is the clock an essential part of nucleolar structure and function?

PART II

Circadian clock disruption

Perturbation of circadian rhythms has been associated with a number of pathologies including obesity, diabetes, and a number of other metabolic diseases (Bass and Takahashi, 2010; Masri et al., 2013a; Sahar and Sassone-Corsi, 2009, 2012). As a matter of fact, mice with disruptions in the circadian clock machinery have numerous consequences. For example, the *Clock* mutant (*Clock∆19*) mice are obese compared to WT littermates and display hyperlipidemia, hepatic steatosis, hyperglycemia, and hypoinsulinemia (Turek et al., 2005). More drastic effects can be observed in *Bmal1* knockout (*Bmal1*-KO) mice that display similar metabolic deficiencies as the *Clock∆19* mice, but also display a severe premature aging phenotype (Kondratov et al., 2003; Rudic et al., 2004). The genetic loss of the core clock components illustrates the importance of the circadian clock in controlling cellular function.

Changes to environmental *zeitgebers*, however, can also change the rhythmic patterns and robustness of the metabolic and transcriptional oscillations observed in normal conditions (Asher and Sassone-Corsi, 2015). Food has been proven to be a powerful pacemaker for peripheral tissues, nutritional composition of various diets is able to differentially alter CCGs expression in the metabolic tissues. For instance, high fat diet (HFD) composed of 60% kcal from fat is able to reprogram circadian hepatic gene expression of unique classes of genes that oscillate exclusively in normal chow-fed mice or HFD-fed mice, these changes result in altered metabolic circadian control in the liver (Eckel-Mahan et al., 2013; Hatori et al., 2012; Kohsaka et al., 2007). Likewise, a body-wide circadian metabolome atlas consisting of eight tissues demonstrates the extensive inter-tissue communication of normal chow-fed mice which is greatly diminished in HFD-fed mice (Dyar et al., 2018; Eckel-

Mahan et al., 2013). By contrast, fasting or the absence of food is one of a few external cues that enhances the expression of the circadian clock, since, in addition to the canonical clock machinery, fasting-induced transcription factors are utilized to promote circadian rhythmicity (Kinouchi et al., 2018; Longo and Panda, 2016). The feeding-fasting cycles, however, are not the only method of altering the circadian clock, the capacity of different external pacemakers to reprogram the circadian clock can be extended to various other recreational activities including physical exercise, travel, and drug use.

Cocaine

In a bidirectional fashion, individuals can develop substance abuse disorders and disrupted circadian rhythms (Logan et al., 2014). In fact, polymorphisms in the *Per2* gene have been associated with a greater predisposition to cocaine addiction and lower levels of the dopamine D2 receptor (Shumay et al., 2012). Cocaine, a drug of abuse known as a psychostimulant, targets the brain's reward system and leads to dopamine buildup. This dopamine accumulation interferes with the daily rhythmic release of the neurochemical in the nucleus accumbens (NAcc) (Schade et al., 1995). The overactivation of the target cells in the NAcc produces unnatural degrees of pleasure and satisfaction greatly affecting the individual's behavior (Nestler, 2005). Indeed, the dopamine receptor-containing postsynaptic neurons in the NAcc contribute to the rhythmic food anticipatory behavior in mice (Gallardo et al., 2014). Although many convincing associations between circadian rhythms and cocaine have been made, how cocaine perturbs the molecular circadian clock in the NAcc remains inadequately addressed.

Chapter 2

BMAL1 associates with NOP58 in the nucleolus and contributes to pre-rRNA processing

Marlene Cervantes, Ignasi Forné, Suman Ranjit, Enrico Gratton, Axel Imhof, and

Paolo Sassone-Corsi

ABSTRACT

The transcription factor BMAL1 is a core element of the circadian clock that contributes to cyclic control of genes transcribed by RNA polymerase II. By using biochemical cellular fractionation and immunofluorescence analyses we reveal a previously uncharacterized nucleolar localization for BMAL1. We used an unbiased approach to determine the BMAL1 interactome by mass spectrometry and identified NOP58 as a prominent nucleolar interactor. NOP58, a core component of the box C/D small nucleolar ribonucleoprotein

complex, associates with Snord118 to control specific pre-ribosomal RNA (rRNA) processing steps. These results suggest a non-canonical role of BMAL1 in rRNA regulation. Indeed, we show that BMAL1 controls NOP58-associated Snord118 nucleolar levels and cleavage of unique pre-rRNA intermediates. Our findings identify an unsuspected function of BMAL1 in the nucleolus that appears distinct from its canonical role in the circadian clock system.

INTRODUCTION

A large array of biological processes follow an approximate 24-hr cycle, leading to circadian rhythms controlling physiology, metabolism, and behavior. Circadian rhythms are governed by a molecular clock system that is present in virtually all mammalian cells (Masri and Sassone-Corsi, 2010). The circadian molecular machinery is based on transcription-translation feedback loops to maintain intrinsic intracellular daily rhythms (Eckel-Mahan and Sassone-Corsi, 2013; Zhang and Kay, 2010). Circadian locomotor output cycles kaput (CLOCK) and Brain and muscle ARNT-like 1 (BMAL1) function as transcription factors activating expression of clock-controlled genes (CCGs) by binding E-box motifs at promoters of target genes transcribed by RNA polymerase II (Partch et al., 2014). Among the CCGs transcribed are genes encoding clock protein repressors Period 1-3 (PER1-3) and Cryptochrome 1-2 (CRY1-2) which in turn negatively regulate rhythmic transcription (Green et al., 2008). In addition to transcription, levels of circadian regulation are provided by a variety of additional mechanisms, including epigenetic control and post-translational modifications (PTMs) such as phosphorylation, acetylation, SUMOylation and ubiquitination of clock proteins that regulate rhythmic activity (Cardone et al., 2005; Feng and Lazar, 2012;

Hirayama et al., 2007; Kondratov et al., 2003). Thus, proper circadian control is obtained through a complex system of interplaying regulatory pathways.

Importantly, post-transcriptional modifications of CCGs transcripts have also been shown to be critical for rhythmic gene regulation. Alternative splicing, polyadenylation, and non-coding RNAs have all been shown to contribute to control the half-life required for rhythmic turnover of circadian transcripts (Kojima et al., 2011). A unique target of rhythmic post-transcriptional modification is the 18S-E ribosomal RNA (rRNA) (Sinturel et al., 2017), a precursor to an essential component of the small ribosomal subunit (Amaldi et al., 1989; Reuveni et al., 2017). Diurnal polyadenylation of 18S-E results in its degradation, decreased ribosomal biogenesis, and reduced protein translation in a time-of-day-dependent manner (Sinturel et al., 2017).

These observations suggest that circadian clock elements may be implicated in the maturation of transcripts generated not exclusively from Pol II. Indeed, the rRNA precursor (pre-rRNA) is transcribed by RNA polymerase I in the nucleolus as a polycistronic transcript that undergoes post-transcriptional processing to produce three mature rRNAs (18S, 5.8S, and 28S) (Nazar, 2004; Woolford and Baserga, 2013). Nucleolar proteins and small nucleolar RNAs (snoRNAs) form small nucleolar ribonucleoprotein complexes (snoRNPs) that mediate post-transcriptional modifications, pseudouridylation, methylation, and cleavage for rRNA maturation (Boisvert et al., 2007). Specifically, snoRNAs direct snoRNPs to target rRNA sites to facilitate post-transcriptional processing (Boisvert et al., 2007). Intriguingly, bioinformatic analysis of circadian nascent and mature RNA sequencing datasets has recently revealed a time-of-day-dependent expression of a number of snoRNAs (Aitken and Semple, 2017). While these notions hint at a potential role of clock proteins in the nucleolus,

including the nucleolar localization of a splicing variant of Period 2 (PER2S) (Avitabile et al., 2014), a functional role within the sub-nuclear organelle has yet to be explored. We have observed that the core clock protein BMAL1 localizes in the nucleolus and its ablation results in aberrant nucleolar organization. Importantly, in mouse Neuro 2a (N2a) cells BMAL1 is associated to nucleolar proteins, Nucleolin (NCL) and Nucleolar RNA helicase 2 (DDX21) (Beker et al., 2019). Using cell fractionation and mass spectrometry we reveal that BMAL1 associates with NOP58, a core component of the box C/D small nucleolar ribonucleoprotein complex. The association is validated by a number of approaches, including Fluorescence Lifetime Microscopy and Fluorescence Resonance Energy Transfer. Finally, we show that BMAL1 is required to maintain Snord118-containing snoRNP levels and plays a previously unappreciated role in pre-rRNA processing.

RESULTS

Nucleolar localization of the circadian clock protein BMAL1

While post-transcriptional polyadenylation of 18S-E rRNA is diurnal (Sinturel et al., 2017), little is known about the contribution of clock proteins in the nucleolus, the specific location of rRNA synthesis and processing (Nazar, 2004; Woolford and Baserga, 2013). Visualization of BMAL1 by immunofluorescence in wild type mouse embryonic fibroblasts (WT MEFs) and human embryonic kidney 293T cells (HEK293T) illustrated that endogenous BMAL1 is not excluded from the nucleolus and rather co-localizes with the nucleolar protein, Fibrillarin (FBL) (Figure 2.1A). Moreover, we performed biochemical isolation of nucleoli using liver tissues harvested from WT mice at six timepoints throughout the circadian cycle, at zeitgeber times (ZT) 0, 4, 8, 12, 16, 20 (Figure 2.1B and Figure 2.S1A). Analysis of endogenous BMAL1

revealed its nucleolar localization at all circadian timepoints. Consistent with the total protein analyses (Figure 2.S1B), FBL, Nucleolar protein 58 (NOP58), and Nucleolar protein 56 (NOP56) levels in the nucleolus were virtually constant along the circadian cycle (Figure 2.1B).

Circadian function is directly linked to changes in BMAL1 phosphorylation state (Hirano et al., 2016). Notably, daily changes in phosphorylated-BMAL1 (p-BMAL1), conventionally visualized as slower migrating bands (Tamaru et al., 2003; Yoshitane et al., 2009), do not affect its nucleolar localization (Figures 1.1B and 1.1C). Moreover, as BMAL1 has also been shown to be rhythmically acetylated and is strongly correlated to its circadian transcriptional activity (Hirayama et al., 2007), we tested whether acetylation alters BMAL1 localization to the nucleolus. We ectopically expressed mutants of BMAL1 for Lysine at position 538, originally shown to be the site of acetylation (AcBMAL1K538) (Hirayama et al., 2007). HEK293T cells transiently co-transfected with GFP-NOP58 and the wild type Myc-BMAL1, Myc-BMAL1K538R preventing acetylation, or the acetylation mimic Myc-BMAL1K538Q, all show localization in the nucleolus despite distinct BMAL1 acetylation statuses (Figure 2.S2). Thus, these post-translational modifications do not appear to be involved in BMAL1 nucleolar localization and confirm that BMAL1 does not undergo rhythmic nucleolar translocation.

Furthermore, circadian analyses of NOP58 by immunofluorescence show the number of nucleoli per nucleus remains constant throughout the 24-hr cycle in mouse livers (Figures 1.1D and 1.1E). Together, these observations show the nucleolar features are consistent throughout the daily cycle and suggest BMAL1 is constitutively present in the nucleolus.

Clock-dependent nucleolar morphological rearrangements

To determine the significance of BMAL1 in the nucleolus we analyzed the expression of nucleolar proteins in livers from WT and *Bmal1*-null (*Bmal1*-KO) mice at ZT8 and ZT20. While BMAL1 ablation does not alter the total levels of ribosome biogenesis factors nor in the nucleolar fractions (Figures 1.2A and 1.2B), it has a substantial impact on nucleolar structure. Indeed, immunofluorescence of NOP58 and FBL show that loss of BMAL1 leads to alterations in nucleolar size and the number of nucleoli per nucleus, both in mouse liver and MEFs (Figures 1.2C and 1.2D). The total nucleolar area in *Bmal1*-KO MEFs appears smaller (Figure 2.2E). Likewise, the number of nucleoli in *Bmal1*-KO MEFs is reduced as compared to WT MEFs, which display greater than 5% more cells with seven or more nucleoli per nucleus (Figures 1.2F and 1.2G). These results suggest that BMAL1 influences the configuration of nucleoli. Since BMAL1 and CLOCK are dimer partners, we tested dominant negative *Clock*-mutant MEFs containing a deletion in the *Clock* gene at Exon 19 (*Clock*Δ19). These cells provide 1) an additional model with a disrupted clock and 2) the potential of CLOCK to influence nucleolar structures similar to its partner, BMAL1. Indeed the *Clock*Δ19 MEFs display smaller and fewer nucleoli (Figures 1.S3A-D). Moreover, similarly to *Bmal1*-KO MEFs, *Clock*Δ19 MEFs maintain comparable levels of NOP58 and FBL (Figure 2.S3E). Importantly, these results were corroborated in WT MEFs stably expressing shRNAs efficiently knocking down BMAL1 levels (Figures 1.2H and 1. S3F). Immunofluorescence imaging of FBL and NOP58 in these cells show reduced nucleolar area and lower number of nucleoli compared to WT MEFs expressing control shGFP (Figures 1.2I-L). Again, a reduction in the number of nucleoli was observed without disruption in the level of nucleolar protein FBL (Figure 2.2H). Our findings show that BMAL1 perturbation in *in vitro* and *in vivo* models

leads to nucleolar-protein rearrangements, reflected by changes in nucleolar structure and allude to dysfunctional nucleoli (Nemeth and Grummt, 2018; Scheer and Hock, 1999).

Altered pre-ribosomal RNA processing in *Bmal1*-KO

The nucleolus is the site of pre-rRNA transcription and maturation, producing three out of four rRNAs, 18S, 5.8S and 28S (Boisvert et al., 2007). To investigate the functional contribution of BMAL1 in the nucleolus, we examined the expression of the polycistronic pre-rRNA transcripts in a circadian manner in WT and *Bmal1*-KO MEFs post-synchronization by dexamethasone at circadian times (CT) 12, 18, 24, 30, 36, and 42. To distinguish pre-rRNA from mature rRNA, pre-rRNA expression was measured at four distinct regions spanning both rRNA and external or internal transcribed spacer (ETS and ITS, respectively) sequences (Figure 2.3A). While pre-rRNA expression does not undergo circadian oscillations (Figure 2.3B), BMAL1 ablation leads to reduced levels of pre-rRNA. During rRNA processing, sequential cleavage of pre-rRNA diverge into two pathways, one containing the upstream 18S intermediates, the other, the downstream 5.8S and 28S intermediates (Henras et al., 2015) (see also Figure 2.3C). Therefore, to discriminate the different cleavage site intermediates indistinguishable by PCR (RT-qPCR), levels of pre-rRNA were examined by Northern analyses using probes discerning pre-rRNA cleavage at different stages (Figures 1.3C-F and Figures 1.S4A-D) (Lapik et al., 2004). Indeed, the specific cleavage intermediate, 36S pre-rRNA, was significantly less abundant in the absence of BMAL1 compared to the WT MEFs (Figure 2.3E). Similarly, Ratio Analysis of Multiple Precursors (RAMP) (Wang et al., 2014), show hybridization patterns that reflect the importance of BMAL1 in efficient pre-

rRNA processing (Figure 2.3F). These results indicate that BMAL1 is likely involved in proper processing of 36S, the 3'-end of pre-rRNA containing 5.8S and 28S rRNAs.

Endogenous BMAL1 nucleolar interactome

Next, we sought to identify whether BMAL1 associates with nucleolar proteins. Notably, in N2a cells, BMAL1-associated proteins include nucleolar proteins, such as NCL and DDX21 (Beker et al., 2019). Thus, we explored the link between BMAL1 and nucleolus-derived proteins by taking an unbiased approach to examine the nucleolar BMAL1 interactome. Endogenous BMAL1 was used for a native co-immunoprecipitation (co-IP) from nucleoplasmic and nucleolar fractions of mouse livers harvested at ZT8 and ZT20. The eluate was subsequently analyzed quantitatively by mass spectrometry (Figure 2.4A). A comparison of the two timepoints revealed a 50-60% overlap of proteins identified at both timepoints (Figure 2.4B and Figure 2.S5A). Each of the fractions analyzed contained a group of exclusive interactors and a subgroup of proteins interacting in both, nucleoplasmic and nucleolar fractions (Figure 2.4C and Figure 2.S5B). Importantly, no uniquely associated nucleoplasmic interactors were identified in the nucleolar fractions, an indication of highly enriched nucleoli. Moreover, when comparing the enrichment of BMAL1-interacting proteins in the nucleoplasmic and nucleolar fractions, we identified the subset of BMAL1 interactors present predominantly in the nucleolar compartment by using a cutoff of four-fold enrichment ($-Log_2$ (Fold change) nucleoplasmic/nucleolar ≥ 2) and a p-value < 0.05 (Figure 2.4C). We applied Gene Ontology (GO) analysis to these BMAL1-nucleolar interactors and identified essential nucleolar-related terms: snoRNA binding and RNA binding (Figure 2.4D). Prominent among the proteins identified in the nucleolus were: box C/D proteins

(NOP58, NOP56, and FBL), box H/ACA protein (NHP2), and previously identified nucleolar RNA helicase, DDX21 (Beker et al., 2019) (Figure 2.4E and Figure 2.S5C). Of note, SIRT7, a prominent nucleolar deacetylase involved in pre-rRNA processing (Chen et al., 2016; Iyer-Bierhoff et al., 2018; Sirri et al., 2019), does not interact with BMAL1 (Figure 2.S5D). Collectively, these data illustrate the BMAL1 interactome contains highly specific nucleolar interactors.

BMAL1 interaction with nucleolar protein NOP58

Our mass spectrometry analyses identified NOP58, which forms snoRNP complexes in the nucleolus that are critical for pre-rRNA processing (Filipowicz and Pogacic, 2002), as a highly significant nucleolar BMAL1-interacting protein. To visualize the interaction between NOP58 and BMAL1, we carried out a combination of Fluorescence Lifetime Microscopy and Fluorescence Resonance Energy Transfer (FLIM-FRET) live cell imaging. For FRET pairing, HEK293T cells were transiently transfected with GFP-NOP58, used as the donor molecule, and RFP-BMAL1, the acceptor molecule (Figure 2.S6A). When in close proximity, energy transfer from the donor molecule to the acceptor reduces the lifetime of the donor (Digman et al., 2008). Visualization by FLIM using a continuous color scheme on the phasor map from red to purple denotes a shift of the phasor points towards shorter lifetime. Accordingly, phasor mapped FLIM analysis of the GFP-NOP58:RFP-BMAL1 or GFP-NOP58 only cells reveal blue puncta unique to the GFP-NOP58:RFP-BMAL1 cells illustrating energy transfer and an interaction (Figures 1.5A and 1.5B). Moreover, histograms of the normalized number of pixels of the fractional intensity of lower lifetime from the GFP-NOP58 only or GFP-NOP58:RFP-BMAL1 cells plotted cumulatively (Figure 2.5C), and individually (Figure 2.S6B),

compare the complexity within each cell and evaluate differences between cells. Thus, the greater intensity shift towards shorter lifetime displayed by the puncta in GFP-NOP58:RFP-BMAL1 cells indicate areas where the two proteins are in close contact. Consistent with the mass spectrometry data, these results validate the BMAL1 and NOP58 association and demonstrate that the interaction is occurring in the nucleoli of live cells.

Next, we tested whether BMAL1 is required for the association between the box C/D proteins, NOP58 and FBL. We performed co-IP of endogenous NOP58 in nucleoli fractionated from livers of WT and *Bmal1*-KO mice (Figure 2.5D). BMAL1 ablation did not alter the NOP58-FBL association.

Noteworthy, CLOCK was identified as a BMAL1 interactor by mass spectrometry in both the nucleoplasmic and nucleolar fractions (Figure 2.S5B). To establish whether BMAL1 requires its canonical partner to interact with NOP58 we examined the interaction of GFP-NOP58 with Myc-BMAL1 in the presence and absence of Myc-CLOCK (Figure 2.5E). These results indicate that heterodimerization with CLOCK is not necessary for interaction of BMAL1 with NOP58. This finding was confirmed by using truncated forms of BMAL1 showing that both PER-ARNT-SIM (PAS) domains, involved in CLOCK dimerization (Huang et al., 2012), are not required for NOP58 interaction (Figure 2.S7). Therefore, the BMAL1 and NOP58 association is likely independent of CLOCK.

Finally, to interrogate whether BMAL1 acetylation, a signature of circadian activity (Hirayama et al., 2007), influences its interaction with NOP58, we transiently transfected the mutated Myc-BMAL1K538 constructs described above with GFP-NOP58 for co-IP in HEK293T cells (Figure 2.5F). NOP58 associates with BMAL1, AcBMAL1K538, BMAL1K538R, and BMAL1K538Q equally, indicating that BMAL1 acetylation is not essential for the

interaction. Taken together, these results show that the NOP58-BMAL1 association is resilient to circadian disruption.

BMAL1 is involved in Snord118 recruitment to box C/D snoRNP

Pre-rRNA processing relies on two dominant classes of small nucleolar ribonucleoprotein (snoRNP) complexes, box C/D protein containing- and box H/ACA protein containing-snoRNPs (Watkins and Bohnsack, 2012). In combination with distinctive box C/D family snoRNAs, NOP58, and the core box C/D proteins FBL, NOP56, and SNU13, form unique snoRNPs with one of two functions directed by the specialized snoRNA within each complex (Caffarelli et al., 1998). Specifically, nucleolar box C/D snoRNPs carrying box C/D snoRNAs such as, MBI-43 (Snord17) or MBII-135 (Snord65) carry out rRNA *2' O*-methylation; snoRNAs U3 (Rnu3a), U8 (Snord118), or U22 (Snord22) guide pre-rRNA processing (Caffarelli et al., 1998; Huttenhofer et al., 2001; Lestrade and Weber, 2006; Watkins and Bohnsack, 2012). Thus, we sought to assess whether BMAL1 impacts the RNA composition of box C/D snoRNP complexes by performing RNA immunoprecipitation followed by quantitative PCR (RIP-qPCR). NOP58 was immunoprecipitated from isolated nucleoli derived from livers of WT and *Bmal1*-KO mice. Analysis of the bound RNA for Rnu3a, a snoRNA known to guide 18S processing (Beltrame and Tollervey, 1995; Kass et al., 1990), displayed no changes in recruitment to the snoRNP complex in *Bmal1*-KO mice (Figure 2.6A). Similarly, Snord17 predicted to guide 28S *2' O*-methylation (Huttenhofer et al., 2001) was equally recruited to the snoRNP upon BMAL1 ablation. In contrast, Snord118, which binds 28S during 5.8S/28S processing (Peculis, 1997), showed significant reduction in association with NOP58 despite being equally expressed in *Bmal1*-KO mice (Figure 2.6B). Moreover,

recruitment of the snoRNP complex to the different modified regions, pre-rRNAs 18S/ITS1, ITS1/5.8S, and ITS2/28S, was not altered in *Bmal1*-KO mice (Figure 2.6C). Thus, BMAL1 appears to direct the specific association of NOP58 with Snord118, a snoRNA required for 5.8S and 28S rRNA maturation.

Mature rRNAs, in association with ribosomal proteins, constitute the fundamental components of a functional ribosome (Amaldi et al., 1989; Reuveni et al., 2017). Misregulation or interruption of rRNA processing significantly alters ribosome biogenesis and function (Meskauskas et al., 2003; Sloan et al., 2017). Therefore, we assessed whether ribosome biogenesis was perturbed in the absence of BMAL1 by analyzing polysome accumulation (Figure 2.6D). A comparison of polysome profiles in WT and *Bmal1*-KO MEFs shows a significantly dampened polysome accumulation, indicating that BMAL1 ablation leads to fewer assembled ribosomes compared to WT MEFs (Figure 2.6E). Accordingly, BMAL1 contributes to snoRNP complex assembly and proper pre-rRNA maturation with a downstream effect on the formation of ribosomes.

DISCUSSION

The proteins that constitute the circadian core clock machinery are classically identified as transcriptional regulators (Eckel-Mahan and Sassone-Corsi, 2013; Masri and Sassone-Corsi, 2010; Partch et al., 2014; Zhang and Kay, 2010). It has also been suggested that, to maintain cellular homeostasis, they may play additional roles in protein translation, post-translational modification and protein translocation (Cardone et al., 2005; Feng and Lazar, 2012; Hirayama et al., 2007; Kondratov et al., 2003). Here we report that the clock protein, BMAL1, is a component of the nucleolus. It is conceivable that other circadian clock proteins may also

localize to the nucleolus, as it appears to be the case for the PER2S splice variant (Avitabile et al., 2014), and as further hinted by the presence of CLOCK in our mass spectrometry analysis. While additional investigations are needed to promote this possibility, it should be stressed that other Pol II-associated transcription factors have also been found to localize in the nucleolus. Indeed, notable examples of transcription factors localized in the nucleolus include the TBP-related factor TRF2, the factor and insulator CTCF, EGR1, C/EBPa and the virus-encoded protein MEQ (Ali et al., 2008; Arabi et al., 2005; Grandori et al., 2005; Kieffer-Kwon et al., 2004; Liu et al., 1997; Muller et al., 2010; Ponti et al., 2014; Torrano et al., 2006). While the possible function of these factors in the nucleolus remains undefined, it is likely to be unconventional with respect to their canonical role in transcriptional regulation of protein-coding genes. In this respect, our findings are relevant as we identify a direct role of BMAL1 in the nucleolus that seems independent of Pol II-mediated transcriptional regulation.

We have demonstrated that BMAL1 ablation in distinct models including mouse livers and MEFs elicits nucleolar rearrangement by decreasing the size and number of nucleoli per nucleus. Consequently, given that nucleolar structure and function are tightly correlated (Nemeth and Grummt, 2018; Scheer and Hock, 1999), we hypothesize that BMAL1 plays a role in nucleolar function. However, to address whether BMAL1 is directly involved in the reorganization of the nucleolus will require in depth structural studies and analysis by phase-separation compartmentalization (Frottin et al., 2019).

To elucidate the consequences of the disruption to the nucleolar structure induced by BMAL1 ablation, we identified the endogenous nucleolar BMAL1-binding partners by mass spectrometry from native, uncrosslinked protein-protein interactions. Notably, BMAL1

associates with box C/D snoRNP proteins, NOP58 and FBL, which are directly involved in pre-rRNA processing (Filipowicz and Pogacic, 2002). Moreover, BMAL1-related proteins, NCL and DDX21, are nucleolar proteins critical for ribosomal biogenesis (Beker et al., 2019). Indeed, confirmation of these interactions *in vivo* and *in vitro* supports a scenario that establishes a causal link between BMAL1 interaction with the snoRNP proteins and impaired pre-rRNA processing of the 3'-end containing 5.8S and 28S rRNAs observed in the BMAL1-null cells. Our study suggests a molecular mechanism by which the function exerted by BMAL1 likely involves the specific interaction with a unique snoRNA, Snord118. Loss-of-function experiments have shown that Snord118 directs 5.8S/28S processing (Peculis, 1997). While the detailed molecular mechanism by which BMAL1 exerts its function within the nucleolus will need further exploration, our results establish the remarkable example of a Pol II transcription factor operating at a completely different level of transcript regulation. Furthermore, it is plausible that the downstream effects of this regulation are complementary to the promotion of protein synthesis mediated by BMAL1 phosphorylation to control global protein translation (Lipton et al., 2015). In conclusion, our findings position BMAL1 in company with unconventional RNA polymerase II-associated transcription factors previously found to have nucleolar localization (Ali et al., 2008; Arabi et al., 2005; Grandori et al., 2005; Kieffer-Kwon et al., 2004; Liu et al., 1997; Muller et al., 2010; Ponti et al., 2014; Torrano et al., 2006). Importantly, this non-canonical function of BMAL1 in the nucleolus appears to operate in a circadian-independent manner.

LIMITATIONS OF THE STUDY

BMAL1 is found to be localized in the nucleolus. Yet, the exact ratio of BMAL1 molecules at chromatin versus the nucleolus remains undetermined. We acknowledge that nucleolar fractions are merely a representation of enriched nucleoli, displaying augmented levels of BMAL1 specifically in the nucleolus with the limitation of not being a full representation of the nucleolar amount with respect to the total nuclear extract. Further studies are needed to investigate this ratio and whether it might be modified in the presence of additional circadian-dependent regulators.

METHODS

Animals

WT and *Bmal1*-KO mice were a generous gift from C. Bradfield (Bunger et al., 2000). Animals were housed under a temperature-controlled, 12-hr light/12-hr dark schedule, and fed *ad libitum*. Age-matched, male mice were sacrificed at specified zeitgeber times (ZT), livers were harvested, flash-frozen in liquid nitrogen and stored at -80ºC until use. All research involving vertebrate animals was performed in accordance with the guidelines of the Institutional Animal Care and Use Committee at the University of California, Irvine.

Cell culture

MEFs from *Bmal1*-KO, *Clock*Δ19 mutant mice and their respective WT were obtained as previously described (Aguilar-Arnal et al., 2013; Hirayama et al., 2007; Sahar et al., 2014), cultured in high-glucose DMEM (HyClone) supplemented with 10% (v/v) FBS (Gibco) and 1% (v/v) Pen/Strep (Gibco) antibiotics. HEK293T cells (ATCC) were maintained in high-

glucose DMEM supplemented with 10% FBS and 1% antibiotics. HEK293T cells were transfected with indicated plasmids using BioT transfection reagent (Bioland Scientific LLC) according to manufacturer's recommendations. All cell lines were tested and free of mycoplasma contamination.

Plasmids

Myc-Bmal1 (Travnickova-Bendova et al., 2002), Myc-Clock (Doi et al., 2006), were previously described. GFP-Nop58 was a generous gift from E. Bertrand (Verheggen et al., 2002). Myc-Bmal1 was used as a template to generate Myc-Bmal1K538R and Myc-Bmal1K538Q point mutations using Q5 Site-Directed Mutagenesis (New England Biolabs) and NEBaseChanger to design mutagenesis primers. The primer sequences used were: Myc-Bmal1K538R: Fwd: 5'-TCCAGGAGGCcagAAGATTCTAAATG-3', Rev: 5'-GAAGAGGCATCAGGGGGA-3'; Myc-Bmal1K538Q: Fwd: 5'-TCCAGGAGGCaggAAGATTCTAAATG-3', Rev: 5'-GAAGAGGCATCAGGGGGA-3'. RFP-Bmal1 was generated by subcloning *Bmal1* from Myc-Bmal1 into the EcoRI and BamHI sites of the pTagRFP-N vector (Evrogen). Control shRNA, pLKO.1-shGFP, was purchased from Addgene and shRNAs targeting *Bmal1* were generated using oligo sequences previously identified by The RNAi Consortium (Moffat et al., 2006) subcloned into the AgeI and EcoRI sites of pLKO.1-TRC (Addgene). The primer sequences used were renamed as: shBmal1 #1: Fwd: 5'-CCGGTCTTCAAGATCCTCAATTATACTCGAGTATAATTGAGGATCTTGAAGATTTTTG-3', Rev: 5'- AATTCAAAAATCTTCAAGATCCTCAATTATACTCGAGTATAATTGAGGATCTTGAAGA-3'; shBmal1 #2: Fwd: 5'-CCGGGCAGTATCAAAGTGCATTAATCTCGAGATTAATGCACTTTGATACTGCTTTTTG-3', Rev:

5’-AATTCAAAAAGCAGTATCAAAGTGCATTAATCTCGAGATTAATGCACTTTGATACTGC-3’; shBmal1 #3: Fwd: 5’-CCGGACATAGGCATCGATATGATAGCTCGAGCTATCATATCGATGCCTATGTTTTTTG-3’, Rev: 5’- AATTCAAAAAACATAGGCATCGATATGATAGCTCGAGCTATCATATCGATGCCTATGT-3’. Vectors for GST-Bmal1-HA fragments were generated by subcloning *Bmal1* sequences from cDNA encoding amino acids residues 1-134 for the F1, 135-265 for the F2, 266-399 for the F3, 400-506 for the F4, 507-626 for the F5 from mouse *Bmal1* (NCBI reference sequence: NM_007489.4) were cloned into the vector pGEX4T1 (GE Healthcare) with a TEV-cleavable N-terminal glutathione S-transferase (GST) tag and a C-terminal hemmaglutinin (HA) tag using EcoRI/NotI restriction sites. The primer sequences used were: GST-Bmal1aa1-134-HA: Fwd: 5’-TCCCCGGAATTCGAGAATCTTTATTTTCAGGGCATGGCGGACCAGAGAATGG-3’, Rev: 5’-CCACCAACCCATACACAGAATACCCTTATGATGTGCCGGATTATGCCTAGCGGCCGCATCGTGAC; GST-Bmal1aa135-265-HA: Fwd: 5’-TCCCCGGAATTCGAGAATCTTTATTTTCAGGGCGCAAACTACAAGCCAACATTTC-3’, Rev: 5’-AAAGGTGGAAGATAAGGACTTCTACCCTTATGATGTGCCGGATTATGCCTAGCGGCCGCATCGTGAC-3’; GST-Bmal1aa266-399-HA: Fwd: 5’-TCCCCGGAATTCGAGAATCTTTATTTTCAGGGCGCCTCTACCTGTAGAATGAAG-3’, Rev: 5’-TTTTACAGACAAGAGAAAAGATCTACCCTTATGATGTGCCGGATTATGCCTAGCGGCCGCATCGTGAC-3’; GST-Bmal1aa400-506-HA: Fwd: 5’-TCCCCGGAATTCGAGAATCTTTATTTTCAGGGCACAACTAATTGCTATAAGTTTAAG-3’, Rev: 5’-GCGGAGGAAATCATGGAAATCTACCCTTATGATGTGCCGGATTATGCCTAGCGGCCGCATCGTGAC-3’; GST-Bmal1aa507-626-HA: Fwd: 5’-

TCCCCGGAATTCGAGAATCTTTATTTTCAGGGCCACAGGATAAGAGGGTCATC-3', Rev: 5'-GACTTGCCATGGCCGCTGTACCCTTATGATGTGCCGGATTATGCCTAGCGGCCGCATCGTGAC-3'. All the vectors were examined and verified by restriction site analysis and sequencing.

Lentiviral production and MEFs transduction

HEK293T cells were transfected with plasmids containing shRNAs, psPAX2, and VSV.G using BioT transfection reagent according to manufacturer's recommendations. After 16hrs, medium was replaced. Virus-containing media was filtered after 48hrs, supplemented with 8μg/ml Polybrene (Millipore) and added to WT MEFs for 16hrs. MEFs were selected for plasmid incorporation using 8μM puromyocin, overnight. Subsequent passages were maintained using growing media supplemented with 2μM puromyocin.

Immunofluorescence analysis

Cells were grown on Nunc Lab-Tek II chamber slides and transfected with plasmids as indicated. Frozen mouse liver tissues were cut to 10μm thick sections using Leica CM1950 Cryostat. Cells and tissue sections were fixed with ice cold 4% PFA for 20min at room temperature (RT) and washed three times with 1x PBS. Samples were then permeabilized (1x PBS, 0.3% Triton X-100) for 15min at RT and blocked (1x PBS, 5% BSA, 10% normal goat serum (NGS)) for 2hrs at RT. Following incubation with primary antibodies diluted in blocking buffer overnight at 4ºC, samples were washed three times with 1x PBS and incubated with secondary antibodies for 2hrs at RT. After three washes with 1x PBS, nuclei were stained using DRAQ7 (Biostatus) or DAPI (Life Technologies) for 15min at RT and subsequently washed twice with 1x PBS. Endogenous and ectopic proteins were detected

using the following antibodies: BMAL1 (Novus, NB100-2288), NOP58 (Abcam, ab155969), FBL (single stain: CST, #2639; double stain: Novus, NB300-269), MYC (Millipore, 05-419). Secondary antibodies: Alexa Fluor 488 Goat anti-Rabbit IgG (Invitrogen, A-11008) and Alexa Fluor 546 Goat anti-Mouse IgG (Invitrogen, A-11003). Quantification of the total area and number of nucleoli were performed on immunofluorescence confocal images (157x157µm/image; Leica, SP5) of cells and liver tissue sections probed with NOP58 (Abcam, ab155969) or FBL (single stain: CST, #2639; double stain: Novus, NB300-269) using ImageJ software in the following sequence: Split channels > for the nuclear channel (DRAQ7 or DAPI): setAutoThreshold (Default dark, BlackBackground) > Convert to Mask > Fill Holes > Watershed > Analyze Particles (Size ≥ 200 pixels, Circularity = 0.00-1.00, Exclude on edges, Add to manager), for the nucleolar channel (NOP58 or FBL): setAutoThreshold (Default dark) > Convert to Mask > Watershed > Analyze Particles (Size ≥ 5 pixels, Circularity = 0.00-1.00, Exclude on edges, Show = Outlines) > overlay ROIs from manager > Measure (%Area).

Nucleolar fractionation

Nucleoli were prepared as previously described (Andersen et al., 2002) with minor modifications. Whole mouse livers were divided into 3 equal pieces and each minced in 5ml of Buffer A (10mM HEPES pH7.9, 1.5mM $MgCl_2$, 10mM KCl, 0.5mM DTT, supplemented with protease inhibitor cocktail (Roche), 0.5mM PMSF, 20mM NaF, 1µM TSA, 10mM NAM). Tissues were homogenized and spun at 1600rpm (600g) for 10min at 4ºC. Pellets were resuspended in 3ml of Buffer S1 (250mM Sucrose, 10mM $MgCl_2$, supplemented with protease inhibitor cocktail (Roche), 0.5mM PMSF, 20mM NaF, 1µM TSA, 10mM NAM), layered over 3ml of Buffer S2 (350mM Sucrose, 0.5mM $MgCl_2$, supplemented with protease

inhibitor cocktail (Roche), 0.5mM PMSF, 20mM NaF, 1μM TSA, and 10mM NAM) and spun at 2500rpm (1430g) for 5min at 4ºC. All three nuclear pellets were combined using Buffer S2, sonicated, layered over 3ml of Buffer S3 (880mM Sucrose, 0.5mM $MgCl_2$, supplemented with protease inhibitor cocktail (Roche), 0.5mM PMSF, 20mM NaF, 1μM TSA, 10mM NAM) and spun at 3500rpm (2800g) for 10min at 4ºC. Supernatant was retained as the enriched nucleoplasmic fraction and diluted with 5x RIPA (250mM Tris pH7.5, 750mM NaCl, 5% NP-40, supplemented with protease inhibitor cocktail (Roche), 0.5mM PMSF, 20mM NaF, 1μM TSA, 10mM NAM). The nucleolar pellet was resuspended in 500μl of Buffer S2 and spun at 3500rpm (2800g) for 5min at 4ºC. The cleaned nucleolar pellet was resuspended in 1x RIPA (50mM Tris pH7.5, 150mM NaCl, 1% NP-40, supplemented with protease inhibitor cocktail (Roche), 0.5mM PMSF, 20mM NaF, 1μM TSA, 10mM NAM). Fractions were briefly sonicated, rocked for 30min at 4ºC, spun at 12500rpm (18000g) for 10min at 4ºC, and enriched lysates collected.

Western blot analysis

Whole cell lysates were prepared from mouse liver tissues by homogenization in 1x RIPA (50mM Tris pH7.5, 150mM NaCl, 5mM EDTA, 1% NP-40, 0.5% Deoxycholate, supplemented with protease inhibitor cocktail (Roche), 0.5mM PMSF, 20mM NaF, 1μM TSA, 10mM NAM), briefly sonicated, rocked for 30min at 4ºC, spun at 12500rpm (18000g) for 10min at 4ºC, and lysates collected. Similarly, MEFs were harvested in 1x RIPA, sonicated, rocked and spun. 20μg of whole cell lysates or nucleolar fractionation lysates were resolved on 6%, 8%, or 10% SDS-PAGE. Antibodies used for Western blot include: BMAL1 (Abcam, ab93806), NOP58 (Abcam, ab155969), NOP56 (Proteintech, 18181-1-AP), FIBRILLARIN (CST, #2639),

NUCLEOLIN (CST, #14574), Ribosomal Protein S6 (CST, #2217), p84 (Genetex, GTX70220), TUBULIN (Sigma, T5168). Secondary antibodies include: HRP-conjugate Goat anti-Rabbit IgG (Millipore, 12-348) and HRP-conjugate Rabbit anti-Mouse IgG (Millipore, AP160P).

RNA extraction, reverse transcription and quantitative real-time PCR analysis

Confluent WT and *Bmal1*-KO MEFs were synchronized by treatment with 100nM Dexamethasone (Sigma) for 30min as described previously (Aguilar-Arnal et al., 2013; Hirayama et al., 2007; Sahar et al., 2014). Total RNA, from either cells or WT and *Bmal1*-KO mouse livers collected at the indicated circadian times (CT or ZT, respectively), were extracted using TRIzol (Invitrogen) following manufacturer's recommendation. 1μg of total RNA was reverse-transcribed to cDNA using iScript cDNA synthesis kit (Bio-Rad Laboratories), according to manufacturer's protocol. cDNA (1:10) was used for quantitative real-time PCR using SsoAdvanced Universal SYBR Green Supermix (Bio-Rad Laboratories) and ran on a CFX96 Touch real-time PCR machine (Bio-Rad Laboratories). Gene expression was normalized to 18S rRNA (1:500 cDNA). Primer sequences used for gene expression analysis were designed with Primer3 software (Koressaar and Remm, 2007; Untergasser et al., 2012). 5'ETS/18S: Fwd: 5'-CTCCTCTCTCGCGCTCTCT-3', Rev: 5'-GGCCGTGCGTACTTAGACAT-3'; 18S/ITS1: Fwd: 5'-CTGAGAAGACGGTCGAACTTG-3', Rev: 5'-CCTCCACAGTCTCCCGTTTA-3'; ITS1/5.8S: Fwd: 5'-ACACCCGAAATACCGATACG-3', Rev: 5'-GTGCGTTCGAAGTGTCGAT-3'; ITS2/28S: Fwd: 5'-GCCTCCTCGCTCTCTTCTTC-3', Rev: 5'-GCCGTTACTGAGGGAATCCT-3'; Rnu3a (U3): Fwd: 5'-ACTGTGTAGAGCACCCGAAAC-3', Rev: 5'-GACTGTGTCCTCTCCCTCTCA-3'; Snord118 (U8): Fwd: 5'-CCTTACCTGTTCCTCCTTTCG-3', Rev: 5'-GAGCAACCAGGATGTTGTCA-3'; Snord17: Fwd: 5'-TGACCTTCTTCCCAGTCTCG-3',

Rev: 5'-GGTGAGATGGAACCCAGAGA-3'; 18S: Fwd: 5'-CGCCGCTAGAGGTGAAATTC-3', Rev: 5'-CGAACCTCCGACTTTCGTTCT-3'.

Northern blot analysis

Total RNA was extracted from WT and *Bmal1*-KO MEFs using TRIzol (Invitrogen) following manufacturer's recommendation. 20µg of total RNA was equally added to 1x TT (1.5M Triethanolamine, 1.5M Tricine), 1mM EDTA, 6.67% Formaldehyde, 50% Formamide, and incubated at 65ºC for 15min. Samples were then mixed with 6x Formaldehyde loading buffer (1mM EDTA, 0.25% Bromophenol blue, 50% Glycerol) and ran on a 0.8% Agarose-Formaldehyde gel (1x TT, 6.67% Formaldehyde) at 4ºC for 15hrs. The gel was prepared for transfer by soaking in 0.05N NaOH for 20min and in 20x SSC (3M NaCl, 0.3M Sodium citrate) for 45min at RT. RNA was transferred overnight onto a positively charged nylon membrane (Amersham Biosciences) by capillary transfer in 10x SSC at RT. The membrane was then rinsed in 2x SSC and UV crosslinked for 15min, incubated in Prehybridization buffer (5x SSC, 5x Denhardt's solution, 0.5% SDS, 25µg/ml Salmon sperm) for 2hrs at 65ºC and hybridized overnight at 65ºC using previously identified probes (Lapik et al., 2004) diluted in prehybridization buffer. After three washes in Wash buffer (2x SSC, 0.1% SDS), the membrane was dried, exposed to a BAS-MS FUJI imaging plate (FUJIFILM) and imaged using Amersham Typhoon imager (GE Healthcare). Probes were labeled at 37ºC for 1hr in a mixture of 1µM Oligo, 1x T4 PNK reaction buffer (New England Biolabs), 20U T4 PNK (New England Biolabs), 50µCi [γ-^{32}P] ATP 3,000Ci/mmol (PerkinElmer). Labeled probes were purified using illustra Microspin G-25 columns (GE Healthcare) following manufacturer's instructions. Probe sequences used were previously identified by (Lapik et al., 2004); probes

were labeled as Pink probe (5'ETS): 5'-AGCTCCCCACGGGAAAGCAATGAGTCTCTC-3'; Gold probe (ITS2): 5'-ACCCACCGCAGCGGGTGACGCGATTGATCG-3'; Blue probe (ITS1): 5'-CTCTCACCTCACTCCAGACACCTCGCTCCA-3'. Imaged blots were quantitated by densitometry analysis on ImageJ software, pre-rRNA intermediates were normalized to 47S/45S. Ratio Analysis of Multiple Precursors (RAMP) analysis was performed as previously described (Wang et al., 2014).

Co-immunoprecipitation

1-4mg of protein were prepared from whole cell lysates of transfected cells or nucleolar fractions from mouse liver tissues in 1x RIPA (50mM Tris pH7.5, 150mM NaCl, 1% NP-40, supplemented with protease inhibitor cocktail (Roche), 0.5mM PMSF, 20mM NaF, 1μM TSA, 10mM NAM). Lysates were pre-cleared with 20μl of Protein G Sepharose beads (Sigma) while rocking at 4ºC for 1hr. After removal of pre-clearing beads, 10% of lysate was retained as input, the remainder of lysates were then incubated with 4μg of BMAL1 antibody (Abcam, ab93806), 4μg of NOP58 antibody (Proteintech, 14409-1-AP), or 5μg of GFP antibody (Abcam, ab290) as indicated. An additional, pooled sample was prepared with equal amount of protein for incubation with equal amount of Rabbit IgG (Santa Cruz Biotechnology, sc-2027 or Invitrogen, 10500C), and rocked overnight at 4ºC. The next day, 40μl of fresh Protein G Sepharose beads were added to the lysates and rocked at 4ºC for 2hrs. Beads were washed three times with 1x RIPA. 50μl sample buffer (240mM Tris-HCl pH 6.8, 40% Glycerol, 8% SDS, 20% β-mercaptoethanol, 0.02% Bromophenol blue) was added directly to the beads and samples were boiled for 10min at 95ºC. 20μl of samples and input were analyzed by Western blot. Antibodies used for Western blot include: BMAL1 (Abcam, ab93806), NOP58

(Abcam, ab155969), FIBRILLARIN (CST, #2639), SIRT7 (SCBT, sc-365344), AcBMAL1 (Millipore, 15396), MYC (Millipore, 05-419), GFP (Abcam, ab6556). Secondary antibodies include: HRP-conjugate Mouse anti-Rabbit light chain (Millipore, MAB201P) and HRP-conjugate Rabbit anti-Mouse IgG (Millipore, AP160P).

***in vitro* co-immunoprecipitation**

GST-fused recombinant BMAL1-HA fragments and GST-empty vectors were expressed in *Escherichia coli* and purified as described in detail previously (Delvecchio et al., 2013). Briefly, fusion proteins were expressed in *E.coli*, BL21 (DE3) and purified using glutathione Sepharose 4 Fast Flow resin according to the manufacturer protocol (GE Healthcare). 1µg of each GST-purified recombinant BMAL1 HA-tagged fragments were incubated overnight at 4ºC while rocking with 1mg of whole cell extracts from HEK293T cells transfected with GFP-NOP58. Lysates were then pre-cleared with 20µl of Protein G Sepharose beads (Sigma) while rocking at 4ºC for 1hr. After removal of pre-clearing beads, 10% of lysate was retained as input, the remainder of lysates were then incubated with 5µg of GFP antibody (Abcam, ab290) and rocked overnight at 4ºC. The next day, 40µl of fresh Protein G Sepharose beads were added to the lysates and rocked at 4ºC for 2hrs. Beads were washed three times with 1x RIPA. 50µl sample buffer (240mM Tris-HCl pH 6.8, 40% Glycerol, 8% SDS, 20% β-mercaptoethanol, 0.02% Bromophenol blue) was added directly to the beads and samples were boiled for 10min at 95ºC. 20µl of samples and input were analyzed by Western blot. Antibodies used for Western blot include: HA (Millipore, 05-904) and GFP (Abcam, ab6556). Secondary antibodies include: HRP-conjugate Mouse anti-Rabbit light chain (Millipore, MAB201P) and HRP-conjugate Rabbit anti-Mouse IgG (Millipore, AP160P).

Liquid chromatography-mass spectrometry

2mg of nucleoplasmic and nucleolar fractions from WT mouse livers harvested at ZT8 and ZT20 were prepared in 1x RIPA (50mM Tris pH7.5, 150mM NaCl, 1% NP-40, supplemented with protease inhibitor cocktail (Roche), 0.5mM PMSF, 20mM NaF, 1μM TSA, 10mM NAM) and 4μg of BMAL1 antibody (Abcam, ab93806) was used for co-immunoprecipitation as described above; after the final wash with 1x RIPA, the beads were washed three times with 50mM NH4HCO3 and incubated with 10 ng/μL trypsin in 1 M urea 50mM NH4HCO3 for 30 minutes, washed with 50mM NH4HCO3 and the supernatant digested overnight (ON) in presence of 1mM DTT. Digested peptides were alkylated and desalted prior to LC-MS analysis. For LC-MS/MS purposes, desalted peptides were injected in an Ultimate 3000 RSLCnano system (Thermo), separated in a 15-cm analytical column (75μm ID home-packed with ReproSil-Pur C18-AQ 2.4 μm from Dr. Maisch) with a 50-min gradient from 5 to 60% acetonitrile in 0.1% formic acid. The effluent from the HPLC was directly electrosprayed into a Qexactive HF (Thermo) operated in data dependent mode to automatically switch between full scan MS and MS/MS acquisition. Survey full scan MS spectra (from m/z 375–1600) were acquired with resolution R=60,000 at m/z 400 (AGC target of 3x106). The 10 most intense peptide ions with charge states between 2 and 5 were sequentially isolated to a target value of 1x105, and fragmented at 27% normalized collision energy. Typical mass spectrometric conditions were: spray voltage, 1.5 kV; no sheath and auxiliary gas flow; heated capillary temperature, 250ºC; ion selection threshold, 33.000 counts. MaxQuant 1.5.2.8 was used to identify proteins and quantify by iBAQ with the following parameters: Database, UP000000589_10090_Mmusculus_151030; MS tol, 10ppm; MS/MS tol, 0.5 Da; Peptide FDR, 0.1; Protein FDR, 0.01 Min. peptide Length, 5; Variable modifications, Oxidation (M); Fixed

modifications, Carbamidomethyl (C); Peptides for protein quantitation, razor and unique; Min. peptides, 1; Min. ratio count, 2. Identified proteins were considered nucleolar-enriched interaction partners if they met both requirements: their MaxQuant iBAQ values displayed greater than two-fold enrichment with $p<0.05$ (two-way ANOVA adjusted for multiple comparisons) when compared to the IgG control and if their MaxQuant iBAQ values displayed greater than four-fold enrichment with $p<0.05$ (two-way ANOVA adjusted for multiple comparisons) when compared to the nucleoplasmic interaction partners. Gene Ontology (GO) analysis was performed on the identified nucleolar-enriched interaction partners using the Database for Annotation, Visualization and Integrated Discovery (DAVID) v6.8 (Huang da et al., 2009). MS data are available via ProteomeXchange with identifier PXD018946.

Fluorescence lifetime imaging

HEK293T cells were plated in 35-mm glass-bottom microwell dishes (MatTek) and transfected with GFP-NOP58 alone or GFP-NOP58 and RFP-BMAL1. After 24hr, FLIM images of the two cell types - donor only (GFP-NOP58) and donor-acceptor (GFP-NOP58:RFP-BMAL1) were measured using a modified Olympus Fluoview FV1000 (Olympus, Waltham, MA) microscope equipped with a Spectra-Physics MaiTai HP laser (Spectra Physics, Santa Clara, CA) and FLIMBox (ISS, Champaign, IL) acquisition card. 900 nm laser line using a 63X water immersion objective (1.2 NA, Olympus Plan-apo, Olympus, Watltham, MA) were used for excitation applying a two photon excitation scheme. The resulting fluorescence was collected using the same objective and was split in two channels using a dichroic mirror (FF495-Di03-25x36, Semrock, Rochester, NY) and then passed through two separate filters

for GFP (520/35 nm, Semrock) and RFP (641/75 nm, Semrock) channels, and collected using two separate photomultiplier tube (H7422P-40, Hamamatsu, Bridgewater, NJ), and recorded using FLIMBox. The pixel dwell time for the acquisitions was set at 32 μs and the images were taken with sizes of 256x256 pixels. To have high signal to noise ratio, 20 – 30 frames were collected. Scanning and field of view were controlled by Olympus software and the data were acquired in passive FLIMBox mode. The data from each pixel were recorded and analyzed using the SimFCS software (developed by Dr. Enrico Gratton in Laboratory for Fluorescence Dynamics, University of California, Irvine, CA). The intensity decays collected at each pixel of the image were transformed to the Fourier space and the phasor coordinates were calculated using the following relations:

$$g_{i,j}(\omega) = \int_0^T I(t) \cdot Cos(n\omega t)dt \Big/ \int_0^T I(t)dt$$

$$s_{i,j}(\omega) = \int_0^T I(t) \cdot Sin(n\omega t)dt \Big/ \int_0^T I(t)dt$$

where, $g_{i,j}(\omega)$ and $s_{i,j}(\omega)$ are the X and Y coordinates of the phasor plot, respectively, and n and ω are the harmonic number and the angular frequency of excitation, respectively, and T is the repeat frequency of laser (80 MHz).

RNA immunoprecipitation followed by quantitative PCR (RIP-qPCR)

1.5mg of nucleolar fractions from WT and *Bmal1*-KO mouse livers harvested at ZT8 were prepared in 1x RIP buffer (25mM Tris pH7.5, 150mM KCl, 5mM EDTA, 0.5mM DTT, 0.5% NP-40, supplemented with protease inhibitor cocktail (Roche), 0.5mM PMSF, 20mM NaF, 1μM TSA, 10mM NAM, 100U/ml RNaseOUT (Invitrogen)) and 4μg of NOP58 antibody (Proteintech, 14409-1-AP) was used for co-immunoprecipitation as described above with a

modification to buffers, S2 and S3, the addition of 100U/ml RNaseOUT (Invitrogen). After the final wash with 1x RIP buffer, 1ml of TRIzol was added to the beads and input samples and RNA was isolated following manufacturer's recommendation. RNA was resuspended in equal volume of DEPC-treated water and reversed transcribed into cDNA using Maxima H Minus cDNA Synthesis Master Mix (Thermo Scientific, Cat#1661). cDNA was used for quantitative real-time PCR using SsoAdvanced Universal SYBR Green Supermix (Bio-Rad Laboratories) and ran on a QuantStudio 3 real-time PCR System (Applied Biosystems). Primer sequences used to identify bound-RNA were designed with Primer3 software (Koressaar and Remm, 2007; Untergasser et al., 2012). Rnu3a (U3): Fwd: 5'-ACTGTGTAGAGCACCCGAAAC-3', Rev: 5'-GACTGTGTCCTCTCCCTCTCA-3'; Snord118 (U8): Fwd: 5'-CCTTACCTGTTCCTCCTTTCG-3', Rev: 5'-GAGCAACCAGGATGTTGTCA-3'; Snord17: Fwd: 5'-TGACCTTCTTCCCAGTCTCG-3', Rev: 5'-GGTGAGATGGAACCCAGAGA-3'; 18S: Fwd: 5'-CGCCGCTAGAGGTGAAATTC-3', Rev: 5'-CGAACCTCCGACTTTCGTTCT-3'; 5'ETS/18S: Fwd: 5'-CTCCTCTCTCGCGCTCTCT-3', Rev: 5'-GGCCGTGCGTACTTAGACAT-3'; 18S/ITS1: Fwd: 5'-CTGAGAAGACGGTCGAACTTG-3', Rev: 5'-CCTCCACAGTCTCCCGTTTA-3'; ITS1/5.8S: Fwd: 5'-ACACCCGAAATACCGATACG-3', Rev: 5'-GTGCGTTCGAAGTGTCGAT-3'; ITS2/28S: Fwd: 5'-GCCTCCTCGCTCTCTTCTTC-3', Rev: 5'-GCCGTTACTGAGGGAATCCT-3'; Actin: Fwd: 5'-GGCTGTATTCCCCTCCATG-3', Rev: 5'-CCAGTTGGTAACAATGCCATGT-3'.

Polysome profiling

WT and *Bmal1*-KO MEFs were treated with 10μg/ml Cycloheximide on a rocker for 5min at RT. One plate of each WT and *Bmal1*-KO MEF cells was retained for standard DNA extraction by Phenol-chloroform. The remainder of cells were washed with 1x PBS containing

200µg/ml of cycloheximide, scraped to collect, and spun at 1500rpm (500g) for 5min. Cell pellets were homogenized in equal volume of Homogenization buffer (300mM NaCl, 50mM Tris-HCl pH8.0, 10mM $MgCl_2$, 1mM EGTA, 1% Triton X-100, 0.1% DOC, 200µg/ml Heparin, 1mM DTT, 200U/ml RNaseOUT (Invitrogen), supplemented with protease inhibitor cocktail (Roche), 200µg/ml Cycloheximide), rocked at 4ºC for 10min, and spun at 12500rpm (18000g) for 15min at 4ºC. Each polysomal lysate was normalized to DNA concentration and layered above a 10-50% sucrose gradient (140mM NaCl, 25mM Tris-HCl pH8.0, 10mM $MgCl_2$, 10%-50% Sucrose) and centrifuged at 31000rpm for 2hrs at 4ºC. Gradients were run through a UA-6 UV/Vis detector (Teledyne Isco) to record polysome profiles. Graphs were digitalized using WebPlotDigitizer software (https://automeris.io/WebPlotDigitizer).

Statistical analysis

Sample size and data presented as mean + s.d. or plotted as individual data points were indicated in the figure legends. Statistical significance was determined by t test, one-way ANOVA, or two-way ANOVA (GraphPad Prism8) as indicated in the figure legends. Statistical significance was assigned as *, **, ***, and **** when p-value cutoffs of 0.05, 0.01, 0.001, and 0.0001, respectively, were met.

RESOURCE AVAILABILITY

Lead Contact: Further information and requests for resources and reactions should be directed to and fulfilled by the Lead Contact, Paolo Sassone-Corsi (psc@uci.edu).

Materials Availability: All unique/stable materials and models generated from this study are available from the Lead Contact with a completed Materials Transfer Agreement.

Data and Code Availability: The MS data generated in this study are available via ProteomeXchange with identifier PXD018946.

ACKNOWLEDGMENTS

We thank all members of the Sassone-Corsi lab for helpful discussion and technical assistance. We are grateful to Dr. Selma Masri for critical scientific discussions. This study was supported by predoctoral fellowships to M.C. from the National Institutes of Health (NIH) (GM117942), the American Heart Association (17PRE33410952), and the UCI School of Medicine Behrens Research Excellence Award. Funding for P.S.-C. was provided by the NIH (AG053592, DK114652), a Novo Nordisk Foundation Challenge Grant, and Institut National de la Sante et la Recherche Medicale (U1233 INSERM, France).

AUTHOR CONTRIBUTIONS

M.C. and P.S.-C. designed the study and analyzed the data. M.C. performed the experiments. I.F. and A.I. conducted the mass spectrometry analysis. S.R. and E.G. conducted the FLIM-FRET analysis. M.C. and P.S.-C. wrote the paper with feedback from all authors.

DECLARATION OF INTERESTS

The authors declare no competing interests.

FIGURES

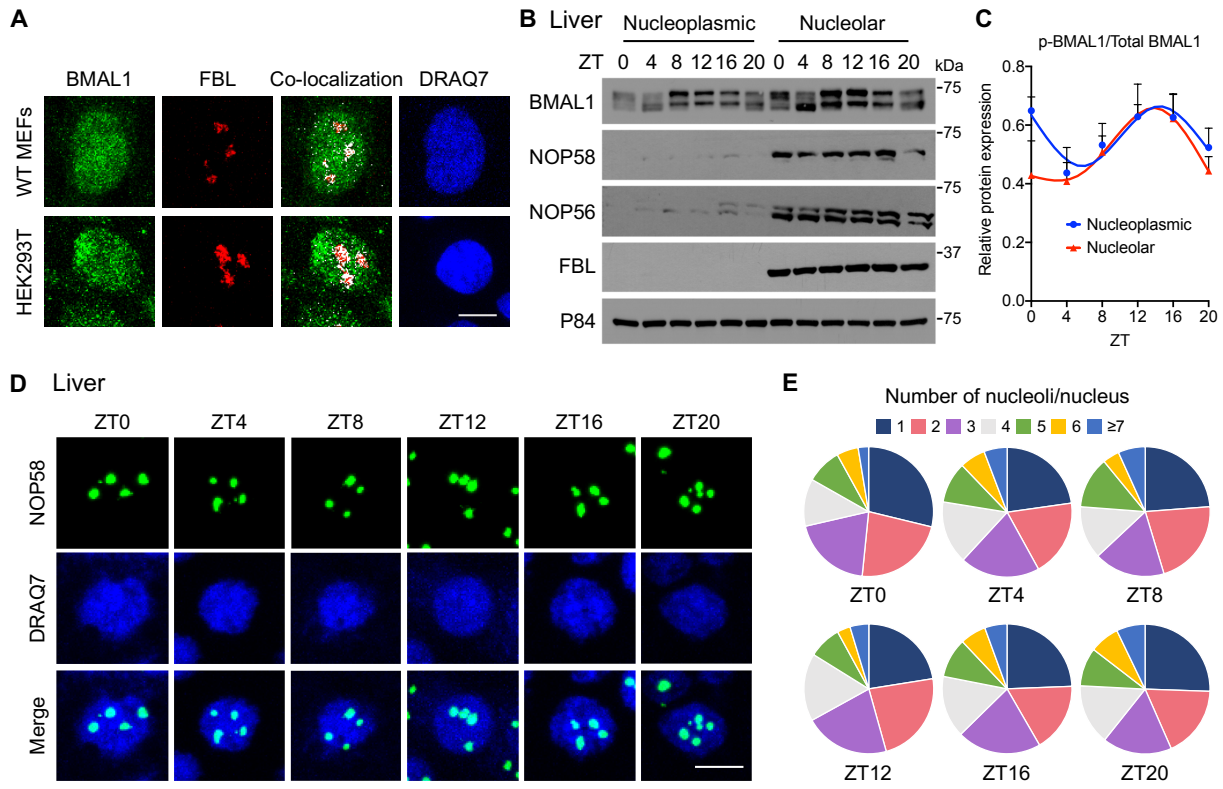

Figure 2.1 BMAL1 localization in circadian-independent nucleoli

A. Representative images of endogenous BMAL1 (green) and FBL (red) in WT MEFs and HEK293T cells with DRAQ7 nuclear stain (blue) and co-localized pixels (white). Scale bar, 10μm. A total of 10 distinct fields of view were imaged/cell type. **B.** Western blot analysis of endogenous BMAL1 and nucleolar proteins, NOP58, NOP56, and FBL in nucleoplasmic and nucleolar fractions prepared from WT mouse liver tissues harvested at ZT0, 4, 8, 12, 16, 20. p84 was used as a loading control. **C.** Quantification of phosphorylated BMAL1 (p-BMAL1) as a ratio of Total BMAL from **B**. Data are presented as mean + SEM. N=5 biological replicates/timepoint/group, no significant differences by two-way ANOVA with Sidak's multiple comparisons test. **D.** Representative images of endogenous NOP58 (green) in WT mouse livers harvested at ZT0, 4, 8, 12, 16, 20 with DRAQ7 nuclear stain (blue). Scale bar, 10μm. A total of 6-9 distinct fields of view were imaged/timepoint. **E.** Pie charts representing the percentage of nuclei displaying the indicated number of nucleoli in WT mouse livers from **D** identified by NOP58 at ZT0, 4, 8, 12, 16, 20. N=3 biological replicates/timepoint, a total of 2,493 cells were counted.

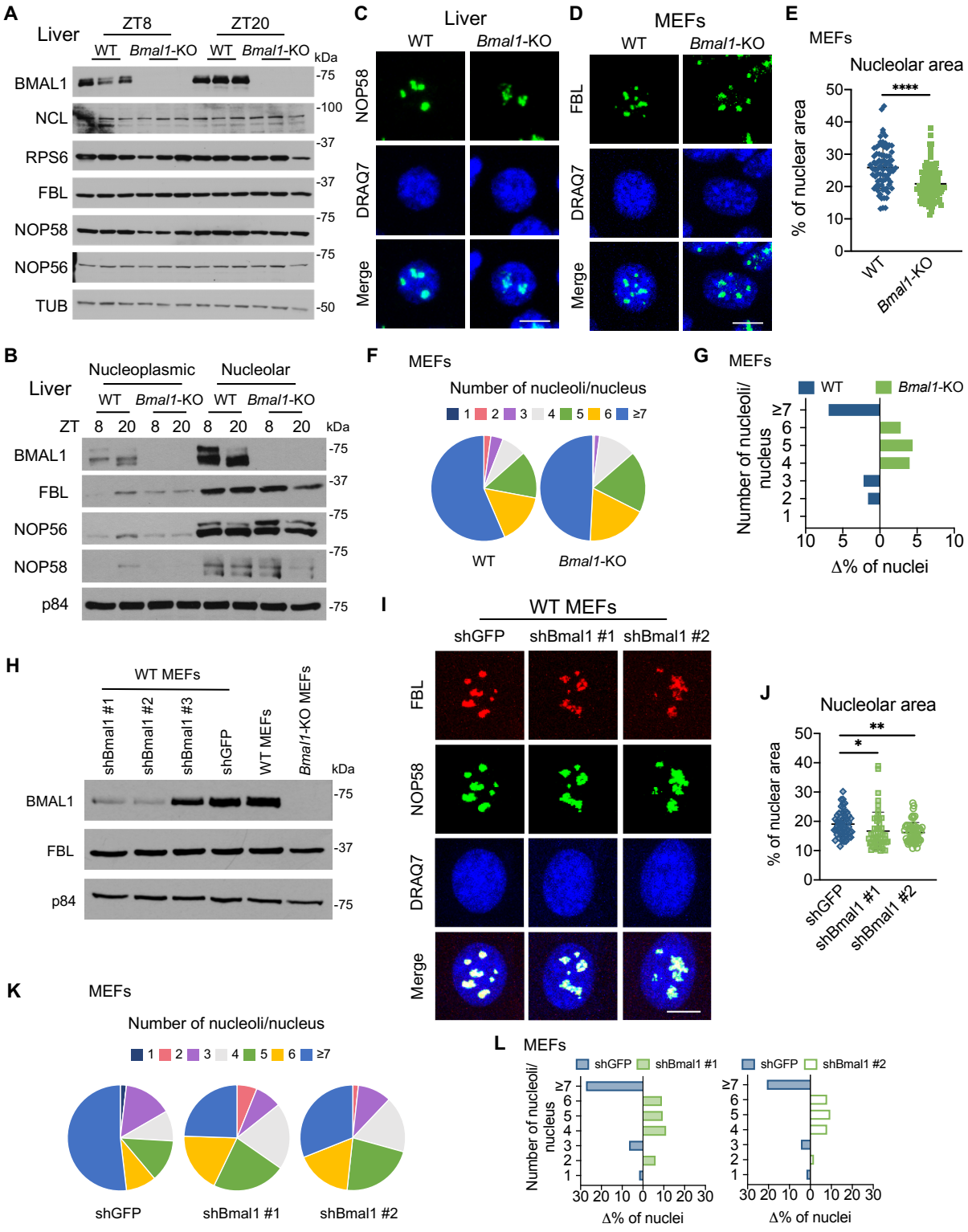

Figure 2.2 *Bmal1*-deficient cells show altered nucleolar structure

A. Western blot analyses of whole cell extracts prepared from WT and *Bmal1*-KO mouse livers collected at ZT8 and ZT20 for ribosome biogenesis proteins, NUCLEOLIN, Ribosomal Protein S6, FIBRILLARIN, NOP58, and NOP56. TUBULIN is used as a loading control. **B.** Western blot analysis of endogenous BMAL1, FBL, NOP56, and NOP58 in nucleoplasmic and nucleolar fractions prepared from WT and *Bmal1*-KO mouse liver tissues harvested at ZT8 and ZT20. p84 was used as a loading control. **C.** Representative images of endogenous NOP58 (green) in WT and *Bmal1*-KO mouse livers harvested at ZT8 with DRAQ7 nuclear stain (blue). Scale bar, 10μm. A total of 10 distinct fields of view were imaged/genotype. **D.** Representative images of endogenous FBL (green) in WT and *Bmal1*-KO MEFs with DRAQ7 nuclear stain (blue). Scale bar, 10μm. A total of 14 distinct fields of view were imaged/genotype. **E.** Total nucleolar area measured as the percent of nuclear area with FBL signal in WT and *Bmal1*-KO MEFs. Individual cells are plotted. N=3 biological replicates/group, ****$p<0.0001$ by unpaired t test with Welch's correction. **F.** Pie charts representing the percentage of nuclei displaying the indicated number of nucleoli in WT and *Bmal1*-KO MEFs from **D** identified by FBL. **G.** Delta percentage of WT and *Bmal1*-KO MEFs that display the indicated number of nucleoli per nucleus. A total of 353 cells were counted. **H.** Western blot analyses of BMAL1 and FBL in whole cell lysates prepared from *Bmal1*-KO and WT MEFs stably expressing shGFP, shBmal1 #1, shBmal1 #2, or shBmal1 #3. p84 was used as a loading control. **I.** Representative images of endogenous FBL (red) and NOP58 (green) in WT MEFs stably expressing shGFP, shBmal1 #1, or shBmal1 #2 with DRAQ7 nuclear stain (blue). Scale bar, 10μm. A total of 8 distinct fields of view were imaged/condition. **J.** Total nucleolar area measured as the percent of nuclear area with FBL and NOP58 signal in WT MEFs stably expressing shGFP, shBmal1 #1, or shBmal1 #2. Individual cells are plotted. N=4 technical replicates/group, *$p<0.05$ and **$p<0.01$ by one-way ANOVA with Tukey's multiple comparisons test. **K.** Pie charts representing the percentage of nuclei displaying the indicated number of nucleoli in MEFs from **I** identified by FBL and NOP58. **L.** Delta percentage of WT MEFs stably expressing shGFP or shBmal1 #1 (left), and shGFP or shBmal1 #2 (right) that display the indicated number of nucleoli per nucleus. A total of 218 cells were counted.

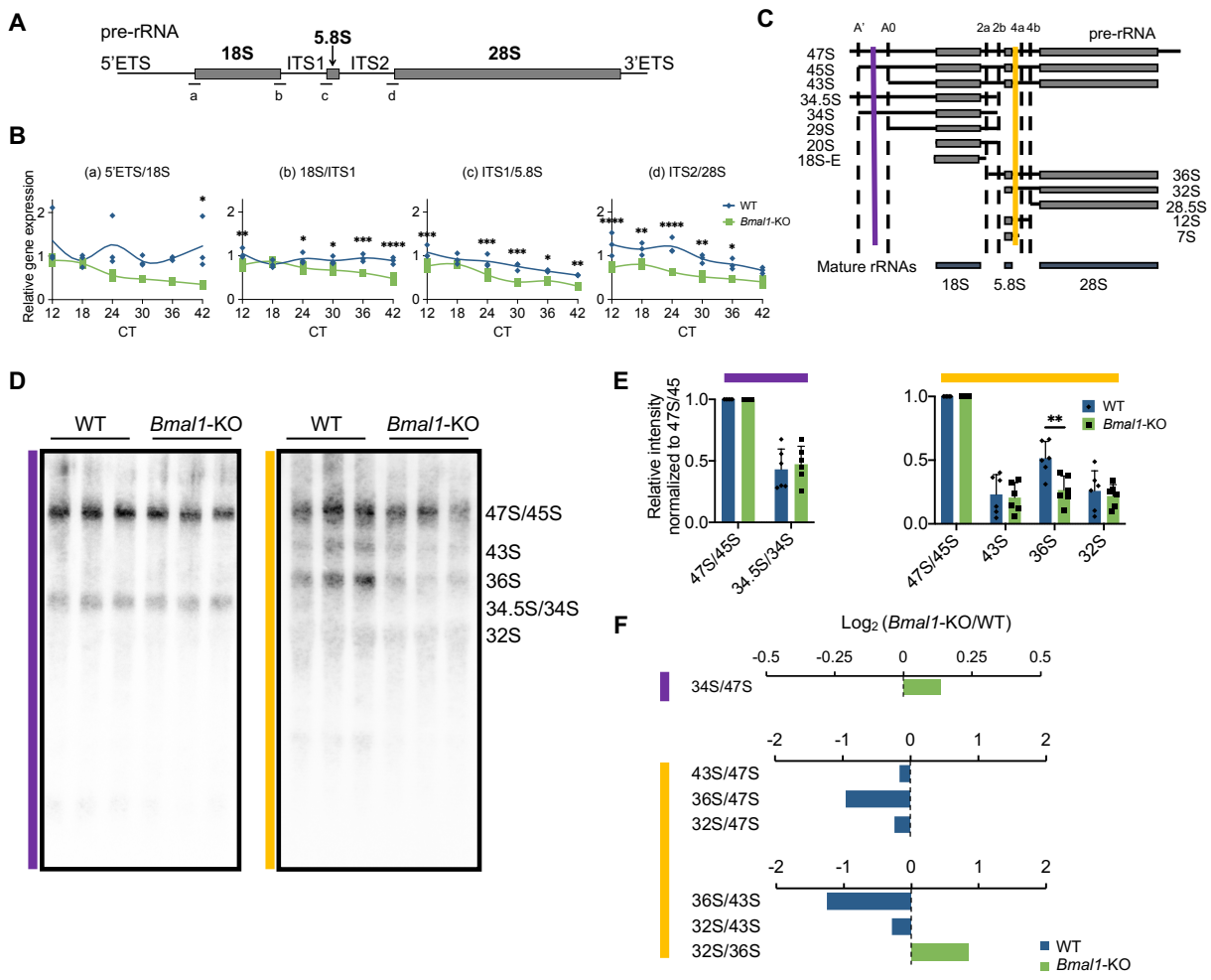

Figure 2.3 Pre-ribosomal RNA processing is altered in the absence of BMAL1

A. Schematic representation of the mammalian pre-rRNA transcript (ETS, external transcribed spacer; ITS, internal transcribed spacer). a-d indicate primer sequence positions designed for reverse transcriptase-quantitative PCR (RT-qPCR) analyses. **B.** pre-rRNA expression profiles at indicated regions a-d from **A** in WT and *Bmal1*-KO MEFs harvested at circadian times (CT) 12, 18, 24, 30, 36, 42 hours post-synchronization. Gene expression normalized to 18S rRNA. Individual data points are plotted. N=3 technical replicates/timepoint/group, *p<0.05, **p<0.01, ***p<0.001, and ****p<0.0001 by two-way ANOVA with Sidak's multiple comparisons test. **C.** Schematic representation of mouse pre-rRNA cleavage intermediates (laterally labeled) as depicted by (Henras et al., 2015). Dotted lines delineate labeled cleavages sites (top). Vertical colored lines (purple and gold) show regions of hybridization by the Northern probes designed by (Lapik et al., 2004). **D.** Northern analyses of pre-rRNA intermediates in WT and *Bmal1*-KO MEFs. Colored lines correspond to colored probes from **C** intermediates identified are labeled on the right. Equal amount of

total RNA was loaded for analysis. **E.** Quantification of each intermediate from **D** normalized to 47S/45S. Colored lines label graphs corresponding to colored probes from **C**. Data are presented as mean + SD. N=6 biological replicates/group, **p<0.01 by two-way ANOVA with Sidak's multiple comparisons test. **F.** Ratio analysis of multiple precursors (RAMP) quantification of each intermediate from **D** Colored lines label graphs corresponding to colored probes from **C**. Data are presented as the Log_2 (*Bmal1*-KO/WT) of the mean ratio of each cleavage pair. N=6 biological replicates/genotype.

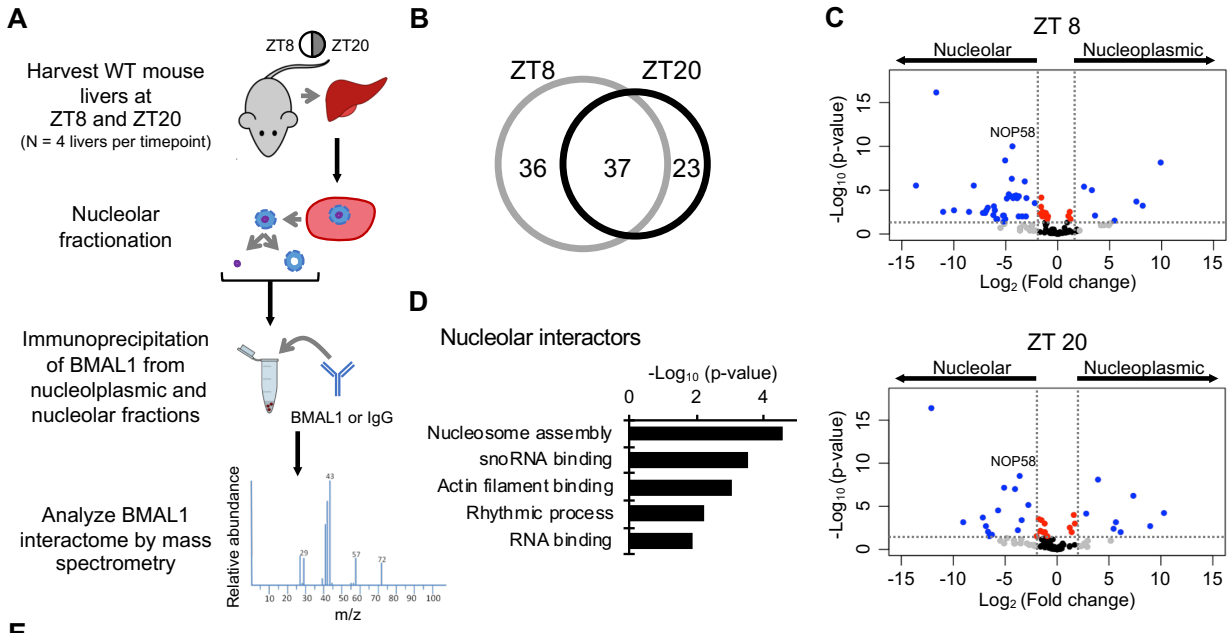

E Nucleolar interactors

ZT8	Protein Name	-Log_2 (Fold change)	p-value
NHP2	H/ACA ribonucleoprotein complex subunit 2	11.69	7.23E-17
NOP58	Nucleolar protein 58	4.36	1.22E-10
NOP56	Nucleolar protein 56	5.06	3.88E-09
DDX21	Nucleolar RNA helicase 2	4.42	5.44E-07
TPM3-RS7	Tropomyosin 3, related sequence 7	3.17	1.10E-06
COL6A3	Collagen type VI alpha 3	8.08	3.04E-06
HIST1H1A	Histone H1.1	13.64	3.09E-06
H2AFY	Histone H2A.1	4.71	3.30E-05
HIST1H33	Histone H3.3	4.01	4.13E-05
RNF213	Ring Finger Protein 213	4.21	4.54E-05

ZT20	Protein Name	-Log_2 (Fold change)	p-value
NHP2	H/ACA ribonucleoprotein complex subunit 2	12.11	3.87E-17
NOP58	Nucleolar protein 58	3.60	2.64E-09
DDX21	Nucleolar RNA helicase 2	5.10	6.95E-08
NOP56	Nucleolar protein 56	4.05	1.14E-07
TPM3-RS7	Tropomyosin 3, related sequence 7	2.77	6.52E-06
PISD	Phosphatidylserine decarboxylase	5.68	3.05E-05
MYBBP1A	MYB binding protein 1a	7.15	1.53E-04
RNF213	Ring Finger Protein 213	3.41	4.10E-04
TPM3	Tropomyosin 3	9.04	6.76E-04
SACM1L	Phosphatidylinositide phosphatase SAC1	6.85	1.83E-03

Figure 2.4 Identification of the BMAL1 nucleolar interactome

A. Schematic representation of the experimental design of the nucleolar BMAL1 interactome analysis. Mass spectrometry analysis was performed on N=4 biological replicates/timepoint. **B.** Venn diagram of the number of total significant BMAL1-interacting proteins at ZT8 and ZT20 compared to IgG control. Significant interactors were identified when having two-fold differences between nucleoplasmic and IgG or nucleolar and IgG, respectively, with $p<0.05$ as determined by two-way ANOVA adjusted for multiple comparisons. **C.** Volcano plots of nucleoplasmic versus nucleolar BMAL1 interactors at ZT8 and ZT20. Significant interactors were identified when having four-fold differences (Log_2 (Fold change) nucleoplasmic/nucleolar > |2| and $p<0.05$ (blue) as determined by two-way ANOVA adjusted for multiple comparisons). **D.** Gene Ontology (GO) analysis of the significant nucleolar BMAL1-interacting proteins (Fisher Exact p-value denotes annotation significance). **E.** Top 10 significant nucleolar BMAL1 interactors listed with p-value and -Log_2 (Fold change) of the comparison between nucleoplasmic/nucleolar. Proteins highlighted in gray appear at both timepoints.

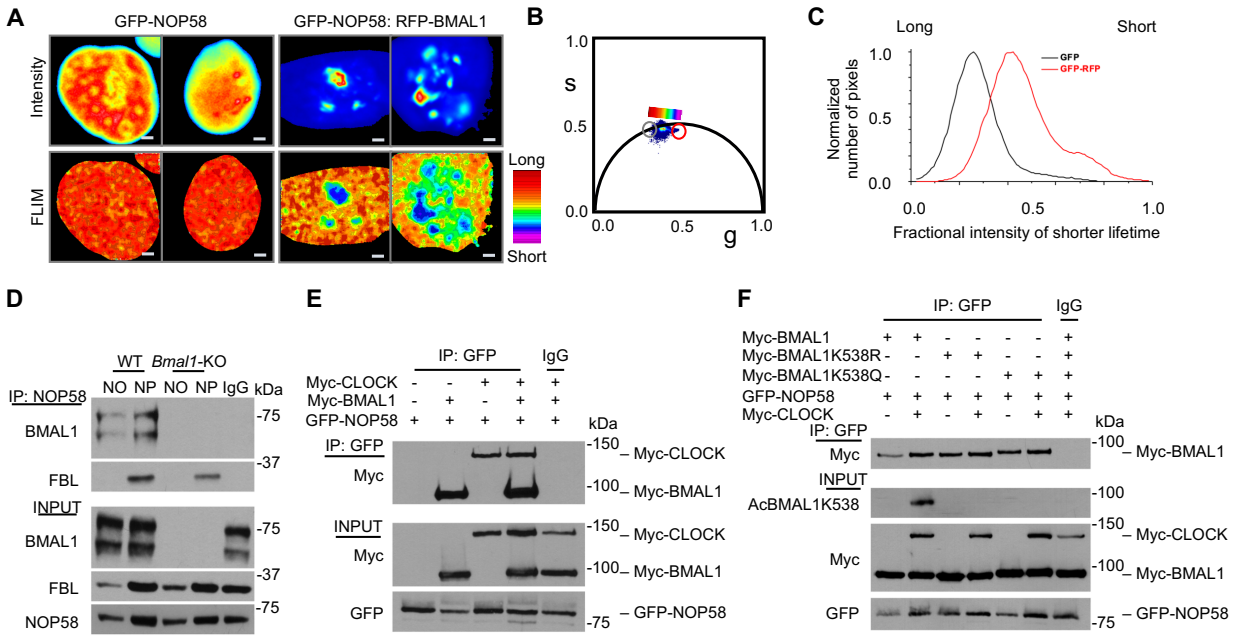

Figure 2.5 BMAL1 interacts with nucleolar protein NOP58

A. Representative images of HEK239T cells transfected with GFP-NOP58 and RFP-BMAL1 as indicated and displayed as auto-scaled fractional intensity images (top), and phasor mapped FLIM images (bottom) color mapped according to the color scheme distribution (left) depicting a range from long to shorter lifetime. **B.** Phasor plot of FLIM images in **A** where red is representative of long lifetime and purple is representative of shorter lifetime and more FRETting. Gray circle denotes GFP-NOP58 cells and red circle denotes GFP-NOP58:RFP-BMAL1 cells. **C.** A cumulative histogram showing the number of pixels plotted against fractional intensity of the shorter lifetime in GFP-NOP58 only (black) and GFP-NOP58:RFP-BMAL1 (red). **D.** Endogenous co-immunoprecipitation analyses were performed in nucleoplasmic (NP) and nucleolar (NO) fractions prepared from WT or *Bmal1*-KO mouse livers. Immunoprecipitation (IP) was performed using BMAL1 or Rabbit IgG followed by Western blot (WB) analyses of BMAL1, FBL, and NOP58 as specified. **E.** Co-immunoprecipitation analyses performed in HEK293T cells co-transfected with GFP-NOP58, Myc-BMAL1, and Myc-CLOCK as indicated. Immunoprecipitation (IP) was performed using GFP or Rabbit IgG followed by Western blot (WB) analysis of MYC and GFP as specified. **F.** Co-immunoprecipitation analyses were performed in HEK293T cells co-transfected with GFP-NOP58 and Myc-BMAL1, Myc-BMAL1K538R, or Myc-BMAL1K538Q mutants. Immunoprecipitation (IP) was performed using GFP or Rabbit IgG followed by Western blot (WB) analyses of MYC, GFP, and AcBMAL1K538 as specified.

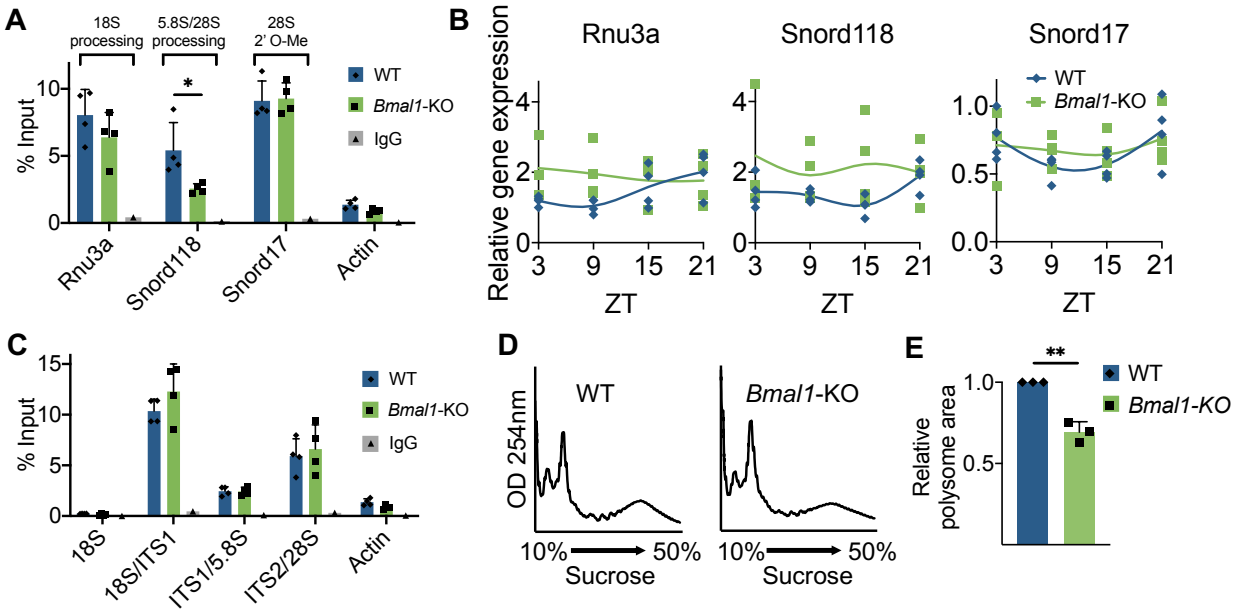

Figure 2.6 BMAL1 links snoRNA recruitment to box C/D snoRNP

A. RNA immunoprecipitation (RIP) using NOP58 or Rabbit IgG in nucleolar fractions isolated from WT and *Bmal1*-KO mouse livers followed by qPCR analyses of snoRNAs: Rnu3a, Snord118, and Snord17. Actin mRNA was used as a negative control. Data are presented as mean + SD. N=4 biological replicates/group, *p<0.05 by two-way ANOVA with Tukey's multiple comparisons test. **B.** Rnu3, Snord118, and Snord17, snoRNAs expression profiles in WT and *Bmal1*-KO mouse livers harvested at ZT3, 9, 15, and 21. Gene expression was normalized to 18S rRNA. Individual data points are plotted. N=4 biological replicates/timepoint/group, no significant differences by two-way ANOVA with Sidak's multiple comparisons test. **C.** RNA immunoprecipitation (RIP) using NOP58 or Rabbit IgG in nucleolar fractions from WT and *Bmal1*-KO mouse livers followed by qPCR analysis for 18S rRNA, 18S/ITS1, ITS1/5.8S, and ITS2/28S pre-RNAs. Actin mRNA was used as a negative control. Data are presented as mean + SD. N=4 biological replicates/group, no significant differences by two-way ANOVA with Tukey's multiple comparisons test. **D.** Polysome profiles of WT and *Bmal1*-KO MEFs. **E.** Quantification of the area under the polysome curve from **D**. Data are presented as mean + SD. N=3 biological replicates/group, **p<0.01 by unpaired t test.

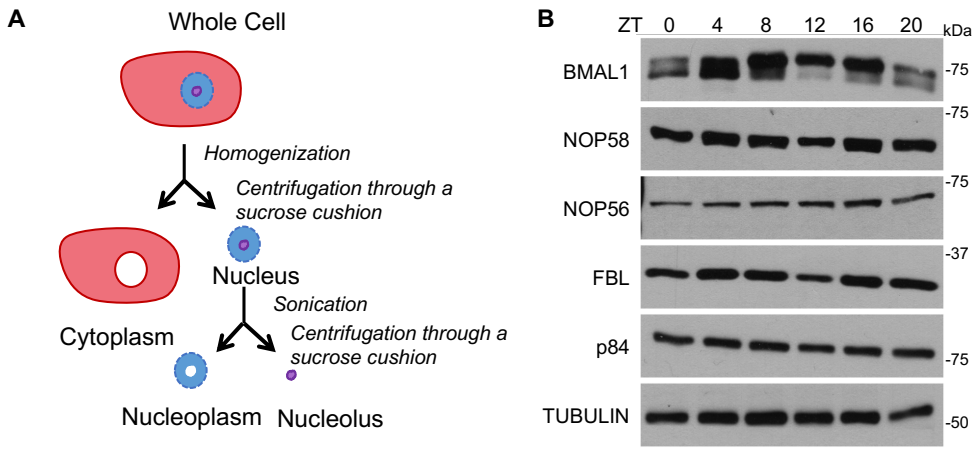

Figure 2.S1 Nucleolar proteins are not circadian

A. Schematic representation of the experimental design used for nucleolar fractionation. **B.** Western blot analyses of whole cell lysates prepared from WT mouse livers collected at ZT0, 4, 8, 12, 16, 20, blotted for BMAL1, NOP58, NOP56, and FBL. p84 and TUBULIN were used as loading controls.

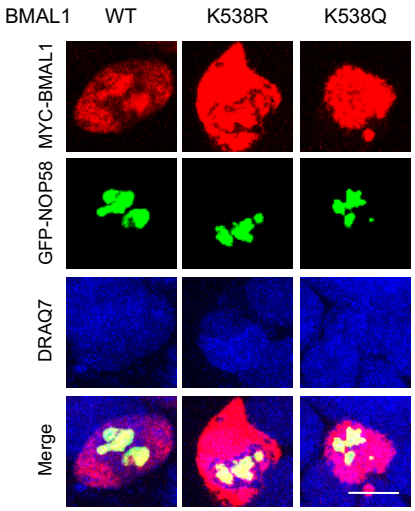

Figure 2.S2 BMAL1 nucleolar localization is acetylation-independent

Representative images of HEK293T cells co-transfected with GFP-NOP58 and Myc-BMAL1 (WT), Myc-BMAL1K538R (K538R), or Myc-BMAL1K538Q (K538Q) mutants. MYC was used to visualize the Myc-BMAL1 variants (red) with DRAQ7 nuclear stain (blue). Scale bar, 10μm. A total of 9 distinct fields of view were imaged/condition.

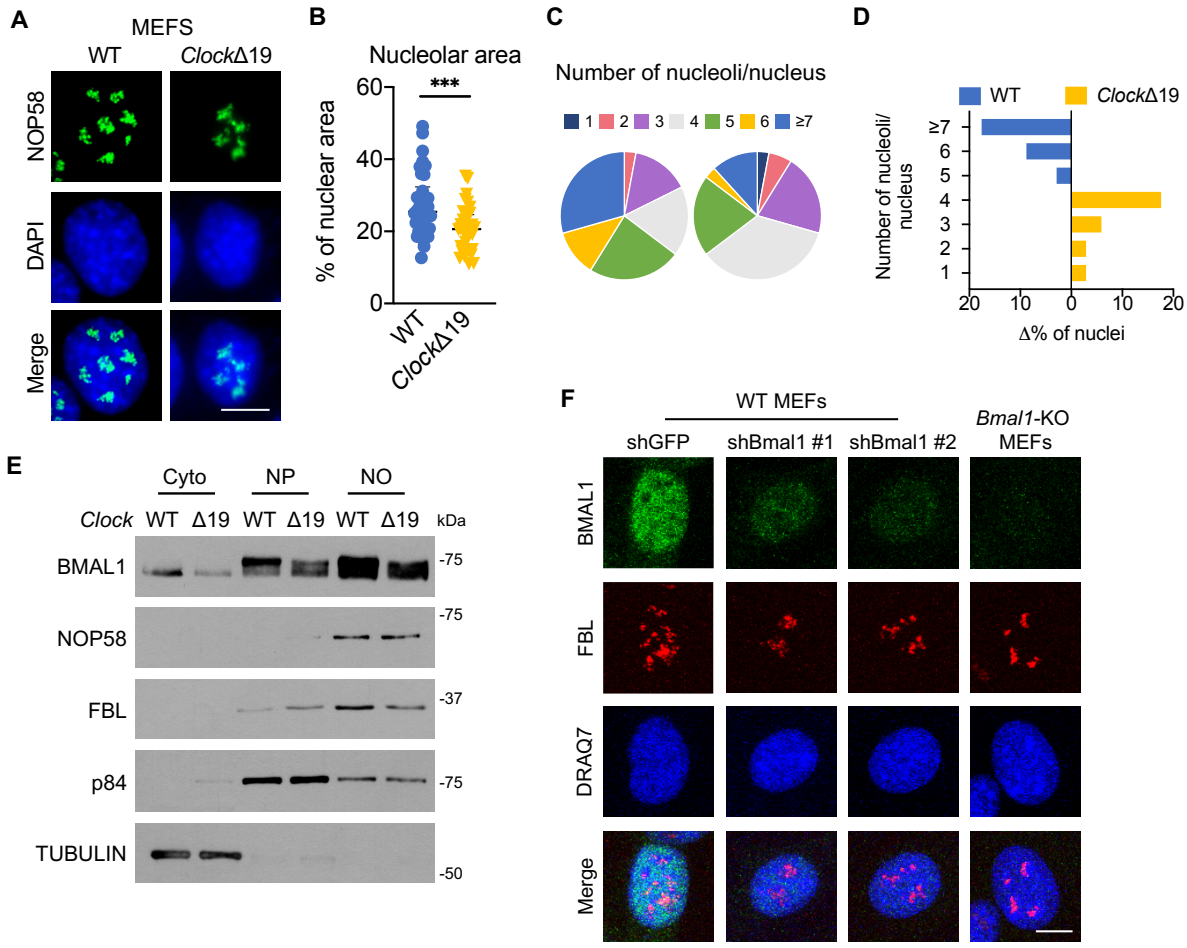

Figure 2.S3 The BMAL1 effect on nucleolar structure

A. Representative images of endogenous NOP58 (green) in WT and *Clock*Δ19 MEFs with DAPI nuclear stain (blue). Scale bar, 10μm. A total of 5 distinct fields of view were imaged/condition. **B.** Total nucleolar area measured as the percent of nuclear area with NOP58 signal in WT and *Clock*Δ19 MEFs. Individual cells are plotted. N=3 technical replicates/group, ***p<0.001 by unpaired t test with Welch's correction. **C.** Pie charts representing the percentage of nuclei displaying the indicated number of nucleoli in WT and *Clock*Δ19 MEFs from **A** identified by NOP58. **D.** Delta percentage of WT and *Clock*Δ19 MEFs that display the indicated number for nucleoli per nucleus. A total of 68 cells were counted. **E.** Western blot analyses of BMAL1, NOP58, and FBL in cytoplasmic (Cyto), nucleoplasmic (NP), and nucleolar (NO) fractions prepared from WT and *Clock*Δ19 MEFs. p84 and TUBULIN were used as loading controls. **F.** Representative images of endogenous BMAL1 (green) and FBL (red) in *Bmal1*-KO and WT MEFs stably expressing shGFP, shBmal1 #1, or shBmal1 #2 with DRAQ7 nuclear stain (blue). Scale bar, 10μm. A total of 5 distinct fields of view were imaged/condition.

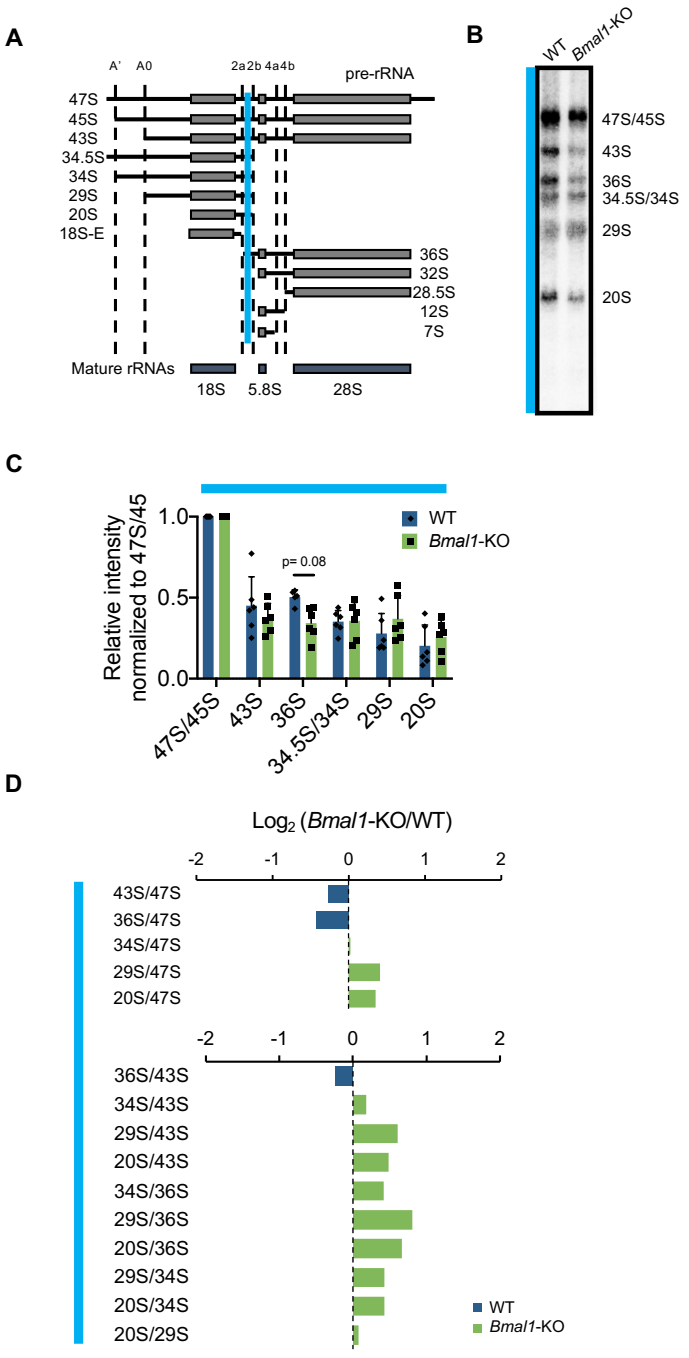

Figure 2.S4 Reduced pre-rRNA processing in *Bmal1*-KO MEFs

A. Schematic representation of mouse pre-rRNA cleavage intermediates (laterally labeled) as depicted by (Henras et al., 2015). Dotted lines delineate labeled cleavages sites (top). Vertical colored line (blue) shows regions of hybridization by the Northern probe designed

by (Lapik et al., 2004). **B.** Northern blot analysis of pre-rRNA intermediates in WT and *Bmal1*-KO MEFs. Colored line (blue) corresponds to colored probe from **A**, intermediates identified are labeled on the right. **C.** Quantification of each intermediate from **B** normalized to 47S/45S. Colored line corresponds to colored probe from **A**. Data are presented as mean + SD. N=6 biological replicates/group, significance tested by two-way ANOVA with Sidak's multiple comparisons test. **D.** Ratio analysis of multiple precursors (RAMP) quantification of each intermediate from **B**. Data are presented as the Log_2 (*Bmal1*-KO/WT) of the mean ratio of each cleavage pair. N=6 biological replicates/genotype.

A All significant nucleolar interactors

ZT8 only				
	ZT8		ZT20	
Protein	Log_2 (Fold Change)	p-value	Log_2 (Fold Change)	p-value
HIST1H1B	8.85	1E-02	3.81	2E-01
COL6A1	8.15	8E-04	1.74	4E-01
BGN	7.71	4E-03	2.22	3E-01
CISD3	7.26	2E-02	2.56	4E-01
HMGN1	7.11	1E-02	0.00	1E+00
TINAGL1	6.99	4E-03	1.55	5E-01
ELOVL2	6.84	3E-02	5.51	7E-02
ABCB10	6.73	1E-03	3.45	7E-02
HIST1H1A	6.67	4E-03	-4.74	3E-02
HMGN2	6.27	4E-02	0.42	9E-01
COL6A2	6.05	2E-03	1.56	4E-01
CBX3	5.81	2E-02	0.00	1E+00
HIST2H2AB	5.53	2E-02	0.00	1E+00
HIST3H2BA	5.26	8E-03	0.00	1E+00
BANF1	5.21	4E-02	0.00	1E+00
PARP1	5.18	8E-03	0.00	1E+00
DIDO1	5.05	2E-02	2.15	3E-01
DCTN2	4.39	2E-02	2.37	2E-01
DCN	3.76	1E-02	0.00	1E+00
H2AFV	3.67	1E-03	-0.45	6E-01
MYH4	3.35	4E-02	0.00	1E+00
HIST2H2AC	3.27	1E-03	0.12	9E-01
MYH10	3.06	1E-02	0.00	1E+00
H2AFY	3.03	2E-03	-0.64	5E-01
HIST1H2B	2.92	3E-03	-0.12	9E-01
H1F0	2.75	2E-03	-0.65	4E-01
HIST1H33	2.65	2E-03	-0.56	5E-01
HIST1H1E	2.54	2E-03	-0.47	5E-01
MYH9	1.92	1E-03	0.61	2E-01
HIST1H1C	1.92	2E-02	-0.91	3E-01
HIST1H4	1.81	7E-03	-0.18	8E-01
MYO1C	1.32	3E-02	0.68	2E-01
EPPK1	1.26	3E-02	0.04	9E-01
TGM2	1.18	8E-03	0.12	8E-01
TPM3-RS7	1.15	2E-02	0.91	5E-02
MYL6	1.13	4E-02	0.53	3E-01

Both				
	ZT8		ZT20	
Protein	Log_2 (Fold Change)	p-value	Log_2 (Fold Change)	p-value
ATP5SL	14.61	5E-07	14.62	5E-07
ARNTL	12.73	2E-08	12.09	5E-08
RAB3IP	12.42	1E-06	12.45	1E-06
LPL	10.12	1E-06	9.51	3E-06
CLOCK	10.12	1E-05	9.47	3E-05
PIGX	10.01	6E-04	7.42	7E-03
LRCH3	9.74	5E-20	9.59	6E-20
ABHD16A	9.72	5E-09	9.95	4E-09
ASGR2	8.95	5E-04	9.86	2E-04
ILKAP	8.33	1E-05	8.74	6E-06
PISD	8.12	3E-07	7.40	1E-06
COL6A3	8.08	3E-06	3.78	6E-03
MYL12B	8.02	5E-03	8.37	4E-03
RALGAPA1	7.30	4E-13	7.97	8E-14
CRACR2B	6.19	2E-04	6.55	1E-04
SACM1L	6.14	4E-03	6.23	4E-03
TMEM102	6.02	4E-03	6.03	4E-03
NIFK	5.91	2E-02	6.65	9E-03
FAM213A	5.87	2E-02	5.10	5E-02
PKP2	5.84	1E-02	4.92	3E-02
RNF213	5.00	6E-06	5.22	3E-06
PPA2	4.66	2E-02	5.76	4E-03
SSFA2	4.43	1E-02	4.35	1E-02
DOCK7	3.18	4E-05	3.39	2E-05
FLNA	3.04	3E-02	3.34	2E-02
GPX4	2.53	5E-03	3.11	1E-03
ZBTB20	2.32	5E-04	2.11	1E-03
HVM58	2.11	3E-04	2.97	5E-06
SLC39A7	2.00	2E-04	1.66	9E-04
NHP2	1.88	1E-04	2.30	1E-05
ASGR1	1.69	6E-06	1.84	2E-06
NOP58	1.34	8E-04	1.35	8E-04
SEC31B	1.27	3E-03	1.67	2E-04
C1RA	1.22	4E-03	1.42	1E-03
FLNB	1.14	2E-02	1.90	6E-04
C1SA	1.07	2E-02	1.29	7E-03
NOP56	1.01	5E-02	1.32	1E-02

ZT20 only				
	ZT8		ZT20	
Protein	Log_2 (Fold Change)	p-value	Log_2 (Fold Change)	p-value
TRY4	7.09	7E-02	8.91	2E-02
TOMM22	2.68	4E-01	7.81	3E-02
P2RX7	4.36	8E-02	7.04	9E-03
ACTA2	4.36	7E-02	6.74	9E-03
HACD3	2.14	5E-01	6.59	3E-02
CAPZB	4.25	1E-01	6.11	4E-02
PZP	2.65	1E-01	5.13	4E-03
SLCO1B2	2.24	3E-01	4.89	5E-02
TPM3	4.60	5E-02	4.85	4E-02
MYBBP1A	2.91	7E-02	4.25	1E-02
IGK-V19-17	2.57	2E-01	3.89	4E-02
SRPRB	2.02	2E-01	2.86	5E-02
HVM10	-0.08	9E-01	1.78	2E-02
NCL	0.98	5E-03	1.63	5E-05
DDX21	1.13	7E-02	1.60	1E-02
C1QA	0.62	2E-01	1.59	2E-03
KV6A4	0.69	2E-01	1.35	1E-02
FMO1	0.62	2E-01	1.22	2E-02
COX4I1	0.14	8E-01	1.22	4E-02
NDUFS5	0.88	1E-01	1.20	4E-02
CAPZA2	0.88	2E-02	1.16	2E-03
FARSB	0.77	4E-02	1.11	5E-03
CYP2C37	0.79	1E-01	1.07	5E-02

B Top 10 Common nucleoplasmic and nucleolar interactors

ZT8					
Nucleoplasmic			Nucleolar		
Protein	Log_2 (Fold change)	p-value	Protein	Log_2 (Fold change)	p-value
LRCH3	9.68	5E-20	LRCH3	9.74	5E-20
ABHD16A	9.41	9E-09	ABHD16A	9.72	5E-09
BMAL1	12.07	5E-08	BMAL1	12.73	2E-08
RAB3IP	12.77	8E-07	ATP5SL	14.61	5E-07
ATP5SL	13.85	1E-06	RAB3IP	12.42	1E-06
LPL	9.72	2E-06	LPL	10.12	1E-06
PISD	6.98	2E-06	ILKAP	8.33	1E-05
ILKAP	8.29	1E-05	CLOCK	10.12	1E-05
CLOCK	9.60	2E-05	ASGR2	8.95	5E-04
ASGR2	9.42	3E-04	PIGX	10.01	6E-04

ZT20					
Nucleoplasmic			Nucleolar		
Protein	Log_2 (Fold change)	p-value	Protein	Log_2 (Fold change)	p-value
LRCH3	9.17	1E-19	LRCH3	9.59	6E-20
ABHD16A	9.37	9E-09	ABHD16A	9.95	4E-09
BMAL1	11.56	9E-08	BMAL1	12.09	5E-08
ATP5SL	14.05	8E-07	ATP5SL	14.62	5E-07
RAB3IP	12.66	9E-07	RAB3IP	12.45	1E-06
LPL	9.72	2E-06	LPL	9.51	3E-06
CLOCK	9.13	4E-05	ILKAP	8.74	6E-06
ASGR2	10.31	1E-04	CLOCK	9.47	3E-05
NDUFA1	9.20	3E-02	ASGR2	9.86	2E-04
TRY4	8.60	3E-02	TRY4	8.91	2E-02

C

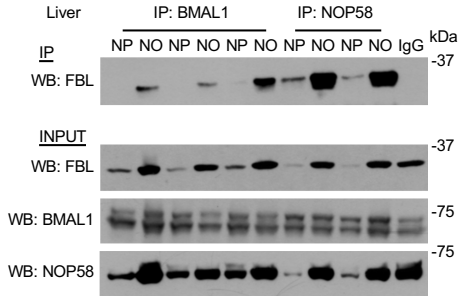

D

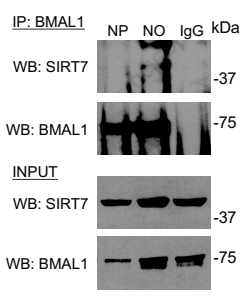

Figure 2.S5 Endogenous BMAL1 nucleoplasmic and nucleolar associations

A. All BMAL1 interactors identified at ZT8, ZT20 or both, listed with p-value and Log_2 (Fold change) of the comparison between nucleolar and IgG. **B.** Top 10 common BMAL1 interactors in nucleoplasmic and nucleolar fractions at ZT8 and ZT20, listed with p-value and Log_2 (Fold change) of the comparison between nucleoplasmic or nucleolar and IgG. BMAL1 and CLOCK are highlighted in gray. **C.** Endogenous co-immunoprecipitation experiments were performed in nucleoplasmic (NP) and nucleolar (NO) fractions prepared from WT mouse livers. Immunoprecipitation (IP) was performed using BMAL1, NOP58 or Rabbit IgG followed by Western blot (WB) analyses of BMAL1, FBL, and NOP58 as specified. **D.** Endogenous co-immunoprecipitation experiments were performed in nucleoplasmic (NP) and nucleolar (NO) fractions prepared from WT mouse livers. Immunoprecipitation (IP) was performed using BMAL1 or Rabbit IgG followed by Western blot (WB) analyses of BMAL1 and SIRT7 as specified.

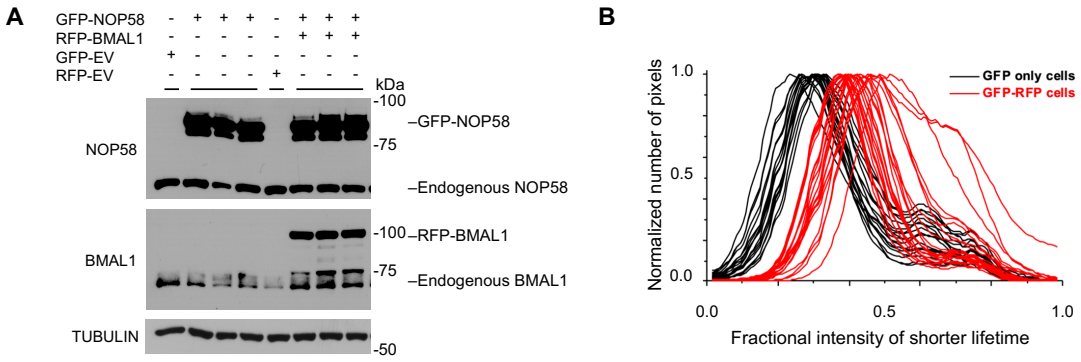

Figure 2.S6 Intranuclear BMAL1-NOP58 interaction

A. Western blot analyses of HEK293T cells transfected with GFP-NOP58, RFP-BMAL1, or the respective empty vectors (EV) as indicated, showing the levels of exogenous GFP- or RFP-tagged proteins compared the respective endogenous protein. TUBULIN was used as a loading control. **B.** Histogram (individual cells plotted) showing the number of pixels plotted against fractional intensity of the shorter lifetime in GFP-NOP58 only (black) and GFP-NOP58:RFP-BMAL1 (red) cells.

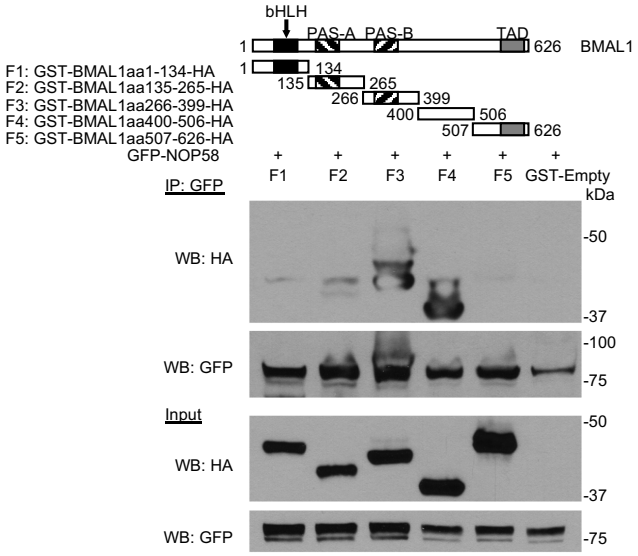

Figure 2.S7 BMAL1 PER-ARNT-SIM (PAS) domain is not required for NOP58 association

Schematic representation of BMAL1 showing the positions of the basic helix–loop–helix (bHLH), PER-ARNT-SIM (PAS)-A, PAS-B, and transactivation domain (TAD). GST-fused BMAL1-HA-tagged fragments are labeled as F1-F5 and are depicted with the range of amino acids (aa) for each peptide fragment. *in vitro* co-immunoprecipitation analyses were performed in whole cell extracts prepared from HEK293T cells co-transfected with GFP-NOP58 and incubated with GST-fused BMAL1 HA-tagged fragments or the GST-empty vector as indicated. Immunoprecipitation (IP) was performed using GFP followed by Western blot (WB) analyses of HA and GFP as specified.

Chapter 3

Cocaine-mediated circadian reprogramming in the striatum through dopamine-driven PPARγ activation

Karen Brami-Cherrier*, Robert G. Lewis*, Marlene Cervantes*, Yu Liu, Paola Tognini, Pierre Baldi, Paolo Sassone-Corsi** and Emiliana Borrelli**

*Equal contribution, **Co-corresponding

ABSTRACT

Substance abuse disorders are linked to alteration of circadian rhythms, although the molecular and neuronal pathways implicated have not been fully elucidated. Addictive drugs, such as cocaine, induce a rapid increase of dopamine levels in the brain. Here we show that acute administration of cocaine triggers reprogramming in circadian gene expression in the striatum, an area involved in psychomotor and rewarding effects of drugs. This process

involves the activation of peroxisome protein activator receptor gamma (PPARγ), a nuclear receptor involved in inflammatory responses. PPARγ reprogramming is altered in mice with cell-specific ablation of the dopamine D2 receptor (D2R) in the striatal medium spiny neurons (MSNs) (iMSN-D2RKO). Administration of a specific PPARγ agonist in iMSN-D2RKO mice elicits substantial rescue of cocaine-dependent control of circadian genes. These findings have potential implications for development of strategies to treat substance abuse disorders.

INTRODUCTION

A large variety of fundamental biological processes, ranging from the sleep-wake cycle and metabolism, to immune responses and behavior, is regulated by the circadian clock (Green et al., 2008; Scheiermann et al., 2013). In mammals, the central clock is located in the suprachiasmatic nucleus (SCN) within the hypothalamus that is entrained by light as an external *zeitgeber* (time-giver) (Welsh et al., 2010). As master regulator of organismal circadian rhythms, the SCN is thought to orchestrate the phase of oscillation of extra-SCN clocks (Albrecht, 2012). Peripheral clocks are present in virtually all organs and cells within the body and recent findings have revealed that clocks communicate in order to achieve systemic homeostasis (Bass and Lazar, 2016; Dyar et al., 2018). Diverse environmental cues, such as feeding behavior, also act as robust *zeitgebers* for peripheral clocks in metabolic tissues through mechanisms that appear SCN-independent(Asher and Sassone-Corsi, 2015; Panda, 2016). From a molecular standpoint, the circadian clock drives oscillations in expression of a large number of genes through transcriptional-translational feedback loops composed of cycling activators and inhibitors (Partch et al., 2014).

Drugs of abuse have been shown to induce severe perturbation of circadian rhythms (Gallardo et al., 2014; Iijima et al., 2002; Mohawk et al., 2012), such as disruption of the sleep/wake cycle, eating habits, blood pressure, hormone secretion and body temperature (Hasler et al., 2012; Logan et al., 2014). Importantly, desynchronization of circadian rhythms has been linked to the switch from recreational consumption to addictive behavior (Korpi et al., 2015). Cocaine, as well as other psychoactive drugs, affects the function of brain circuits such as the basal ganglia by increasing neurotransmitter release to the medium spiny neurons (MSNs), which are the principle striatal neurons and the striatum's only output neurons. This is the case for cocaine-mediated activation of dopamine (DA) signaling in MSNs that leads to long-term adaptations of cellular programs and behavioral responses(Di Chiara and Bassareo, 2007; Girault, 2012). Importantly, there are indications that DA signaling impacts central and peripheral circadian rhythms (Logan et al., 2019; McClung et al., 2005). In the striatum, DA levels oscillate in a circadian manner (Castaneda et al., 2004; Ferris et al., 2014) and are involved in the regulation of the neuronal circadian clock gene expression (Hood et al., 2010; Imbesi et al., 2009). To date, however, characterization of the molecular mechanisms by which drugs of abuse alter circadian rhythms in a tissue-specific manner remains incomplete.

Under physiological conditions, the endogenous clocks coordinate transcriptional and metabolic cycles in distinct organs(Asher and Sassone-Corsi, 2015; Panda, 2016). The capacity of peripheral clocks to be highly flexible through transcriptional and metabolic reprogramming is highlighted by experiments involving nutritional challenges such as fasting, high fat diet, ketogenic diet or caloric restriction(Brown, 2016; Challet, 2019; Ribas-Latre and Eckel-Mahan, 2016). It is unclear whether neuronal clocks are capable of similar

reprogramming. We hypothesized that the short and long-term adaptation of neuronal circuits in response to cocaine would involve changes in circadian rhythmicity within the ventral striatum and in particular the Nucleus Accumbens (NAcc).

Our recent findings show that D2R-mediated signaling in MSNs critically modulates striatal responses to cocaine(Kharkwal et al., 2016; Radl et al., 2018). These results indicate that D2R signaling plays a critical role in the mechanisms by which drugs of abuse affect striatal physiological responses. Thus, we explored how the circadian program of striatal neurons is influenced by acute administration of cocaine in WT mice and in mutants with D2R ablation exclusively in D2R-expressing MSNs (iMSN-D2RKO mice)(Anzalone et al., 2012; Kharkwal et al., 2016). Our results show that cocaine induces a drastic reprogramming of the diurnal transcriptome in the NAcc. There is a remarkable difference in the number, type and cycling profiles of cocaine-driven oscillatory genes in iMSN-D2RKO mice. Using combined metabolomic and transcriptomic approaches, we show that D2R in iMSNs contributes to cocaine-induced activation of peroxisome protein activator receptor gamma (PPARγ), a nuclear receptor implicated in inflammatory responses(Khan et al., 2019; Kliewer et al., 1994). PPARγ drives a significant fraction of *de novo* cocaine-induced transcriptional response, which is impaired in the absence of D2R signaling in iMSNs. Pharmacological activation of PPARγ by pioglitazone(Lee et al., 2003) in iMSN-D2RKO mice leads to restoration of the cocaine-induced profile of circadian gene expression. Our findings unveil a D2R signaling- PPARγ connection in circadian regulation linked to cocaine-mediated rewiring in striatal neurons.

RESULTS

Response of core clock genes to cocaine in both WT and iMSN-D2RKO mice

We previously reported that iMSN-D2RKO mice display reduced motor activity in basal conditions(Anzalone et al., 2012) and absence of cocaine-induced hyperlocomotion(Kharkwal et al., 2016). We sought to study the effects of cocaine in WT and iMSN-D2RKO mice by analyzing circadian motor activity along the daily cycle, four days before and four days after acute cocaine administration (Figure 3.1a and Figure 3.1b). Circadian motor activity was quantified as infrared beam breaks per minute at each circadian time in mice housed in home cages. Interestingly, acute cocaine does not affect the diurnal pattern of locomotor activity either in WT or iMSN-D2RKO mice, indicating that D2R deletion in iMSNs does not alter the physiology and function of the SCN central clock (Figure 3.1c). Nevertheless, circadian motor activity of iMSN-D2RKO mice was decreased with respect to WT mice in the active phase before ($p<0.0001$) and after ($p=0.0004$) cocaine administration (Figure 3.1d and Figure 3.1e), consistent with results obtained in non-circadian behavioral settings(Anzalone et al., 2012; Dobbs et al., 2016; Kharkwal et al., 2016). To determine the effect of cocaine challenge on the striatal expression of clock genes, WT and iMSN-D2RKO mice received an intraperitoneal (i.p.) injection of either cocaine (Coc 20 mg kg^{-1}) or saline (Sal), shortly after the beginning of the resting phase (zeitgeber time, ZT3). Animals from both groups were sacrificed every 4 hours (n=5 or 6/time point) and tissue punches from the NAcc collected at six time points to cover the full circadian cycle (Figure 3.1f). To investigate the direct effect of cocaine in the NAcc of WT and iMSN-D2RKO mice on the core-clock machinery, we analyzed the expression of *Bmal1, Cry1, Dbp* and *Per1* in saline and cocaine-treated mice (Figure 3.1g). We observed a significant effect of time for all tested

core-clock genes (p≤0.0005), indicating that expression of all genes follows the typical circadian cycle in both genotypes. There was no substantial alteration in the expression profiles of these clock genes upon cocaine treatment (*Bmal1*: p=0.7389; *Cry1*: p=0.7529; *Per1*: p=0.6765), as well as a clock output gene, as exemplified by *Dbp* expression profile (p=0.1495) (see Table 3.S1). A slight but nevertheless significant difference was found in *Per1* expression level between WT and iMSND2RKO mice (p=0.0022). Thus, acute cocaine treatment, whether in the presence or absence of D2R in iMSNs, does not alter the rhythmic expression of this group of circadian genes.

Reprogramming of the striatal circadian transcriptome by cocaine

Cocaine intake induces an increase of DA accumulation in the synaptic cleft through blockade of the DA transporter prolonging activation of postsynaptic neurons(Beuming et al., 2008; Nestler, 2005). The dopaminergic mesolimbic pathway connecting the ventral tegmental area to the NAcc and cortex is critically involved in the effects of drugs of abuse(Luscher and Malenka, 2011).

To analyze the acute cocaine-dependent genome-wide rhythmicity, RNAs were extracted from NAcc punches from brains harvested every four hours throughout a full circadian cycle (Figure 3.1f) and processed for RNA-seq analyses. Rhythmic transcripts were identified using the non-parametric test JTK_CYCLE(Hughes et al., 2010), an algorithm that includes Bonferroni-adjusted multiple comparisons and incorporates a window of 20-28 hours for the determination of diurnal periodicity. Out of a combined 2314 cycling transcripts identified, 1157 (50%) were rhythmic only in the saline condition. An additional 294 (~13%) were cycling in both saline- and cocaine-treated mice and, notably, 863 (~37%)

de novo oscillating transcripts were identified upon cocaine challenge (Figure 3.2a). The phases of oscillation of genes diurnal in both conditions were similar (Figure 3.2b and Figure 3.2c). The newly cocaine-induced oscillating transcripts display a peak at around ZT7, which is absent in saline condition. Moreover, 13% of the common oscillating genes showed a decrease in amplitude, while 35% displayed an increase upon cocaine treatment with respect to saline conditions (Figure 3.2d). Thus, the circadian program of cycling genes in the NAcc is profoundly modified upon acute cocaine administration.

Pathway analyses were performed using Database for Annotation, Visualization and Integrated Discovery (DAVID) (Figure 3.2e) and Reactome (Figure 3.S1a-c). Both approaches identified analogous pathways in the common rhythmic transcripts between saline- and cocaine-treated NAcc. Gene Ontology (GO) annotation revealed clusters in the protein folding and rhythmic process pathways in both treatments. The saline-only specific circadian transcripts were enriched in RNA splicing, cell projection, and protein monoubiquitination pathways. Conversely, the cocaine-only specific transcripts were highly enriched in the transmembrane transport, ER to Golgi vesicle mediated transport and cell projection pathways (see Figure 3.2e and Figure 3.S1a and Figure 3.S1b). These results highlight the effect of a single, acute cocaine challenge on circadian function in the NAcc.

Cocaine-driven circadian reprogramming is dependent on D2 receptors

Both D1R- and D2R-mediated signaling play a fundamental role in the psychomotor and rewarding properties of cocaine(Vallone et al., 2000). Importantly, mice carrying selective ablation of D2R in the iMSNs display impaired cellular and motor response to acute cocaine administration(Kharkwal et al., 2016). To determine the role of D2R-mediated signaling in

the regulation of circadian gene oscillation in the NAcc, iMSN-D2RKO mice were treated with saline or cocaine (as shown in Figure 3.1f), as previously described for their WT counterparts. RNA-seq analyses along the circadian cycle showed a substantial difference in the number of oscillatory genes as compared to WT mice in the saline condition (Figure 3.3a). Indeed, we observed a drastic decrease in the number of genes oscillating in iMSN-D2RKO mice (359 transcripts) as compared to the same condition in WT mice (1399 transcripts); 53 oscillating genes were common to both genotypes (Figure 3.3a). The phase of the overlapping genes was similar in both genotypes (Figure 3.S2a and Figure 3S.2b) with a higher percentage of genes with greater amplitude in iMSN-D2RKO mice (Figure 3.S2c). Moreover, transcripts exclusively diurnal in iMSN-D2RKO had phase distributions at approximately ZT4 and ZT16 (Figure 3.3b and Figure 3.3c). Genes oscillating only in iMSN-D2RKO mice clustered in GO annotations including transmembrane transport and steroid metabolic process (Figure 3.3d and Figure 3.S2d and Figure 3.S2e). It is relevant that annotation analyses of genes oscillating in both WT and iMSN-D2RKO mice include classic terms required for normal neuronal function (Figure 3.S2f and Figure 3.S2g).

Acute cocaine treatment revealed a unique circadian signature in the NAcc of iMSN-D2RKO mice. Notably, a total of 1131 cycling genes were found in the cocaine-treated WT. Of these, 25 were common to iMSN-D2RKO mice. An additional 171 genes were rhythmic in iMSN-D2RKO mice only (Figure 3.3e). Phase distribution analyses also revealed unique features of cocaine-induced reprogramming of circadian gene expression in WT and iMSN-D2RKO mice. Notably, a unique phase distribution peak observed at ~ZT18 in WT mice was almost completely absent in iMSN-D2RKO mice (Figure 3.3f and Figure 3.3g). On the other hand, genes oscillating in both conditions display a peak at ZT6-ZT8 (Figure 3.S3a and Figure

3.S3b) and maintain similar amplitudes (Figure 3.S3c). GO term analyses revealed unique pathways enriched in WT vs iMSN-D2RKO mice (Figure 3.3h and Figure 3.S3d and Figure 3.S3e), such as protein folding, transport, cell projection in WT, and transcription, negative regulation of apoptotic process, positive regulation of cytosolic Ca^{2+} concentration in iMSN-D2RKO. Moreover, GO annotation analyses showed a common enrichment of genes that belong to the circadian regulation of gene expression in both genotypes (Figure 3.S3f and Figure 3.S3g). Taken together our results demonstrate that D2R signaling in iMSNs is critical for basal and cocaine-driven circadian oscillations in the NAcc.

Cocaine-induced circadian response of PPARγ-target genes

To explore the molecular mechanisms by which cocaine induces *de novo* oscillations of striatal genes, we used MotifMap(Daily et al., 2011) to identify transcription factor binding motifs selectively represented in rhythmic genes under saline conditions and after cocaine challenge. A profound reorganization in transcription factor pathway usage was observed upon cocaine challenge, with a significant enrichment of genes containing PPARγ binding sites for genes oscillating in WT mice (Figure 3.4a). Indeed, 372 out of 863 cocaine-induced newly oscillating genes are PPARγ targets (Figure 3.2a and Figure 3.4b-c). Importantly, cocaine-induced enrichment of PPARγ binding sites is not observed in the iMSN-D2RKO cocaine-treated mice. Thus, ablation of D2R from iMSNs significantly reduces the cocaine-induced PPARγ oscillatory program observed in WT mice (Figure 3.4b). Among the cocaine-induced PPARγ target genes, none were common oscillators in both genotypes. The significant fraction of *de novo* cycling PPARγ target genes induced by the first exposure to cocaine in WT mice, prompted us to further explore the involvement of this nuclear factor.

Phase oscillation analyses of PPARγ cycling targets revealed a specific phase distribution in cocaine treated WT mice at ZT6-ZT8 and ZT18 (Figure 3.4d). GO biological process analyses of the PPARγ-target genes in WT cocaine-treated mice revealed transport, translation initiation, positive regulation of apoptotic process, and transcription as key annotations (Figure 3.4e and Figure 3.S4a). Taken together, our data underscore the involvement of PPARγ signaling pathway in cocaine-induced transcriptional reprogramming of the NAcc clock. This unique cocaine-induced transcriptional feature is absent in mice with ablation of D2R from iMSNs.

D2R-driven PPARγ nuclear enrichment upon cocaine

PPARγ localizes in the cytoplasm and upon activation translocates to the nucleus to activate transcription of specific genes(Mangelsdorf et al., 1995). We performed immunofluorescence analyses using a nuclear-specific PPARγ antibody to quantify the induction of nuclear PPARγ staining in the NAcc of WT and iMSN-D2RKO mice upon cocaine treatment. For this purpose, mice of both genotypes were administered either saline or cocaine (20 mg kg^{-1}) at ZT3 and sacrificed at ZT7. A diffuse nuclear PPARγ staining was observed in NAcc neurons in saline conditions in both genotypes (Figure 3.5a). After cocaine we observed a significant increase in nuclear PPARγ staining in WT NAcc neurons, which was absent in iMSN-D2RKO mice. Quantification of PPARγ nuclear intensity per cell, as well as of the number of cells with nuclear PPARγ staining, shows a statistically significant increase of nuclear PPARγ localization upon cocaine in WT as compared to iMSN-D2RKO NAcc neurons (Figure 3.5b, p=0.0030; Figure 3.5c, p=0.0124). To establish the identity of the MSNs

showing the heightened intensity of PPARγ nuclear staining, we performed *in-situ* hybridization coupled to immunohistochemistry using probes specific for the two subtypes of MSNs. This allowed for the unambiguous identification of D2R-expressing iMSNs from D1R-expressing dMSNs. Double *in-situ* hybridization/immunohistochemistry analyses were performed using riboprobes for *enkephalin* (Enk)(Baik et al., 1995), an iMSNs specific marker or the dopamine D1 receptor (*D1R)*, a dMSN specific marker, together with the specific PPARγ antibody. These experiments demonstrated that the cocaine-driven increase in PPARγ nuclear staining occurs in iMSNs ($p=0.0030$) and not in dMSNs ($p=0.9991$) (Figure 3.5d and Figure 3.5e). Importantly, the increase of PPARγ in iMSNs nuclei after cocaine was not observed in the NAcc of iMSN-D2RKO mice ($p=0.8693$) (Figure 3.5d and Figure 3.5e). These results point to a cocaine-mediated D2R-dependent activation of PPARγ.

Lack of PPARγ activation and function in iMSN-D2RKO mice

To ascertain whether the metabolic consequences of acute cocaine treatment may be linked to PPARγ activation, we performed mass-spectrometry (MS) metabolomics analyses from isolated NAcc at ZT7 after either saline or cocaine (20 mg kg^{-1}; i.p.) administration at ZT3. We identified a significant effect of cocaine on lipid metabolism (Figure 3.6a). Among 180 metabolites analyzed, 145 were lipids including: phospholipids, acylcarnitines and sphingolipids. In WT, but not in iMSN-D2RKO mice, phosphatidylcholine levels were significantly decreased after cocaine treatment while most lysophosphatidylcholines increased. D2R activation is involved in the conversion of phosphatidylcholine into lysophosphatidylcholine and arachidonic acid (AA)(Kanterman et al., 1991; Neve et al., 2004), the latter being a precursor of prostaglandins(Kuehl and Egan, 1980; Piomelli et al.,

1991). Importantly, prostaglandins are well-characterized PPARγ natural ligands(Nosjean and Boutin, 2002). Interestingly, AA release in the striatum is regulated by D1R and D2R in an opposite manner (Piomelli et al., 1991; Schinelli et al., 1994); D1R signaling inhibits while D2R signaling increases AA release. Based on these findings, we reasoned that the efficient turnover of phosphatidylcholine levels in response to cocaine would be dampened in mice with D2R ablation in iMSNs. We thereby analyzed the levels of the PGJ2-type prostaglandin (15-deoxy-$\Delta^{12,14}$-PGJ2)(Scher and Pillinger, 2005), a prostaglandin that specifically binds and activates PPARγ (Forman et al., 1995), in the NAcc of WT and iMSN-D2RKO mice. Indeed, we observed that in response to cocaine, there is a significantly lower level of 15-deoxy-$\Delta^{12,14}$-PGJ2 in the NAcc of iMSN-D2RKO mice as compared to saline treated mice ($p=0.0153$) (Figure 3.6b). In contrast, WT mice show no significant change in 15-deoxy-$\Delta^{12,14}$-PGJ2 levels after cocaine treatment, a response that mirrors results obtained in human cocaine users(Samikkannu et al., 2014). These findings point to D2R signaling as a key player in the cocaine-driven prostaglandin production involved in PPARγ activation.

We next assessed the downstream effects of PPARγ activation by analyzing the expression of specific genes from the list of PPARγ circadian putative targets (Figure 3.4c). Among these genes, *Adora2a* (Adenosine A2a Receptor), *Kcnd1* (Potassium Voltage-Gated Channel Subfamily D Member 1), and *Gabrδ* (Gamma-Aminobutyric Acid Type A Receptor Delta Subunit) are not oscillatory under normal conditions in WT mice (Figure 3.6c). However, upon cocaine treatment, their expression displayed *de novo* oscillatory profiles. In contrast, in cocaine treated iMSN-D2RKO mice, these genes were not cyclically expressed, their circadian expression parallels that of saline-control mice (Figure 3.6c). Next, we analyzed the molecular mechanism of control at the promoter level by chromatin

immunoprecipitation assays (ChIP) using NAcc nuclear extracts from both WT and iMSN-D2RKO cocaine-treated mice harvested at ZT7. Using PPARγ nuclear-specific antibodies, we show that PPARγ chromatin recruitment to *Adora2a* and *Kcnd1* promoters was significantly reduced in iMSN-D2RKO animals as compared to WT (Figure 3.6d) (*Adora2a:* p=0.0361 and *Kcnd1*: p=0.0252). An analogous trend was observed for the *Gabrδ* promoter (p=0.1549). These results support a scenario in which PPARγ activation by cocaine leads to the *de novo* program of D2R signaling-dependent circadian genes in the NAcc.

Rescue of PPARγ function using the specific agonist pioglitazone

To validate the critical role played by PPARγ in D2R signaling-dependent circadian reprogramming upon cocaine, WT and iMSN-D2RKO mice were subjected to oral gavage with pioglitazone, a specific PPARγ activator(Swanson et al., 2011) that crosses the blood brain barrier(Kiyota et al., 1997). Pioglitazone or vehicle, were administered at ZT1, 2 hours before the acute cocaine injection (Figure 3.7a). Expression of the *Adora2a*, *Kcnd1* and *Gabrδ* genes was analyzed at ZT7 and at ZT19 (Figure 3.7b). Pioglitazone treatment before cocaine reestablished the induction of *Adora2a* (p=0.0388), *Kcnd1* (p<0.0001), and *Gabrδ* (p=0.0019) gene expression in iMSN-D2RKO mice at ZT7, which nicely paralleled WT expression levels (Figure 3.7b). Thus, PPARγ activation operates as a direct link between cocaine, D2R-signaling(Kanterman et al., 1991; Neve et al., 2004) and downstream gene expression (Figure 3.7c). These results identify PPARγ as a critical factor that intervenes in the transcriptional reprogramming of the striatal clock upon acute cocaine treatment.

DISCUSSION

Drugs of abuse, such as cocaine, are known to alter human physiology and circadian rhythms(Hasler et al., 2012). While relevant information about the molecular mechanisms by which cocaine affects short or long-term neuronal plasticity has been accumulated(Luscher and Bellone, 2008), little is known about how it interplays with the circadian system. Deciphering how cocaine alters circadian regulation may provide critical knowledge to design strategies aimed at mitigating the daily dysfunctions of drug addicts. Previous studies have addressed this question through the analysis of chronically treated WT mice(Ozburn et al., 2017) or mutant mice for specific clock genes(Abarca et al., 2002; Brager et al., 2013; Iijima et al., 2002; McClung et al., 2005). In this study, we first sought to decipher how a single acute cocaine treatment affects genome-wide circadian oscillations within the NAcc, and secondly to dissect the D2R-mediated signaling pathways in striatal neurons. For this purpose, we exploited mouse models in which genetic ablation of D2R is targeted uniquely to striatal iMSNs. We demonstrate that cocaine generates a profound reprogramming of circadian gene expression and identified PPARγ as one critical player that elicits the acute effects of cocaine through D2R-mediated signaling.

D2R is essential for the psychomotor and rewarding effects of psychoactive drugs such as cocaine(Caine et al., 2002; Kharkwal et al., 2016; Welter et al., 2007). Indeed, constitutive D2R knockout mice self-administer higher amounts of cocaine as compared to WT littermates(Caine et al., 2002). Importantly, lower striatal D2R levels have been observed in cocaine abusers as well as in rodent models(Czoty et al., 2010; Nader et al., 2006; Volkow et al., 2001). Thus, ablation of D2R from the main striatal population, as achieved in iMSN-D2RKO mice, represents an ideal model to study the mechanisms by which cocaine affects

striatal signaling and circuitry. Previous studies revealed the importance of D2R for intrastriatal connections (i.e. collaterals between iMSN and dMSN) necessary for the psychomotor effects of cocaine(Anzalone et al., 2012; Dobbs et al., 2016; Kharkwal et al., 2016; Lewis et al., 2020).

Our findings place D2R in a central position in the modulation of circadian rhythmicity in the striatum. Indeed, D2R ablation in iMSNs leads to a significant reduction in the number of oscillating genes in the NAcc. Our data reinforce emerging evidence suggesting that cocaine-mediated increase of dopamine is involved in maintaining circadian rhythms in brain areas including the retina, olfactory bulb, striatum, midbrain and hypothalamus(Korshunov et al., 2017). Remarkably, cocaine administration is significantly less effective on circadian reprogramming in the absence of D2R.

Previous reports have indicated that D2R-mediated signaling modulates *Clock* and *Per2* gene expression(Hood et al., 2010; Imbesi et al., 2009). Our results show that D2R also modulates *Per1* expression (Supplementary Table 1). Cocaine treatment does not lead to major alterations in the circadian oscillation of the core clock genes *Bmal1, Cry1* and *Dbp* in striatal neurons. On the other hand, we observe induction of newly oscillatory genes. This is remarkable when considering the extensive changes in circadian gene expression observed between WT and iMSN-D2RKO mice. Altogether these observations point to a D2R signaling-driven cocaine-induced reprogramming of the NAcc. Our study allows the identification of PPARγ as a key mediator of cocaine-induced rhythmic transcriptional reprogramming.

While originally characterized for its role in adipogenesis and glucose metabolism, PPARγ has been recently linked to neurological disorders such as neurodegeneration and neuro-inflammation(Chaturvedi and Beal, 2008; Jiang et al., 2008). Importantly, we have

demonstrated that D2R ablation prevents cocaine-driven PPARγ activation and the consequent *de novo* oscillation of PPARγ target genes. Dependence on D2R can be circumvented by the administration of the specific PPARγ agonist pioglitazone. Our results support recent findings suggesting the involvement of PPARγ in cocaine use disorder. Indeed, pioglitazone treatment during abstinence has a positive effect on cocaine addiction by reducing cocaine self-administration(Miller et al., 2018). GO analyses of the cocaine treated WT and iMSN-D2RKO NAcc transcriptomes shows that the most significant annotation in iMSN-D2RKO is transcription factors which is absent in WT mice. This notion supports a modulatory role of D2R signaling in NAcc-dependent molecular responses to cocaine. Thus, while dMSNs have been critically involved in cocaine-mediated responses(Bateup et al., 2008; Cates et al., 2019; Hikida et al., 2010; Kelz et al., 1999; Parekh et al., 2019; Zhang et al., 2006), the modulatory role of D2R signaling needs to be further highlighted. Along these lines, it is tempting to speculate that alteration of cocaine-induced circadian reprogramming in absence of D2R might also occur in cocaine abusers where the levels of D2R are dampened(Volkow et al., 2001). Notably, the full D2R knockout mice show heightened intake of cocaine as measured in cocaine self-administration studies(Caine et al., 2002). Since the iMSN-D2RKO mice show multiple features of the full D2R knockout mice, it is tempting to speculate that they might also self-administer higher amounts of cocaine. Future studies will address this question.

Our findings reveal the fundamental role of D2R in circadian physiology of the brain's reward system. D2R signaling plays a crucial role in the reprogramming of diurnal transcription driven by acute cocaine in the NAcc. Unsuspected to date, D2R-mediated signaling triggers a regulatory circuit that leads to PPARγ activation. This response underlies

the cyclic activation of a large number of *de novo* oscillatory genes. These results well exemplify the complexity underlying the effects of cocaine in the brain by adding a member of the nuclear receptor family to the molecular circuitry previously implicated in the response to cocaine(Chandra and Lobo, 2017; Everitt and Robbins, 2013; Lobo and Nestler, 2011; Walker et al., 2018; Yager et al., 2015). Finally, the identification of the PPARγ pathway as a mediator of D2R signaling represents an important promising target for the clinical treatment of drug addiction.

METHODS

Animals

iMSN-D2RKO mice were generated by mating $D2R^{flox/flox}$ mice with $D2R^{flox/flox/D1R\text{-}CRE+/-}$ mice(Anzalone et al., 2012). In $D2R^{flox/flox/D1R\text{-}CRE+/-}$ mice, the DA D1R promoter drives the CRE recombinase. The ability of this CRE to eliminate D2R in iMSNs(Anzalone et al., 2012) resides in the common expression of D1R and D2R in embryonic MSN precursors(Aizman et al., 2000). Absence of D2R from iMSNs was previously shown by binding analyses on striatal extracts using a D2R-specific 3H-labeled ligand, as well as by double *in-situ* hybridization experiments using GAT1 as marker of MSNs and D2R exon 2 specific probes(Anzalone et al., 2012).

Mice were maintained on a standard 12h light/ 12h dark cycle; food and water were available *ad libitum* in ~25ºC and 40-60% humidity. Animals' care and use was in accordance with guidelines of the Institutional Animal Care and Use Committee at the University of California, Irvine. Genotype identification was performed by Southern blot and PCR analyses of DNA extracted from tails biopsies.

Drugs

Before pharmacological treatments, mice were handled for at least 3 days for 5 min. On the day of the test, mice were habituated to the novel home cage for 2 hours and then administered either cocaine or saline. Cocaine (Sigma Cat. #C5776) was dissolved in saline (NaCl 0.9%) and injected intraperitoneally (i.p.) at the dose of 20 mg kg^{-1}. Pioglitazone (Cayman Chemical Cat. # 71745) was dissolved in DMSO to have a stock solution of 10 mg mL^{-1}. Pioglitazone solution was diluted 1:1 in PBS and administered 2 hours prior to either cocaine or saline injection by oral gavage at a dose of 60 mg kg^{-1}.

Locomotor activity analysis

Activity was measured on individually housed mice n=4-5/group for 11 days using Actimetrics optical beam motion detection (Philips Respironics). Data was collected using Minimitter Vital View v5.0 data acquisition software and analyzed through Matlab R2013a v9.7.0.1296695 software and Clocklab software v2.72.

Quantitative RT–PCR

Striatum samples were homogenized in TRIzol lysis reagent (Thermo Fisher) following manufacturer's instructions. Total RNA was reverse-transcribed using iScript Reverse Transcription Supermix (Biorad Cat. N. 1708840). Gene expression was analyzed by Real-Time PCR (BIO-RAD Real-Time System; BIO-RAD CFX Manager Software v3.1) using SsoAdvanced Universal SYBR Green Supermix (Biorad Cat. N. 172-5270). The sequences of the primers used for RT-PCR are Kcnd1 Forward: 5'-TCCGTTTGGCAAAGAGTGGT-3', Kcnd1 Reverse: 5'-AGCTCGTCTGTGAACTCGTG-3'; Gabrd Forward: 5'-GGCGCCAGGGCAATGAAT-3',

Gabrd Reverse: 5'-GTCAATGCTGGCCACCTCTA-3'; Adora2a Forward: 5'-TTCATCGCCTGCTTTGTCCT-3', Adora2a Reverse: 5'-AATGATGCCCTTCGCCTTCA-3'; Bmal1 Forward: 5'-GCAGTGCCACTGACTACCAAGA-3', Bmal1 Reverse: 5'-TCCTGGACATTGCATTGCAT-3'; Per1 Forward: 5'-ACCAGCGTGTCATGATGACATA-3', Per1 Reverse: 5'-GTGCACAGCACCCAGTTCCC-3'; Dbp Forward: 5'-AATGACCTTTGAACCTGATCCCGCT-3', Dbp Reverse: 5'-GCTCCAGTACTTCTCATCCTTCTGT-3'; Cry1 Forward: 5'-CAGACTCACTCACTCAAGCAAGG-3', Cry1 Reverse 5'-TCAGTTACTGCTCTGCCGCTGGAC-3'.

RNA-seq analysis

RNA library preparation and sequencing were performed at the UCI Genomics High-throughput Facility, University of California, Irvine. Briefly, total RNA was monitored for quality control using the Agilent Bioanalyzer Nano RNA chip and Nanodrop absorbance ratios for 260/280 nm and 260/230 nm. Library construction was performed according to the Illumina TruSeq® Stranded mRNA Sample Preparation Guide. The input quantity for total RNA was 700 ng and mRNA was enriched using oligo dT magnetic beads. The enriched mRNA was chemically fragmented for 3 minutes. First strand synthesis used random primers and reverse transcriptase to make cDNA. After second strand synthesis the ds cDNA was cleaned using AMPure XP beads and the cDNA was end repaired and then the 3' ends were adenylated. Illumina barcoded adapters were ligated on the ends and the adapter ligated fragments were enriched by nine cycles of PCR. The resulting libraries were validated by qPCR and sized by Agilent Bioanalyzer DNA high sensitivity chip. The concentrations for the libraries were normalized and then multiplexed together. The multiplexed libraries were

sequenced on four lanes using single end 100 cycles chemistry on the HiSeq 2500. The version of HiSeq control software was HCS 2.2.58 with real time analysis software, RTA v1.18.64. Sequence alignment was performed using TopHat v2.1.1 while assembly and expression estimation was done using Cufflinks v0.12.1(Trapnell et al., 2013). Reads were mapped to the mouse genome mm10 and expression values were estimated as FPKM.

DETAILS: FASTQ files were obtained from the sequencing facility and processed through the standard Tuxedo protocol(Trapnell et al., 2013). Reads were then aligned to the UCSC mm10 mouse reference genome using TopHat and Bowtie2 v2.3.4. Assembled transcripts were obtained via Cufflinks with the mm10 reference annotation file. Genome assembly was obtained using Cuffmerge and expression levels (summarized to genes) were calculated using Cuffquant and then normalized via Cuffnorm to FPKM values. For each condition, 24 hr time series data from six time points with three replicates each were collected. In total, expression levels of 24138 unique genes were considered for further analysis. Data was further split to pairwise time series format for comparative analysis (e.g. WT Saline vs WT Cocaine treatment, KO Saline vs KO Cocaine treatment etc).

Bioinformatics and pathway analysis

Bioinformatics analysis was performed on RNA-seq data using JTK_CYCLE(Hughes et al., 2010) v3.1 and pipelines for CircadiOmics (circadiomics.ics.uci.edu)(Patel et al., 2012). Pathway analysis was performed using DAVID(Huang da et al., 2009) and Reactome(Fabregat et al., 2017; Sidiropoulos et al., 2017) software.

Details: Statistical and bioinformatics analyses were performed based on pairwise comparisons, where the effect of cocaine treatment was analyzed while controlling the

genotype or the difference between genotypes (WT or KO) were compared while controlling the treatment. Dixon's test was performed on replicates of transcriptomic data to reduce outlier effects, filtering out up to 1 outlier replicate from each time point. For transcriptomic data, genes with consistently low expression values (FPKM < 1) were filtered out from further analysis to reduce noise. Time series data was then used to determine circadian behavior of genes using JTK_CYCLE, including the p-value for whether the time series is considered circadian, its periodicity (between 20-28 hrs), amplitude and phase. A gene is considered circadian if its JTK_CYCLE p-value passed the cutoff of 0.01. Heatmaps of circadian transcripts were generated using the R package gplots v3.0.3, where the values on each row were normalized and rows were sorted by the JTK_CYCLE phase.

The Database for Annotation, Visualization and Integrated Discovery (DAVID) pathway and Reactome analysis tools were used to identify enriched KEGG pathways for circadian genes in each condition. Pathways were ranked by the number of genes found annotated with the pathway information or with the negative natural log of p-values for enrichment, which behave similarly to z-scores where larger values indicate higher confidence.

Putative TFBS information from MotifMap(Daily et al., 2011) were used to determine the enriched TFs in each condition. Fisher's test was conducted comparing the relative abundance of binding sites in the promoter regions (-10000 bps to +2000 bps of transcription start site) of circadian genes in each condition, as opposed to the genomic background (defined as all 24138 genes from the RNA-seq data with FPKM > 0 at any time point). In addition, a filtering parameter of BBLS>1, FDR<0.25 was used to obtain high quality binding sites while TFs with motifs that are too short or degenerate (more than 50000 binding sites under the filtering criteria) were removed as they tend to be unreliable.

TFs were ranked by the negative log of their Fisher p-values. Enrichment results from different pairwise comparisons were also compared in a meta-analysis to identify condition-specific TFs, in particular PPARγ which was found to be exclusively enriched in WT-Cocaine condition.

PPARγ targeted genes were filtered using a combination of MotifMap data and ChIP-Seq data from GSE64458(Soccio et al., 2015). Binding sites were searched within a smaller promoter region of -3000 bps to +1000 bps of the TSS while filtering parameters for MotifMap were kept the same as mentioned above. Other visualization and statistical analyses were performed in R or in python using pandas and scikit-learn.

Metabolomics analysis

Metabolomic analyses were performed using p180 from the Biocrates facility (Innsbruck, Austria). Metabolite levels were measured at ZT7 after an intraperitoneal injection of saline or cocaine at a dose of 20 mg kg^{-1} at ZT3, 5 replicates each.

Statistical and bioinformatics analyses were performed based on pairwise comparisons, where the effect of cocaine treatment was analyzed while controlling the genotype or the difference between genotypes (WT or KO) were compared while controlling the treatment. Dixon's test was performed to reduce outlier effects, filtering out up to 1 outlier replicate from each condition. Heatmaps for the metabolite profiles were generated using the RStudio software. Row z-scores are displayed and were calculated using the 'heatmap.2' function of the gplots package.

Immunohistochemistry and fluorescent in situ hybridization analysis

Single immunostaining was performed on vibratome sections as described previously(Brami-Cherrier et al., 2005) using anti- PPARγ antibody (1:1000; Novus Biotechnologies Cat. #NB120-19481). Nuclei staining was obtained using Draq7 (Biostatus, Cat# DR70250). For quantifications, frames of 375x375 µm/image (n=4) were analyzed. ROIs were drawn around individual cells using LASX software v3.7.0 (Leica); mean gray values/cell were obtained and background subtracted. Double immunohistochemistry/in situ hybridization staining were obtained using striatal sections which were hybridized with digoxigenin (DIG)-Enkephalin or (DIG)-D1R riboprobes (RNA labeling mix; Roche, Cat# 11277073910)(Anzalone et al., 2012). After incubating the probe for overnight (ON) at 60°C, sections were washed with PBS (Phosphate Buffered Saline) 3 times (5min), permeabilized with Triton 0.3% in PBS (15 min), blocked with normal horse serum 5% for 1h and incubated ON with rabbit PPARγ antibody (1:1000) at 4°C. On day 3, after 3 washes in PBS, sections were incubated for 1h with an anti-rabbit Alexa488 (1:600, Life technologies) followed by an incubation for 1h with anti–DIG-AP (1:5000, Roche) antibody. To amplify the signal, the HNPP (2-hydroxy-3-naphtoic acid-2'-phenylanilide phosphate) fluorescent Detection Set (Roche) was used. Quantifications were performed on confocal images (SP5, Leica) of coronal striatal slices (3 slices/animal and 3 brains/genotype/condition) using LASX v3.7.0. The number of MSNs showing the induction of PPARγ was quantified in frames of 246x246 µm/image (n=3); iMSNs were defined as the number of PPARγ$^+$ and Enkephalin$^+$ cells while dMSNs as PPARγ$^+$ and D1R$^+$ colocalizing cells.

Chromatin immunoprecipitation

Chromatin immunoprecipitation (ChIP) procedure was performed(Murakami et al., 2016). Punches of striatum from frozen brains of two mice were pooled. Tissue was minced and double crosslinked with DSG for 20 min and 1% formaldehyde for 10 min followed by adding glycine (0.125 M final concentration) at room temperature for 10 min. After homogenizing tissue pellets in PBS, 1 ml of lysis buffer was added. Samples were sonicated (20 cycles, every cycle: 30 sec ON / 30 sec OFF, power high) to generate 200-500 base pairs fragments and centrifuged at 14000g at 4^{o}C. Supernatants were diluted in a dilution buffer (1.1% Triton X100, 1.2 mM EDTA, 16.7 mM Tris-HCl, 167 mM NaCl). The diluted chromatin was incubated with 2 mg of anti- PPARγ antibody (Abcam Cat. # ab41928), overnight at 4^{o}C. To monitor the specificity of ChIP assays, samples were also immunoprecipitated with a specific-antibody isotype matched control immunoglobulin (IgG). 10ul of Dynabeads Protein G (Invitrogen, Cat. # 10003D) were added to the supernatant and incubated for 2 hrs at 4^{o}C. Beads were recovered, washed in low salt buffer, high salt buffer, LiCl buffer, followed by washing in TE for three times. Elution buffer (300 mM NaCl, 0.5% SDS, 10 mM Tris-HCl, 5mM EDTA) was added to the washed beads, treated with RNase at 37^{o}C for 2 hrs and Proteinase K at 65^{o}C overnight. Equal amount of Phenol-Chloroform-Isoamyl alcohol was added to the samples and the aqueous phase was recovered. DNA was precipitated by adding 100% Ethanol, NaOAc and glycogen and kept at -20^{o}C overnight. Samples were centrifuged at 14000g for 30 min at 4^{o}C and washed with 70% ethanol followed by centrifugation at 14000g for 30 min at 4^{o}C. Quantitative PCRs were performed using SsoAdvanced Universal SYBR Green Supermix (Biorad Cat. N. 172-5270), according to the manufacturer's protocol. Primers used for ChIP analysis by RT-PCR: Kcnd1 Forward: 5'-CTCACGAGGCTAGGCAGTTC -3', Kcnd1

Reverse: 5'-CCTTGATCGGGTGACTTGTT -3'; Gabrd Forward: 5'- CTGTTCACCTGCAATCAGGA-3', Gabrd Reverse: 5'- GGTCTGCCCTTGAGAAATGA -3'; Adora2a Forward: 5'-AAAGATGTGGGGGAGGAGTC -3', Adora2a Reverse: 5'- TTGCCCTTTATCGGAGCTAA -3'.

Prostaglandins PGJ2 analysis

15-deoxy-$\Delta^{12,14}$-PGJ2 Elisa KIT (Enzo Life Sciences Cat. # ADI-900-023) was used to determine striatal Prostaglandin J2 concentration. ELISA tests were performed following manufacturer's instructions. Samples were prepared as follows: striatal punches of the NAcc were minced in Phosphate buffer and the solution was then acidified by addition of HCl (2M) to pH 3.5. Samples were centrifuged and the supernatant was passed through a C18 column (Pierce) and eluted with 20µl of ethyl acetate. After evaporation (O/N, RT), samples were reconstituted in 250µl of Assay Buffer and used for the Elisa assay.

Additional statistical analyses

For all non-circadian statistics, data were analyzed either by Student's t-test, or by two- or three-way ANOVA (GraphPad Prism8.3.0), followed by Tukey's or Bonferroni's post hoc analyses, as appropriate. Statistical significance was assigned with p-value < 0.05. For circadian analysis, JTK_Cycle was used with a p-value < 0.01 cutoff.

RESOURCE AVAILABILITY

The GEO accession number for the RNA-seq data set reported in this paper is GSE142657 (https://www.ncbi.nlm.nih.gov/geo/query/acc.cgi?acc=GSE142657). RNA-seq data was used for Figure 2, Figure 3, and Figure 4, and Supplementary Figures 1-4. UCSC mm10 mouse

reference genome was used for alignment. All the transcriptomic data associated with this work is publicly available on the resource circadiomics.ics.uci.edu. PPARγ ChIP-seq data used for Figure 4 was downloaded from GEO, accession number GSE64458 (https://www.ncbi.nlm.nih.gov/geo/query/acc.cgi?acc=GSE64458) (Soccio et al., 2015).

ACKNOWLEDGEMENTS

We thank all the members of the Sassone-Corsi and Borrelli laboratories for scientific discussion and technical assistance. We also thank Siwei Chen for computational assistance. We greatly appreciate Melanie Oakes, Christophe Magnan, Seung-Ah Chung and Valentina Ciobanu at the UCI Genomics High-Throughput Facility. R.G.L. was supported by the University of California, Irvine School of Medicine Dean's Fellowship and the Dr. Lorna Carlin Scholar Award. M.C. was supported by predoctoral fellowships from the National Institutes of Health (NIH) (GM117942) and the American Heart Association (17PRE33410952). P.T. by Human Frontier Science Program LT 000576/2013. This work was supported by grants from NIH (DA 035600 to E.B. and P.S.-C.) and by the French Institut National de la Santé et de la Recherche Médicale (INSERM).

AUTHOR CONTRIBUTIONS

K.B.-C., R.G.L., M.C., and P.T. performed the experiments and analyzed the data. Y.L. and P.B. performed the bioinformatics analysis. P.S.-C. and E.B. designed the study, analyzed the data and wrote the manuscript.

DECLARATION OF INTERESTS

The authors declare no conflicts of interests.

FIGURES

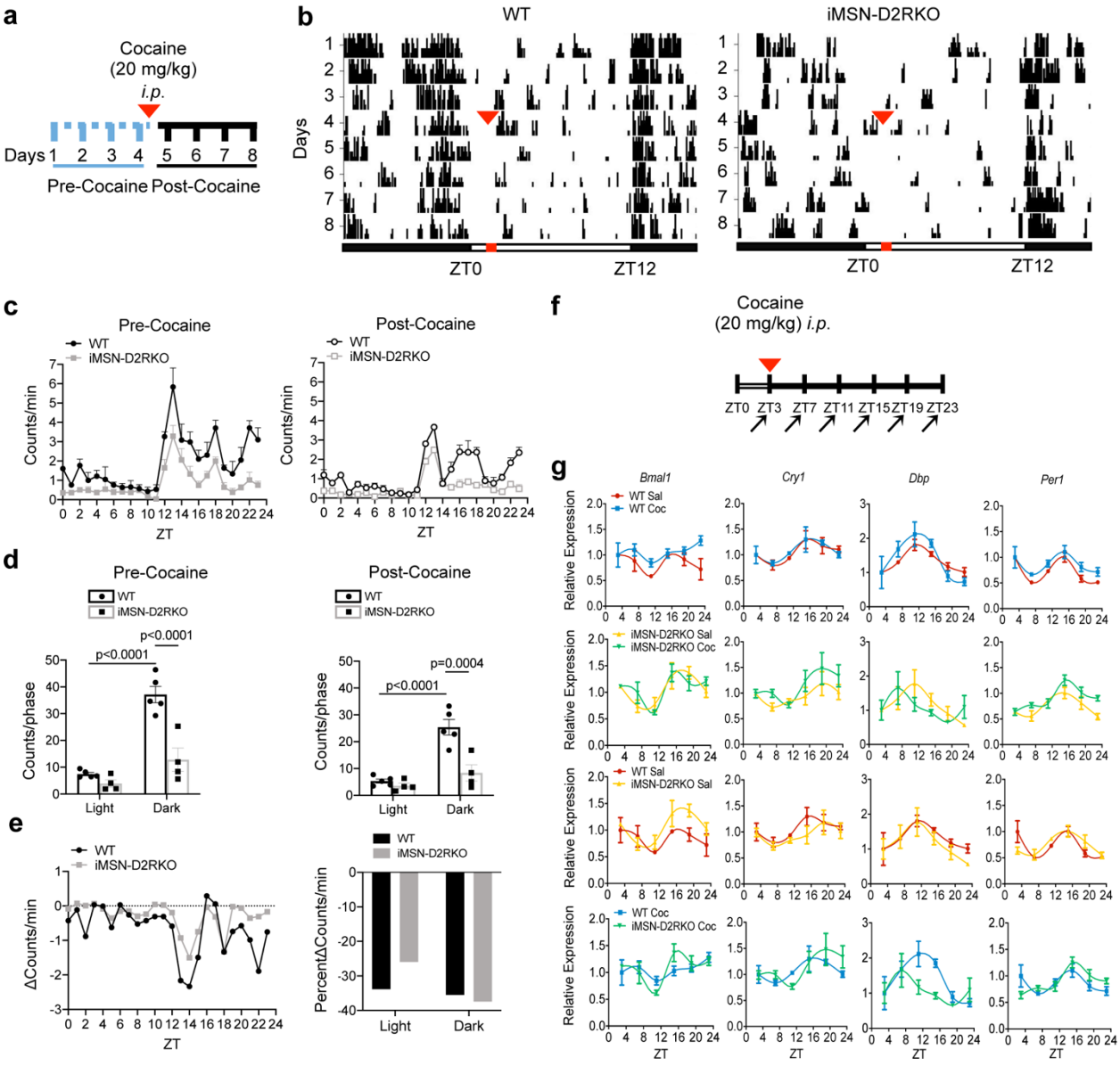

Figure 2.1 Effects of acute cocaine on circadian clock genes

a, Schematic of the experimental design in **b**. **b**, Actograms of 24 h locomotor activity in 12h-Light/12h-Dark cycles in WT (n=5) and iMSN-D2RKO mice (n=4) during the 4 days preceding and following cocaine administration. Cocaine (20 mg kg^{-1}, i.p.) was given once at ZT3 on day 4 (red arrowheads in 1a and 1b). **c**, Locomotor activity analyses from b in WT (circles) and iMSN-D2RKO (squares) mice. Graphical representation of the number of beam breaks/min/circadian time (ZT) during the days preceding (Pre-Cocaine; left) or following cocaine injection (Post-Cocaine; right). **d**, Total beam breaks per phase in WT (circles) (n=5)

and iMSN-D2RKO (squares) (n=4); inactive phase (Light), active phase (Dark), Pre-cocaine (two-way ANOVA, Genotype: $F_{(1, 14)} = 27.31$, $p=0.0001$; Time: $F_{(1, 14)} = 52.41$, $p<0.0001$; Interaction: $F_{(1, 14)} = 15.20$, $p=0.0016$) and Post-cocaine (two-way ANOVA, Genotype: $F_{(1, 14)} = 18.15$, $p=0.0008$; Time: $F_{(1, 14)} = 31.86$, $p<0.0001$; Interaction: $F_{(1, 14)} = 12.01$, $p=0.0038$). Tukey's multiple comparison test p-values as indicated. **e**, Left: The mean change in counts/min at each time point in pre-cocaine vs post-cocaine time in WT (circles) and iMSN-D2RKO (squares). Right: same as **e**) *left,* but represented as percent change during the light (ZT0-11) and dark (ZT12-23) phases. **f**, Schematic of the circadian experimental design in g. Mice were injected with cocaine (20 mg kg^{-1}, i.p) at ZT3 and NAcc samples were collected every 4 hours following cocaine injection at ZT 3, 7, 11, 15, 19 and 23 (arrows). **g**, Expression of core clock and clock-controlled genes: *Bmal1, Cry1, Dbp*, and *Per1* in WT saline (Sal; red circles) or cocaine (Coc; blue squares) and iMSN-D2RKO (Sal; yellow upward triangles) or (Coc; green downward triangles) analyzed by quantitative real-time PCR (n=3/genotype). (*three-way ANOVA;* For statistics see Table 3.S1). Data are presented as mean values ± SEM.

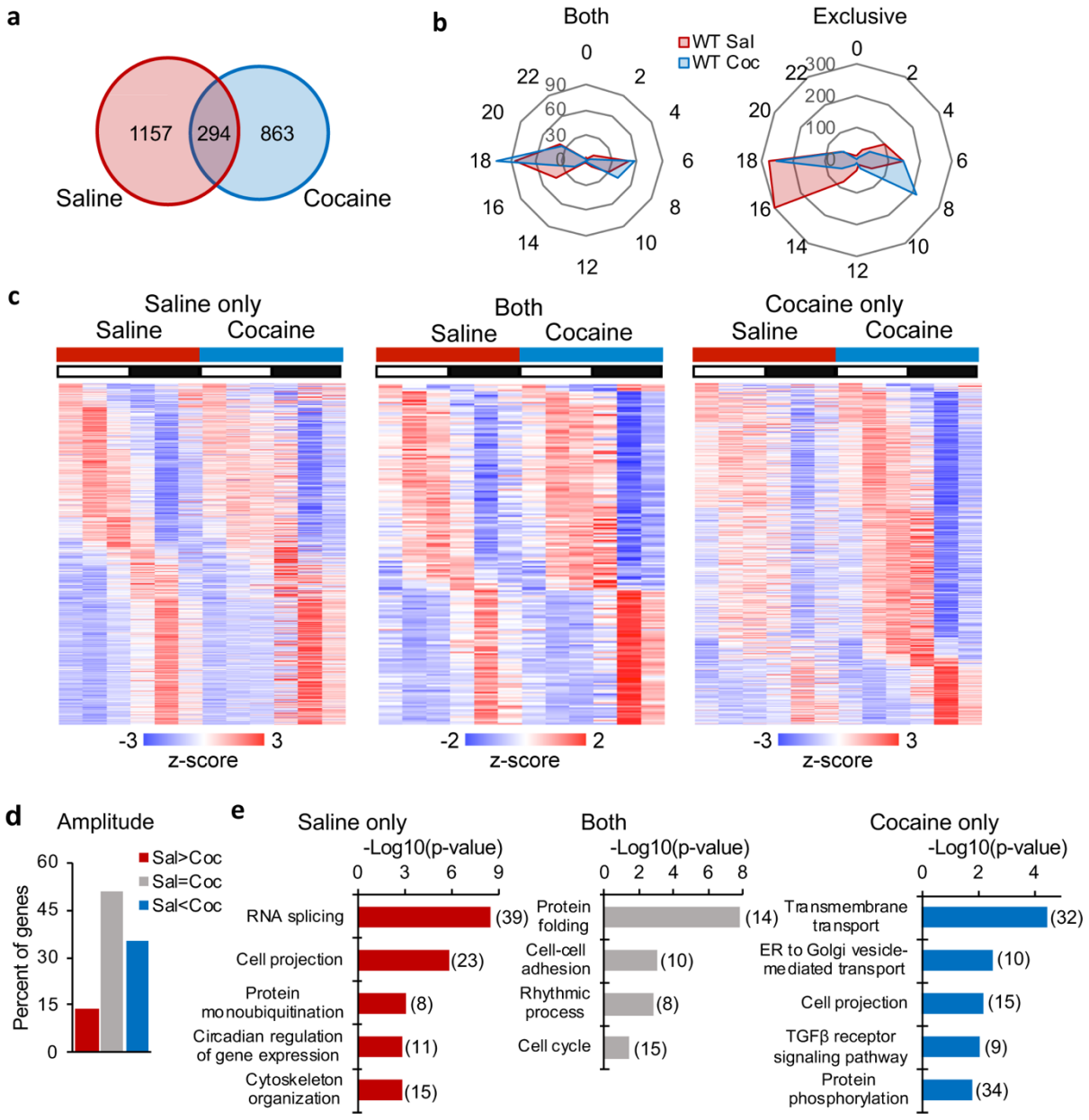

Figure 3.2 Cocaine rewires the striatal circadian transcriptome in WT mice

a, Venn diagram representing the striatal rhythmic genes in saline and cocaine treated WT mice (n = 3, JTK_Cycle, cutoff p<0.01). **b**, Radar plots representing the phase analysis of genes whose expression is circadian in both saline (Sal) and cocaine (Coc) treated mice (left) and genes exclusively circadian in saline or cocaine conditions (right). **c**, Heat maps representing genes significantly circadian (n=3, JTK_cycle, cutoff p<0.01) in saline- (left), in cocaine-treated mice (right) and commonly circadian in saline and cocaine treated mice (middle). White and black bars indicate the light (ZT3, 7, 11) and dark (ZT15, 19, 23) timepoints respectively. **d**, Amplitude analysis of striatal transcripts rhythmic in both saline (Sal) and

cocaine (Coc) injected mice. The percentage of genes with amplitude higher, lower or equal to saline condition is reported. **e**, DAVID Gene Ontology Biological Process analysis of circadian genes oscillating in saline only (left), both (middle) and cocaine only (right). Bar charts represent the -Log10(p-value) of each enriched term. The number of genes identified in each pathway is shown in parenthesis.

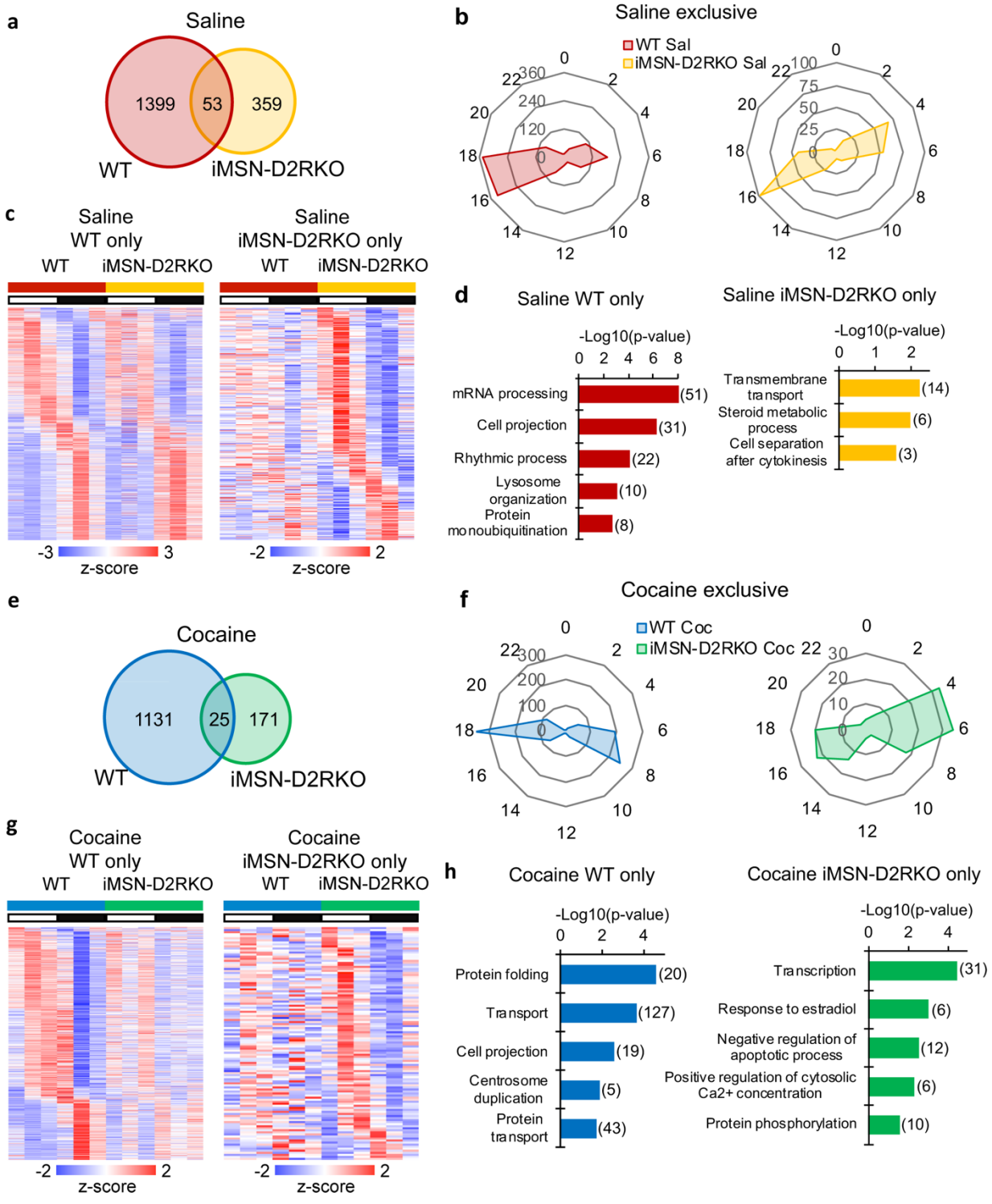

Figure 3.3 D2R ablation from iMSN reorganizes the striatal circadian transcriptome

a, Venn diagram of striatal oscillating genes in saline treated WT and iMSN-D2RKO mice (n = 3, JTK_Cycle, cutoff p<0.01). **b**, Radar plots displaying the phase analysis of genes whose

expression is exclusively circadian in WT mice (left) or in iMSN-D2RKO saline-treated (Sal) mice (right). **c**, Heat maps of genes significantly circadian (n=3, JTK_Cycle, cutoff p<0.01) only in WT (left) or in iMSN-D2RKO (right) saline-treated mice. White and black bars indicate the light (ZT3, 7, 11) and dark (ZT15, 19, 23) timepoints respectively. **d**, DAVID Gene Ontology Biological Process analysis of circadian genes oscillating in saline WT only (left) and in saline iMSN-D2RKO only (right). Bar charts represent the -Log10(p-value) of each enriched term. The number of genes identified in each pathway is shown in parenthesis. **e**, Venn diagram of striatal oscillating genes in cocaine treated WT and iMSN-D2RKO mice (n = 3, JTK_Cycle, cutoff p<0.01). **f**, Radar plots displaying the phase analysis of genes whose expression is exclusively circadian in WT (left) or in iMSN-D2RKO cocaine-treated (Coc) mice (right). **g**, Heat maps of genes significantly circadian (n=3, JTK_Cycle, cutoff p<0.01) only in WT (left) or in iMSN-D2RKO (right) cocaine-treated mice. White and black bars indicate the light (ZT3, 7, 11) and dark (ZT15, 19, 23) timepoints respectively. **h**, DAVID Gene Ontology Biological Process analysis of circadian genes oscillating in cocaine WT only or in cocaine iMSN-D2RKO only. Bar charts represent the -Log10(p-value) of each enriched term. The number of genes identified in each pathway is shown in parenthesis.

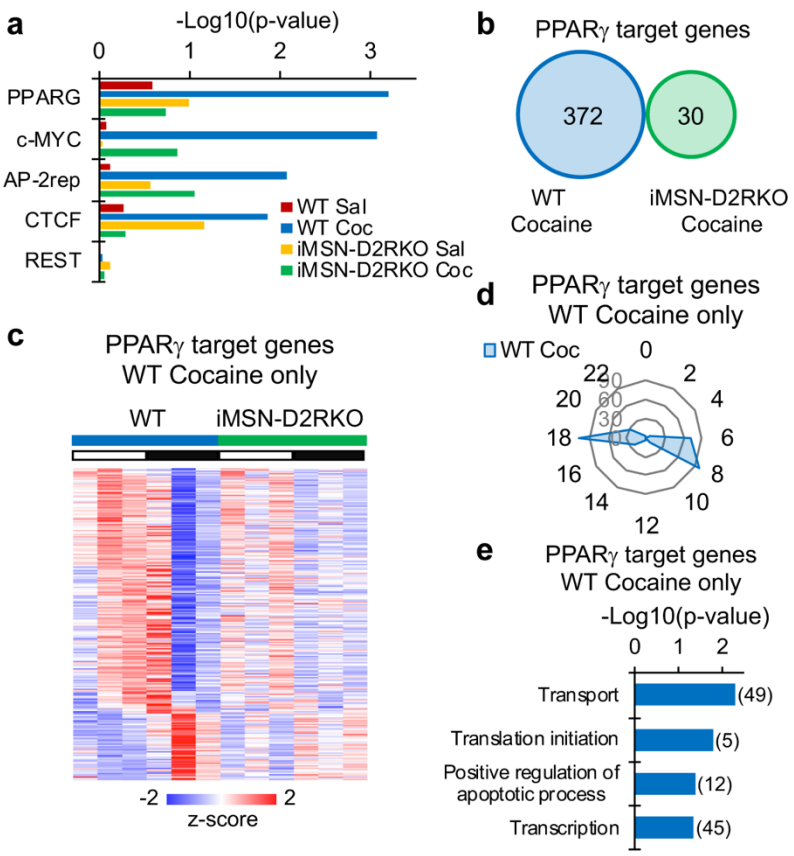

Figure 3.4 Cocaine-driven *de novo* oscillation of PPARγ target genes

a, Comparison of transcription factor binding site (TFBS) analysis between WT saline (Sal), WT cocaine (Coc), iMSN-D2RKO saline, and iMSN-D2RKO cocaine. The charts report the -Log10(p-value). **b**, Venn diagram representing the rhythmic PPARγ target transcripts after cocaine treatment in WT and iIMSN-D2RKO mice (n = 3, JTK_Cycle, cutoff p<0.01). **c**, Heat map displaying PPARγ target genes oscillating only in WT cocaine-treated mice compared to iMSN-D2RKO cocaine-treated mice (n=3, JTK_Cycle, cutoff p<0.01). White and black bars indicate the light (ZT3, 7, 11) and dark (ZT15, 19, 23) timepoints respectively. **d**, Radar plots displaying the phase analysis of PPARγ target genes whose expression is exclusively circadian in WT cocaine-treated (Coc) mice. **e**, DAVID Gene Ontology Biological Process analysis of oscillatory PPARγ target genes in cocaine-treated WT mice (n=3, JTK_Cycle, cutoff p<0.01). Bar charts represent the -Log10(p-value) of each enriched term. The number of genes identified in each pathway is shown in parenthesis.

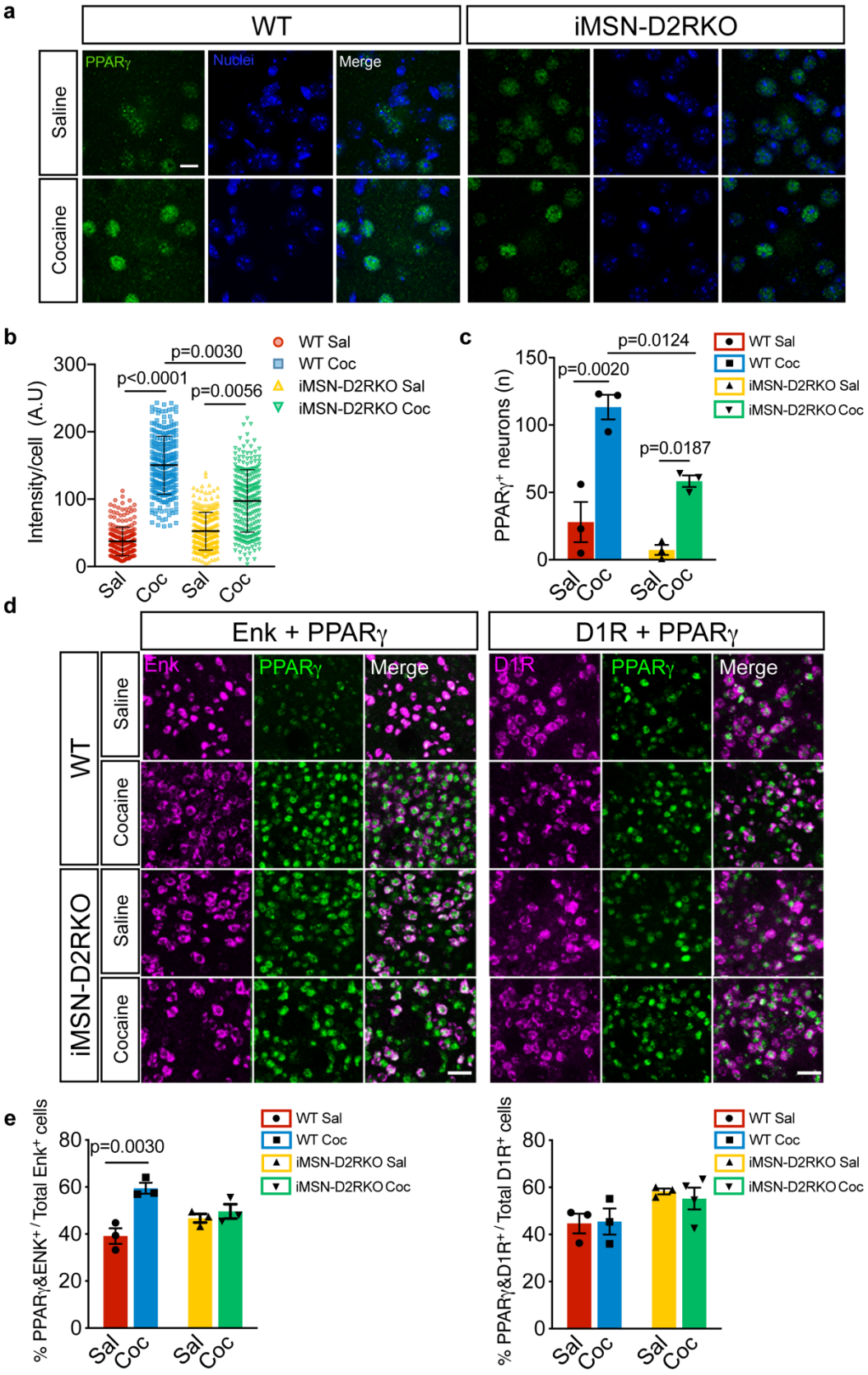

Figure 3.5 Cocaine-induced nuclear PPARγ is impaired in iMSN-D2RKO mice

a, Immunolabeling of PPARγ and nuclei on striatal sections of saline and cocaine treated WT and iMSN-D2RKO mice. Scale bar: 25 μm. **b**, Quantification of the fluorescent intensity of PPARγ immunolabeling in WT and iMSN-D2RKO mice treated with saline (Sal; WT: red circles; iMSN-D2RKO: yellow upward triangles) or cocaine (Coc; WT: blue squares; iMSN-D2RKO: green downward triangles). Data were analyzed by two-way ANOVA using the mean ± SD of intensity/cell for each biological replicate (n=4/group) (Genotype: $F_{(1, 12)} = 8.458$, $p=0.0131$; Treatment: $F_{(1, 12)} = 91.23$, $p<0.0001$; Interaction: $F_{(1, 12)} = 12.81$, $p=0.0038$), Tukey's multiple comparison test. **c**, Quantification of PPARγ positive neurons with the indicated treatment (n=3/group). Significance was calculated using two-way ANOVA (Genotype: $F_{(1, 8)} = 16.87$, $p=0.0034$; Treatment: $F_{(1, 8)} = 54.77$, $p<0.0001$; Interaction: $F_{(1, 8)} = 3.474$, $p=0.0993$) Tukey's multiple comparison test. **d**, Double *in-situ*/immunofluorescence for *Enkephalin* (Enk) or *D1R* mRNA and PPARγ protein in cocaine treated WT and iMSN-D2RKO mice. Scale bar: 50 μm. **e**, Percentage of PPARγ- and Enk- or D1R-positive cells in cocaine and saline treated WT and iMSN-D2RKO mice (Enk: n=3/group; D1R: n=3 WT Sal, n=3 WT Coc, n=3 iMSN-D2RKO Sal, n=4 iMSN-D2RKO Coc). Two-way ANOVA (Enk: Genotype: $F_{(1, 8)} = 0.1782$, $p=0.6841$; Treatment: $F_{(1, 8)} = 18.69$, $p=0.0025$; Interaction: $F_{(1, 8)} = 10.53$, $p=0.0118$; D1R: Genotype: $F_{(1, 9)} = 7.117$, $p=0.0257$; Treatment: $F_{(1, 9)} = 0.06215$, $p=0.8087$; Interaction: $F_{(1, 9)} = 0.1943$, $p=0.6697$). Tukey's multiple comparison test. Data in c and e are presented as mean values ± SEM.

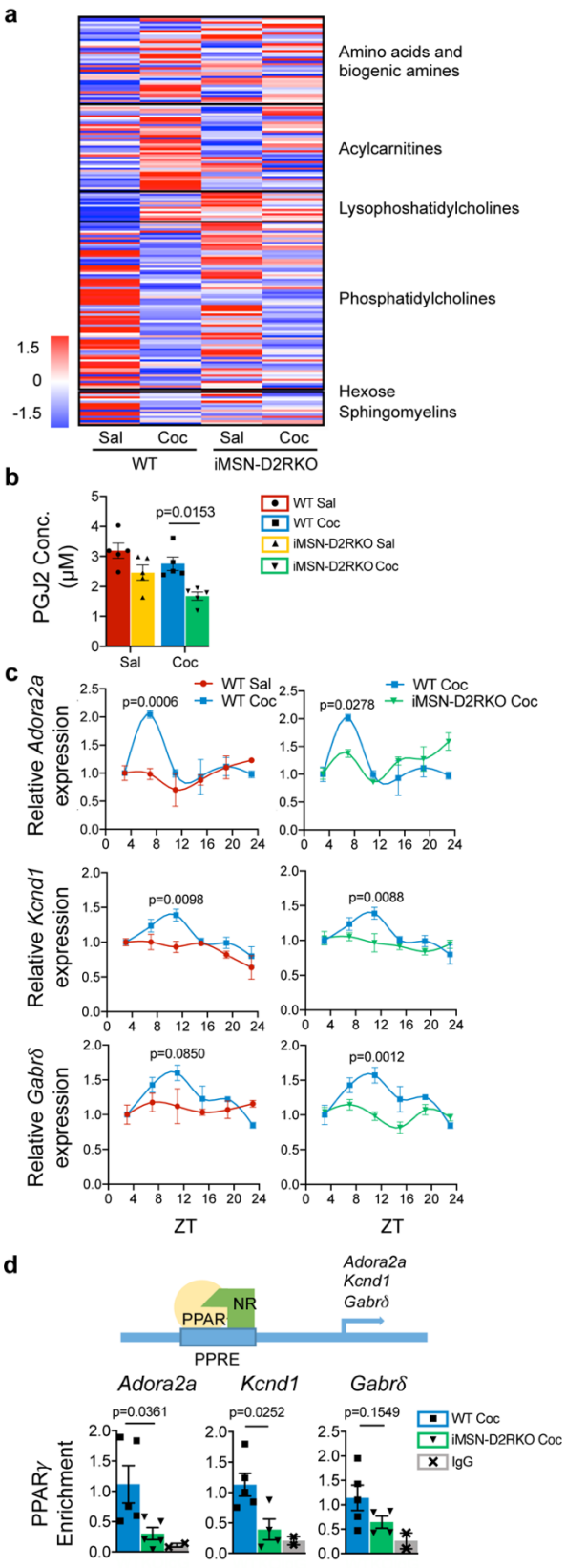

Figure 3.6 PPARγ signaling is altered in iMSN-D2RKO mice

a, Heatmap of the 180 metabolites analyzed in WT and iMSN-D2RKO mice, either saline or cocaine-treated (n=5/group). Metabolites were measured at ZT7 after saline or cocaine was injected at ZT3. Classes of metabolites measured are indicated on the right. **b**, Prostaglandin PGJ2-type (15-deoxy-$\Delta^{12,14}$-PGJ2) concentration assessed by enzyme-linked immunosorbent assay (ELISA) at ZT7 in WT and iMSN-D2RKO mice treated with saline (Sal: WT, red circles; iMSN-D2RKO, yellow upward triangles) or cocaine (Coc: WT, blue squares; iMSN-D2RKO, green downward triangles) (n=5/group/genotype). Two-way ANOVA (Genotype: $F_{(1, 16)}$ = 0.1696, p=0.0008; Treatment: $F_{(1, 16)}$ = 7.719, p=0.0134; Interaction: $F_{(1, 16)}$ = 0.6034, p=0.4486). Tukey's multiple comparison test p-values as indicated. **c**, Circadian expression of selected PPARγ target genes *Adora2a*, *Kcnd1*, *Gabrδ* as determined by quantitative real time PCR (n=3/group). WT Sal (red circles), WT Coc (blue squares), iMSN-D2RKO Coc (green downward triangles). Two-way ANOVA *Adora2a* WT Sal vs WT Coc: Treatment: $F_{(1, 24)}$ = 4.372, p=0.0473; Time: $F_{(5, 24)}$ = 4.253, p=0.0065; Interaction: $F_{(5, 24)}$ = 3.983, p=0.0090; *Adora2a* WT Coc vs iMSN-D2RKO Coc: Genotype: $F_{(1, 24)}$ = 0.4260, p=0.5201; Time: $F_{(5, 24)}$ = 7.429, p=0.0002; Interaction: $F_{(5, 24)}$ = 4.363, p=0.0058; *Kcnd1* WT Sal vs WT Coc: Treatment: $F_{(1, 24)}$ = 10.98, p=0.0029; Time: $F_{(5, 24)}$ = 6.118, p=0.0009; Interaction: $F_{(5, 24)}$ = 1.640, p=0.1878; *Kcnd1* WT Coc vs iMSN-D2RKO Coc: Genotype: $F_{(1, 24)}$ = 5.302, p=0.0303; Time: $F_{(5, 24)}$ = 4.360, p=0.0058; Interaction: $F_{(5, 24)}$ = 2.743, p=0.0426; *Gabrδ* WT Sal vs WT Coc: Treatment: $F_{(1, 24)}$ = 2.940, p=0.0993; Time: $F_{(5, 24)}$ = 2.690, p=0.0456; Interaction: $F_{(5, 24)}$ = 2.124, p=0.0972; *Gabrδ* WT Coc vs iMSN-D2RKO Coc: Genotype: $F_{(1, 24)}$ = 15.59, p=0.0006; Time: $F_{(5, 24)}$ = 5.308, p=0.0020; Interaction: $F_{(5, 24)}$ = 3.961, p=0.0092. Bonferroni's multiple comparison test p-values as indicated. **d**, Chromatin recruitment of PPARγ at PPAR response element (PPRE) binding site contained in *Adora2a* (p=0.0361; WT Coc (blue squares) n=5, iMSN-D2RKO Coc (green downward triangles) n=5, IgG (grey X's) n=2), *Kcnd1* (p=0.0252; WT Coc n=5, n=4 iMSN-D2RKO Coc, IgG n=2) and *Gabrδ* promoters (p=0.1549; WT Coc n=5, iMSN-D2RKO Coc n=4, IgG n=2. unpaired Student's t-test. Data are presented as mean values ± SEM.

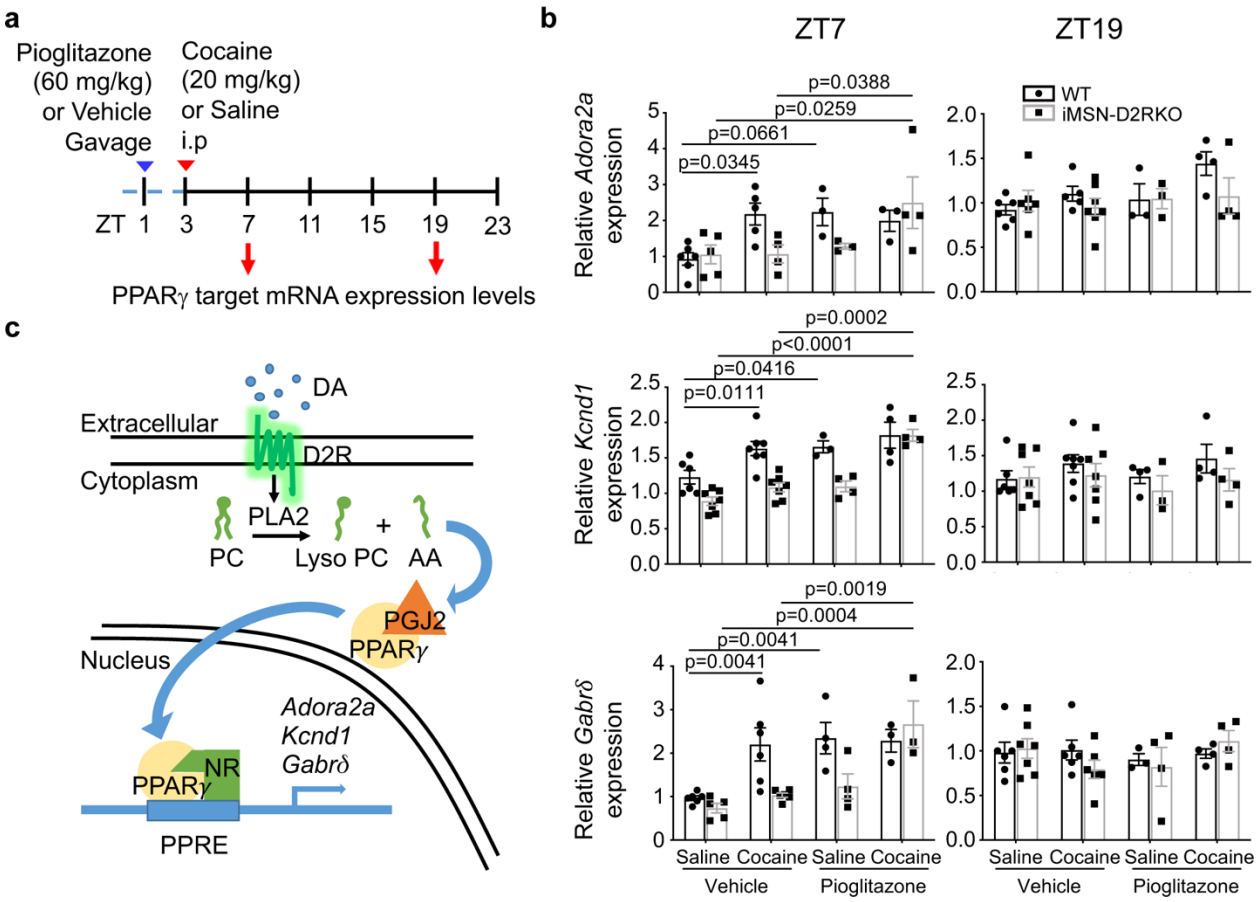

Figure 3.7 Pharmacological activation of PPARγ restores PPARγ signaling iMSN-D2RKO mice

a, Schematic representation of the experimental design, arrowheads indicate the time and treatment of Pioglitazone (blue) and Cocaine treatments (red). **b**, Expression of selected PPARγ target genes *Adora2a, Kcnd1*, and *Gabrδ* as determined by quantitative real time PCR at ZT7 and ZT19 in presence or absence of Pioglitazone (60 mg kg^{-1}) prior to saline or cocaine (20 mg kg^{-1}) (*Adora2a* ZT7: Genotype: $F_{(1, 25)}$ = 2.003, p=0.1693; Treatment: $F_{(3, 25)}$ = 4.682, p=0.0099; Interaction: $F_{(3, 25)}$ = 2.479, p=0.0845 (Vehicle and Saline: WT n=6, iMSN-D2RKO n=5; Vehicle and Cocaine: WT n=5, iMSN-D2RKO n=4; Pioglitazone and Saline: WT n=3, iMSN-D2RKO n=3; Pioglitazone and Cocaine: WT n=3, iMSN-D2RKO n=4); *Kcnd1* ZT7: Genotype: $F_{(1, 34)}$ = 26.20, p<0.0001; Treatment: $F_{(3, 34)}$ = 20.05, p<0.0001; Interaction: $F_{(3, 34)}$ = 3.130, p=0.0383 (Vehicle and Saline: WT n=6, iMSN-D2RKO n=7, Vehicle and Cocaine WT n=7, iMSN-D2RKO n=7; Pioglitazone and Saline: WT n=3, iMSN-D2RKO n=4, Pioglitazone and Cocaine WT n=4, iMSN-D2RKO n=4); *Gabrδ* ZT7 Genotype: $F_{(1, 29)}$ = 7.445, p=0.0107; Treatment: $F_{(3, 29)}$ = 11.26, p<0.0001; Interaction: $F_{(3, 29)}$ = 3.378, p=0.0315 (Vehicle and Saline: WT n=6, iMSN-D2RKO n=5, Vehicle and Cocaine: WT n=6, iMSN-D2RKO n=6; Pioglitazone and Saline: WT n=4, iMSN-D2RKO n=4; Pioglitazone and Cocaine: WT n=3, iMSN-D2RKO n=3); *Adora2a* ZT19: Genotype: $F_{(1,30)}$ = 1.352, p=0.2540; Treatment: $F_{(3, 30)}$ =

2.071, p=0.1250; Interaction: $F_{(3, 30)}$ = 1.406, p=0.2603 (Vehicle and Saline: WT n=6, iMSN-D2RKO n=6; Vehicle and Cocaine: WT n=5, iMSN-D2RKO n=7; Pioglitazone and Saline: WT n=3, iMSN-D2RKO n=3; Pioglitazone and Cocaine WT n=4, iMSN-D2RKO n=4); *Kcnd1* ZT19: Genotype: $F_{(1, 34)}$ = 1.903, p=0.1767; Treatment: $F_{(3, 34)}$ = 0.7013, p=0.5578; Interaction: $F_{(3, 34)}$ = 0.3919, p=0.7596 (Vehicle and Saline: WT n=6, iMSN-D2RKO n=7; Vehicle and Cocaine WT n=7, iMSN-D2RKO n=7; Pioglitazone and Saline: WT n=4, iMSN-D2RKO n=3; Pioglitazone and Cocaine: WT n=4, iMSN-D2RKO n=4); *Gabrδ*ZT19 Genotype: $F_{(1, 32)}$ = 0.09598, p=0.7587; Treatment: $F_{(3, 32)}$ = 0.8134, p=0.4959; Interaction: $F_{(3, 32)}$ = 0.8259, p=0.4893 (Vehicle and Saline: WT n=6, iMSN-D2RKO n=7; Vehicle and Cocaine WT n=6, iMSN-D2RKO n=6; Pioglitazone and Saline WT n=3, iMSN-D2RKO n=4; Pioglitazone and Cocaine: WT n=4, iMSN-D2RKO n=4)). Tukey's multiple comparison test p-values as indicated. Data are presented as mean values ± SEM. **c**, Simplified overview depicting D2R-mediated cocaine effect on circadian transcription of PPARγ target genes through PPARγ activation by prostaglandins (PGJ2). Dopamine (DA) activation of D2R stimulates Phospholipase A2 (PLA2) converting phosphatidylcholine (PC) to lysophosphatidylcholine (Lyso PC) and arachidonic acid (AA); AA is later converted into Prostaglandin (PGJ2). PGJ2 induces PPARγ nuclear translocation and transcriptional activation.

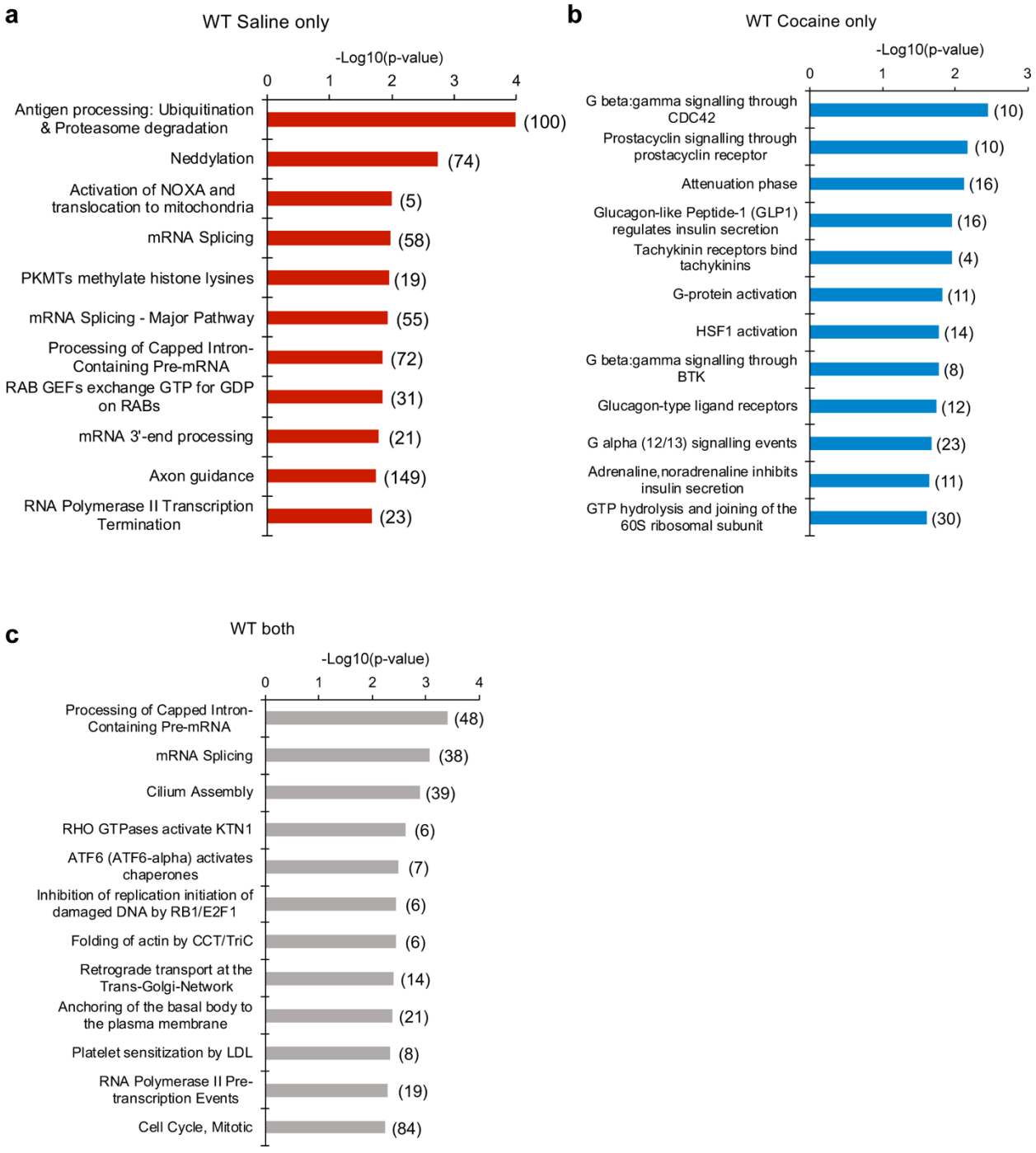

Figure 3.S1 Pathway analyses in WT and iMSN-D2RKO mice

a-c, Reactome Pathway analysis of circadian genes oscillating in saline only **a**, cocaine only **b**, and both **c**. Bar charts represent the -Log10(p-value) of each enriched term. The number of genes identified in each pathway is shown in parenthesis.

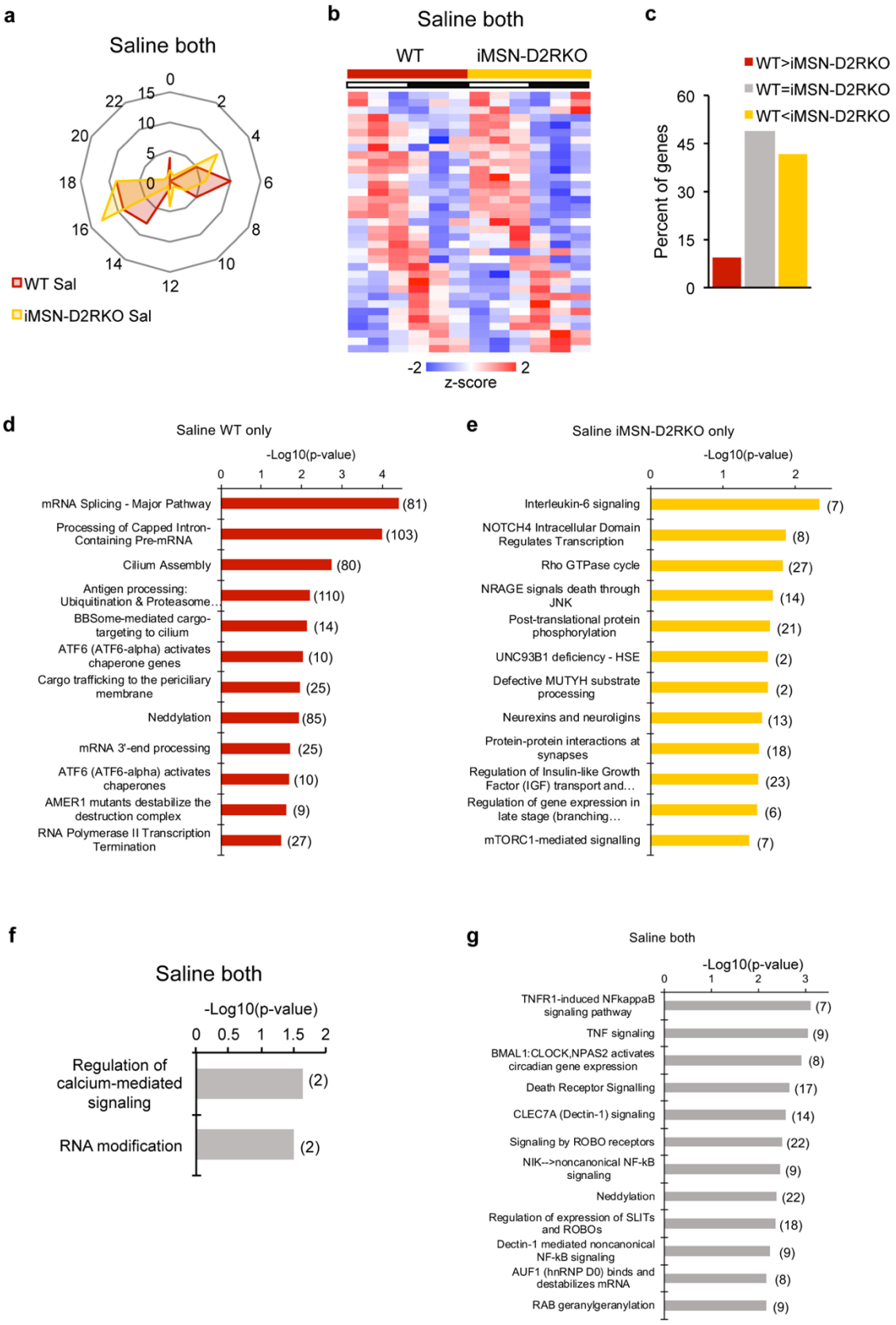

Figure 3.S2 Phase and pathway analyses in WT and iMSN-D2RKO saline-treated mice

a, Radar plots representing the phase analysis of genes whose expression is circadian in both WT and iMSN-D2RKO saline-treated (Sal) mice. **b**, Heat maps representing genes significantly circadian (n=3, JTK_cycle, cutoff p<0.01) in both WT and iMSN-D2RKO saline-treated mice. White and black bars indicate the light (ZT3, 7, 11) and dark (ZT15, 19, 23) timepoints respectively. **c**, Amplitude analysis of NAcc transcripts rhythmic in "both" WT and iMSN-D2RKO saline-treated mice. The percentage of genes with amplitude higher, lower or equal to WT is reported. **d** and **e**, Reactome Pathway analysis of circadian genes oscillating in WT only **d**, and iMSN-D2RKO only **e**, saline-treated mice. Bar charts represent the -Log10(p-value) of each enriched term. The number of genes identified in each pathway is shown in parenthesis. **f**, DAVID Gene Ontology Biological Process analysis of circadian genes oscillating in both WT and iMSN-D2RKO saline-treated mice. Bar charts represent the -Log10(p-value) of each enriched term. **g**, Reactome Pathway analysis of circadian genes oscillating in both WT and iMSN-D2RKO saline-treated mice. Bar charts represent the -Log10(p-value) of each enriched term. The number of genes identified in each pathway is shown in parenthesis.

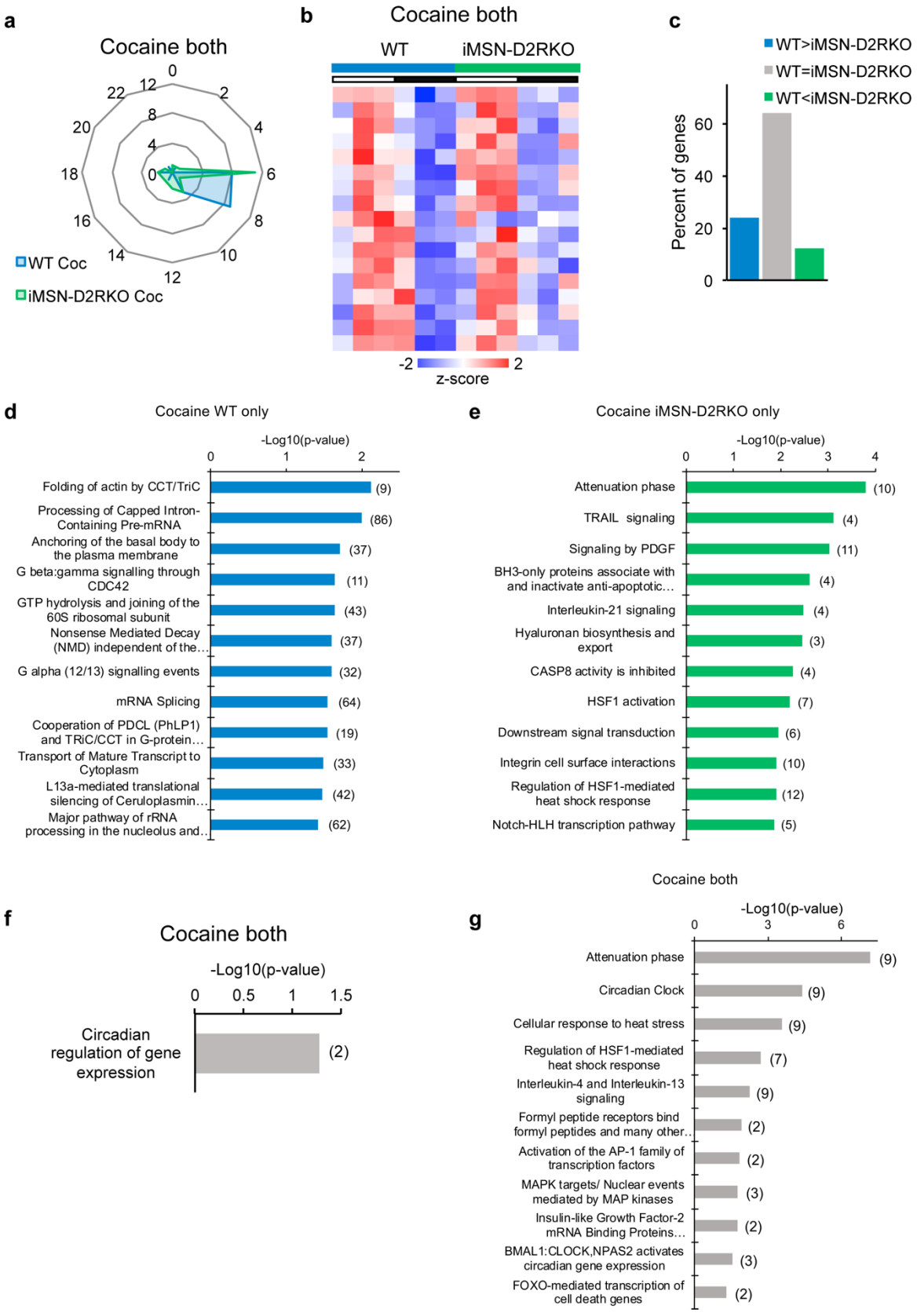

Figure 3.S3 Phase and pathway analyses in WT and iMSN-D2RKO cocaine-treated mice

a, Radar plots representing the phase analysis of genes whose expression is circadian in both WT and iMSN-D2RKO cocaine-treated (Coc) mice. **b**, Heat maps representing genes significantly circadian (n=3, JTK_cycle, cutoff p<0.01) in both WT and iMSN-D2RKO cocaine-treated mice. White and black bars indicate the light (ZT3, 7, 11) and dark (ZT15, 19, 23) timepoints respectively. **c**, Amplitude analysis of striatal transcripts rhythmic in "both" WT and iMSN-D2RKO cocaine-treated mice. The percentage of genes with amplitude higher, lower or equal to WT is reported. **d** and **e**, Reactome Pathway analysis of circadian genes oscillating in WT only **d**, and iMSN-D2RKO only **e**, cocaine-treated mice. Bar charts represent the -Log10(p-value) of each enriched term. The number of genes identified in each pathway is shown in parenthesis. **f**, DAVID Gene Ontology Biological Process analysis of circadian genes oscillating in both WT and iMSN-D2RKO cocaine-treated mice. Bar charts represent the -Log10(p-value) of each enriched term. **g**, Reactome Pathway analysis of circadian genes oscillating in both WT and iMSN-D2RKO cocaine-treated mice. Bar charts represent the -Log10(p-value) of each enriched term. The number of genes identified in each pathway is shown in parenthesis.

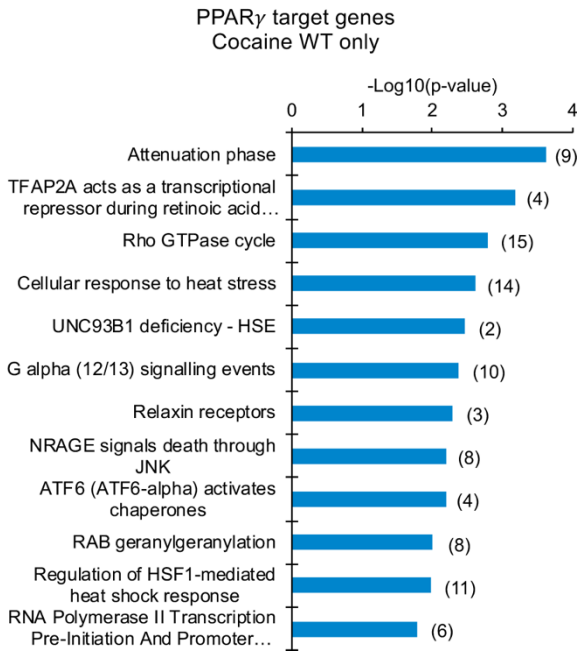

Figure 3.S4 Pathway analysis of PPARγ target genes in WT cocaine-treated mice

Reactome pathway analysis of oscillatory PPARγ target genes in cocaine-treated WT mice (n=3, JTK_Cycle, cutoff $p < 0.01$). Bar charts represent the -Log10(p-value) of each enriched term. The number of genes identified in each pathway is shown in parenthesis.

TABLE

Table 3.S1 Statistics for Figure 3.1g

Bmal1	**SS**	**DF**	**MS**	**F (DFn, DFd)**	**P value**
Time	1.811	5	0.3622	F (5, 48) = 6.805	P<0.0001
Treatment	0.1942	1	0.1942	F (1, 48) = 3.649	P=0.0621
Genotype	0.2022	1	0.2022	F (1, 48) = 3.798	P=0.0572
Time x Treatment	0.4559	5	0.09119	F (5, 48) = 1.713	P=0.1497
Time x Genotype	0.2632	5	0.05264	F (5, 48) = 0.9889	P=0.4345
Treatment x Genotype	0.1025	1	0.1025	F (1, 48) = 1.926	P=0.1716
Time x Treatment x Genotype	0.1459	5	0.02917	F (5, 48) = 0.5481	P=0.7389
Cry1	SS	DF	MS	F (DFn, DFd)	P value
Time	1.743	5	0.3487	F (5, 48) = 5.429	P=0.0005
Treatment	0.006013	1	0.006013	F (1, 48) = 0.09362	P=0.7609
Genotype	0.1796	1	0.1796	F (1, 48) = 2.796	P=0.1010
Time x Treatment	0.3174	5	0.06349	F (5, 48) = 0.9885	P=0.4346
Time x Genotype	0.08598	5	0.0172	F (5, 48) = 0.2678	P=0.9285
Treatment x Genotype	0.1282	1	0.1282	F (1, 48) = 1.996	P=0.1641
Time x Treatment x Genotype	0.17	5	0.034	F (5, 48) = 0.5294	P=0.7529
Per1	SS	DF	MS	F (DFn, DFd)	P value
Time	0.9461	5	0.1892	F (5, 48) = 6.215	P=0.0002
Treatment	0.005365	1	0.005365	F (1, 48) = 0.1762	P=0.6765
Genotype	0.3202	1	0.3202	F (1, 48) = 10.52	P=0.0022
Time x Treatment	0.685	5	0.137	F (5, 48) = 4.500	P=0.0019
Time x Genotype	0.1803	5	0.03607	F (5, 48) = 1.185	P=0.3307
Treatment x Genotype	0.0006089	1	0.0006089	F (1, 48) = 0.02000	P=0.8881
Time x Treatment x Genotype	0.08812	5	0.01762	F (5, 48) = 0.5789	P=0.7159
Dbp	SS	DF	MS	F (DFn, DFd)	P value
Time	7.595	5	1.519	F (5, 48) = 6.853	P<0.0001
Treatment	0.7277	1	0.7277	F (1, 48) = 3.283	P=0.0762
Genotype	0.002965	1	0.002965	F (1, 48) = 0.01338	P=0.9084
Time x Treatment	0.9625	5	0.1925	F (5, 48) = 0.8685	P=0.5092
Time x Genotype	0.364	5	0.07281	F (5, 48) = 0.3285	P=0.8933
Treatment x Genotype	0.0834	1	0.0834	F (1, 48) = 0.3763	P=0.5425
Time x Treatment x Genotype	1.899	5	0.3799	F (5, 48) = 1.714	P=0.1495

Chapter 4

Summary and Conclusions

The molecular circadian clock is a complex set of proteins that act in synchrony to regulate clock-controlled gene expression. Recent studies have provided evidence that the canonical clock function is one of many functions provided by the core clock proteins. The study we have presented in Chapter 2 elucidates an unappreciated role for BMAL1 in pre-rRNA processing. In a multilevel discovery, we have found that BMAL1 holds a non-canonical, non-circadian role. Our data illustrates BMAL1 localizes to the nucleolus and its absence results in altered nucleolar structure displaying a larger morphology and a reduced nucleoli-to-nucleus ratio. Additionally, we have identified the endogenous BMAL1 nucleolar interactome and characterize the specific interaction with the snoRNP nucleolar protein, NOP58. In association with the snoRNP complex, BMAL1 is required for the proper recruitment of

snoRNA, Snord118, to regulate proper processing of the 36S pre-rRNA species. Finally, the misregulation of pre-rRNA maturation in the BMAL1-deficient cells results in reduced ribosome biogenesis.

Based on our findings it is tempting to propose the biological significance of BMAL1 in the nucleolus. Given the robust premature aging phenotype attributed to BMAL1 (Kondratov et al., 2003), we believe a link can be made between the altered nucleolar structure we observe in our clock-deficient models to that of the enlarged nucleolar phenotype observed in aging models (Tiku and Antebi, 2018). Moreover, we define a BMAL1 function that is non-circadian. Is this a function retained in the nucleolus from early developmental stages? The role of the circadian clock in embryonic stem cells remains elusive, ESC express core clock proteins but lack rhythmicity and circadian activity (Yagita et al., 2010). Future studies are required to address these proposals, but our data provide the first strong evidence of novel links to other vital, non-circadian, non-canonical roles of circadian clock factors.

In Chapter 3 we took an alternative strategy and studied the effects of cocaine on the circadian clock in the brain's reward system. We used mice lacking the dopamine D2 receptor in the specific D2R-expressing medium spiny neurons of the nucleus accumbens (iMSN-D2RKO). WT mice and littermate iMSN-D2RKO mice were treated with a single dose of cocaine at the beginning of the light phase (ZT3). Cocaine had a marginal effect on the intensity of locomotor activity in both the WT and iMSN-D2RKO mice, however the mice maintained a circadian rhythmic behavior. Similarly, circadian striatal gene expression of the core clock genes was virtually unaltered with the exception of *Per2*. However, global RNA sequencing analysis in the NAcc of these mice revealed substantially greater differences in

the circadian transcriptome. Only 20% of the WT saline oscillating genes were conserved after cocaine treatment. On the other hand, about 4% of WT rhythmic genes were also rhythmic in the saline treated iMSN-D2RKO mice. By contrast, in the cocaine treated mice, only about 2% of genes were rhythmically preserved between the WT and iMSN-D2RKO. Furthermore, this analysis compared the uniquely oscillating genes in each treatment-genotype condition and detected genes that became newly oscillating either after cocaine treatment or in the absence of D2R. Motif analysis of the known promoters of these *de novo* rhythmic genes uncovered PPARγ as a key transcription factor involved in cocaine-mediated gene rhythmicity with limited activation on the iMSN-D2RKO transcripts. Indeed, we visualized the nuclear translocation of PPARγ in iMSNs of cocaine treated WT mice, but not in the iMSN-D2RKO mice. We measured the activation of PPARγ first, through the levels of its natural ligand, prostaglandin (PGJ2). Cocaine increased the levels of PGJ2 in the WT mice but did not increase the abundance of the ligand in the iMSN-D2RKO mice. Secondly, we measured the activation and expression of PPARγ target genes, we found cocaine induced rhythmic gene expression only in WT mice and not in the mice lacking D2R. These data highlighted the role of D2R in the circadian reprogramming response to cocaine. To bypass the dopamine receptor, we pharmacologically activated PPARγ with pioglitazone and were able to rescue the response to cocaine in the iMSN-D2RKO mice.

Our understanding of the detrimental consequences of drugs of abuse in various brain regions are extensively defined based on decades of research. However, the vast majority of the studies are limited to a single snapshot in time. In our study, we have extended our knowledge to encompass the effects of cocaine on multiple time points consisting of a full circadian cycle, allowing us to distinguish day and night differences in the

NAcc. Still, many unanswered questions remain and will require follow-up studies. For example, how does the time of day a user engages in drug use change the molecular effects we see on the circadian clock? Treating mice with cocaine during their active versus rest phases are likely to elicit separate stressors with differential response mechanisms. An epidemiological study also indicates the timing effects can differ based on the drug of abuse, caffeine, alcohol, cannabis, or cocaine (Gordon, 2019). Furthermore, how different is the rhythmic response in first time users compared to addicts? And how reversible is the reprogramming we identified on the clock? Future studies are essential to untangle the complex web linking drugs of abuse and the circadian clock. Identifying the central molecular mechanisms will allow for more targeted approaches to combating perturbations to the clock in drug abuse and addition.

REFERENCES

Abarca, C., Albrecht, U., and Spanagel, R. (2002). Cocaine sensitization and reward are under the influence of circadian genes and rhythm. Proc Natl Acad Sci U S A *99*, 9026-9030.

Aguilar-Arnal, L., Hakim, O., Patel, V.R., Baldi, P., Hager, G.L., and Sassone-Corsi, P. (2013). Cycles in spatial and temporal chromosomal organization driven by the circadian clock. Nat Struct Mol Biol *20*, 1206-1213.

Aitken, S., and Semple, C.A. (2017). The circadian dynamics of small nucleolar RNA in the mouse liver. J R Soc Interface *14*.

Aizman, O., Brismar, H., Uhlen, P., Zettergren, E., Levey, A.I., Forssberg, H., Greengard, P., and Aperia, A. (2000). Anatomical and physiological evidence for D1 and D2 dopamine receptor colocalization in neostriatal neurons. Nat Neurosci *3*, 226-230.

Akashi, M., Tsuchiya, Y., Yoshino, T., and Nishida, E. (2002). Control of intracellular dynamics of mammalian period proteins by casein kinase I epsilon (CKIepsilon) and CKIdelta in cultured cells. Mol Cell Biol *22*, 1693-1703.

Albrecht, U. (2012). Timing to perfection: the biology of central and peripheral circadian clocks. Neuron *74*, 246-260.

Ali, S.A., Zaidi, S.K., Dacwag, C.S., Salma, N., Young, D.W., Shakoori, A.R., Montecino, M.A., Lian, J.B., van Wijnen, A.J., Imbalzano, A.N.*, et al.* (2008). Phenotypic transcription factors epigenetically mediate cell growth control. Proceedings of the National Academy of Sciences of the United States of America *105*, 6632-6637.

Amaldi, F., Bozzoni, I., Beccari, E., and Pierandrei-Amaldi, P. (1989). Expression of ribosomal protein genes and regulation of ribosome biosynthesis in Xenopus development. Trends in biochemical sciences *14*, 175-178.

Andersen, J.S., Lyon, C.E., Fox, A.H., Leung, A.K., Lam, Y.W., Steen, H., Mann, M., and Lamond, A.I. (2002). Directed proteomic analysis of the human nucleolus. Curr Biol *12*, 1-11.

Anzalone, A., Lizardi-Ortiz, J.E., Ramos, M., De Mei, C., Hopf, F.W., Iaccarino, C., Halbout, B., Jacobsen, J., Kinoshita, C., Welter, M.*, et al.* (2012). Dual control of dopamine synthesis and release by presynaptic and postsynaptic dopamine D2 receptors. J Neurosci *32*, 9023-9034.

Arabi, A., Wu, S., Ridderstrale, K., Bierhoff, H., Shiue, C., Fatyol, K., Fahlen, S., Hydbring, P., Soderberg, O., Grummt, I.*, et al.* (2005). c-Myc associates with ribosomal DNA and activates RNA polymerase I transcription. Nat Cell Biol *7*, 303-310.

Asher, G., and Sassone-Corsi, P. (2015). Time for food: the intimate interplay between nutrition, metabolism, and the circadian clock. Cell *161*, 84-92.

Avitabile, D., Genovese, L., Ponti, D., Ranieri, D., Raffa, S., Calogero, A., and Torrisi, M.R. (2014). Nucleolar localization and circadian regulation of Per2S, a novel splicing variant of the Period 2 gene. Cell Mol Life Sci *71*, 2547-2559.

Baik, J.H., Picetti, R., Saiardi, A., Thiriet, G., Dierich, A., Depaulis, A., Le Meur, M., and Borrelli, E. (1995). Parkinsonian-like locomotor impairment in mice lacking dopamine D2 receptors. Nature *377*, 424-428.

Bass, J., and Lazar, M.A. (2016). Circadian time signatures of fitness and disease. Science *354*, 994-999.

Bass, J., and Takahashi, J.S. (2010). Circadian integration of metabolism and energetics. Science *330*, 1349-1354.

Bateup, H.S., Svenningsson, P., Kuroiwa, M., Gong, S., Nishi, A., Heintz, N., and Greengard, P. (2008). Cell type-specific regulation of DARPP-32 phosphorylation by psychostimulant and antipsychotic drugs. Nat Neurosci *11*, 932-939.

Beker, M.C., Caglayan, B., Caglayan, A.B., Kelestemur, T., Yalcin, E., Caglayan, A., Kilic, U., Baykal, A.T., Reiter, R.J., and Kilic, E. (2019). Interaction of melatonin and Bmal1 in the regulation of PI3K/AKT pathway components and cellular survival. Sci Rep *9*, 19082.

Beltrame, M., and Tollervey, D. (1995). Base pairing between U3 and the pre-ribosomal RNA is required for 18S rRNA synthesis. EMBO J *14*, 4350-4356.

Beuming, T., Kniazeff, J., Bergmann, M.L., Shi, L., Gracia, L., Raniszewska, K., Newman, A.H., Javitch, J.A., Weinstein, H., Gether, U.*, et al.* (2008). The binding sites for cocaine and dopamine in the dopamine transporter overlap. Nat Neurosci *11*, 780-789.

Boisvert, F.M., van Koningsbruggen, S., Navascues, J., and Lamond, A.I. (2007). The multifunctional nucleolus. Nat Rev Mol Cell Biol *8*, 574-585.

Brager, A.J., Stowie, A.C., Prosser, R.A., and Glass, J.D. (2013). The mPer2 clock gene modulates cocaine actions in the mouse circadian system. Behav Brain Res *243*, 255-260.

Brami-Cherrier, K., Valjent, E., Herve, D., Darragh, J., Corvol, J.C., Pages, C., Arthur, S.J., Girault, J.A., and Caboche, J. (2005). Parsing molecular and behavioral effects of cocaine in mitogen- and stress-activated protein kinase-1-deficient mice. J Neurosci *25*, 11444-11454.

Brown, S.A. (2016). Circadian Metabolism: From Mechanisms to Metabolomics and Medicine. Trends Endocrinol Metab *27*, 415-426.

Bunger, M.K., Wilsbacher, L.D., Moran, S.M., Clendenin, C., Radcliffe, L.A., Hogenesch, J.B., Simon, M.C., Takahashi, J.S., and Bradfield, C.A. (2000). Mop3 is an essential component of the master circadian pacemaker in mammals. Cell *103*, 1009-1017.

Buttgereit, F., Smolen, J.S., Coogan, A.N., and Cajochen, C. (2015). Clocking in: chronobiology in rheumatoid arthritis. Nat Rev Rheumatol *11*, 349-356.

Caffarelli, E., Losito, M., Giorgi, C., Fatica, A., and Bozzoni, I. (1998). In vivo identification of nuclear factors interacting with the conserved elements of box C/D small nucleolar RNAs. Mol Cell Biol *18*, 1023-1028.

Caine, S.B., Negus, S.S., Mello, N.K., Patel, S., Bristow, L., Kulagowski, J., Vallone, D., Saiardi, A., and Borrelli, E. (2002). Role of dopamine D2-like receptors in cocaine self-administration: studies with D2 receptor mutant mice and novel D2 receptor antagonists. J Neurosci *22*, 2977-2988.

Cardone, L., Hirayama, J., Giordano, F., Tamaru, T., Palvimo, J.J., and Sassone-Corsi, P. (2005). Circadian clock control by SUMOylation of BMAL1. Science *309*, 1390-1394.

Castaneda, T.R., de Prado, B.M., Prieto, D., and Mora, F. (2004). Circadian rhythms of dopamine, glutamate and GABA in the striatum and nucleus accumbens of the awake rat: modulation by light. J Pineal Res *36*, 177-185.

Cates, H.M., Lardner, C.K., Bagot, R.C., Neve, R.L., and Nestler, E.J. (2019). Fosb Induction in Nucleus Accumbens by Cocaine Is Regulated by E2F3a. eNeuro *6*.

Challet, E. (2019). The circadian regulation of food intake. Nat Rev Endocrinol *15*, 393-405.

Chandra, R., and Lobo, M.K. (2017). Beyond Neuronal Activity Markers: Select Immediate Early Genes in Striatal Neuron Subtypes Functionally Mediate Psychostimulant Addiction. Front Behav Neurosci *11*, 112.

Chaturvedi, R.K., and Beal, M.F. (2008). PPAR: a therapeutic target in Parkinson's disease. J Neurochem *106*, 506-518.

Chen, S., Blank, M.F., Iyer, A., Huang, B., Wang, L., Grummt, I., and Voit, R. (2016). SIRT7-dependent deacetylation of the U3-55k protein controls pre-rRNA processing. Nat Commun *7*, 10734.

Czoty, P.W., Gage, H.D., and Nader, M.A. (2010). Differences in D2 dopamine receptor availability and reaction to novelty in socially housed male monkeys during abstinence from cocaine. Psychopharmacology (Berl) *208*, 585-592.

Dahlberg, A.E. (1989). The functional role of ribosomal RNA in protein synthesis. Cell *57*, 525-529.

Daily, K., Patel, V.R., Rigor, P., Xie, X., and Baldi, P. (2011). MotifMap: integrative genome-wide maps of regulatory motif sites for model species. BMC Bioinformatics *12*, 495.

Dallmann, R., Viola, A.U., Tarokh, L., Cajochen, C., and Brown, S.A. (2012). The human circadian metabolome. Proceedings of the National Academy of Sciences of the United States of America *109*, 2625-2629.

Delvecchio, M., Gaucher, J., Aguilar-Gurrieri, C., Ortega, E., and Panne, D. (2013). Structure of the p300 catalytic core and implications for chromatin targeting and HAT regulation. Nat Struct Mol Biol *20*, 1040-1046.

Di Chiara, G., and Bassareo, V. (2007). Reward system and addiction: what dopamine does and doesn't do. Curr Opin Pharmacol *7*, 69-76.

Dieci, G., Preti, M., and Montanini, B. (2009). Eukaryotic snoRNAs: a paradigm for gene expression flexibility. Genomics *94*, 83-88.

Digman, M.A., Caiolfa, V.R., Zamai, M., and Gratton, E. (2008). The phasor approach to fluorescence lifetime imaging analysis. Biophys J *94*, L14-16.

Dobbs, L.K., Kaplan, A.R., Lemos, J.C., Matsui, A., Rubinstein, M., and Alvarez, V.A. (2016). Dopamine Regulation of Lateral Inhibition between Striatal Neurons Gates the Stimulant Actions of Cocaine. Neuron *90*, 1100-1113.

Doi, M., Hirayama, J., and Sassone-Corsi, P. (2006). Circadian regulator CLOCK is a histone acetyltransferase. Cell *125*, 497-508.

Dyar, K.A., Lutter, D., Artati, A., Ceglia, N.J., Liu, Y., Armenta, D., Jastroch, M., Schneider, S., de Mateo, S., Cervantes, M.*, et al.* (2018). Atlas of Circadian Metabolism Reveals System-wide Coordination and Communication between Clocks. Cell *174*, 1571-1585 e1511.

Eckel-Mahan, K., and Sassone-Corsi, P. (2013). Metabolism and the circadian clock converge. Physiol Rev *93*, 107-135.

Eckel-Mahan, K.L., Patel, V.R., de Mateo, S., Orozco-Solis, R., Ceglia, N.J., Sahar, S., Dilag-Penilla, S.A., Dyar, K.A., Baldi, P., and Sassone-Corsi, P. (2013). Reprogramming of the circadian clock by nutritional challenge. Cell *155*, 1464-1478.

Everitt, B.J., and Robbins, T.W. (2013). From the ventral to the dorsal striatum: devolving views of their roles in drug addiction. Neurosci Biobehav Rev *37*, 1946-1954.

Fabregat, A., Sidiropoulos, K., Viteri, G., Forner, O., Marin-Garcia, P., Arnau, V., D'Eustachio, P., Stein, L., and Hermjakob, H. (2017). Reactome pathway analysis: a high-performance in-memory approach. BMC Bioinformatics *18*, 142.

Feng, D., and Lazar, M.A. (2012). Clocks, metabolism, and the epigenome. Molecular cell *47*, 158-167.

Ferris, M.J., Espana, R.A., Locke, J.L., Konstantopoulos, J.K., Rose, J.H., Chen, R., and Jones, S.R. (2014). Dopamine transporters govern diurnal variation in extracellular dopamine tone. Proc Natl Acad Sci U S A *111*, E2751-2759.

Filipowicz, W., and Pogacic, V. (2002). Biogenesis of small nucleolar ribonucleoproteins. Current opinion in cell biology *14*, 319-327.

Forman, B.M., Tontonoz, P., Chen, J., Brun, R.P., Spiegelman, B.M., and Evans, R.M. (1995). 15-Deoxy-delta 12, 14-prostaglandin J2 is a ligand for the adipocyte determination factor PPAR gamma. Cell *83*, 803-812.

Frottin, F., Schueder, F., Tiwary, S., Gupta, R., Korner, R., Schlichthaerle, T., Cox, J., Jungmann, R., Hartl, F.U., and Hipp, M.S. (2019). The nucleolus functions as a phase-separated protein quality control compartment. Science *365*, 342-347.

Gallardo, C.M., Darvas, M., Oviatt, M., Chang, C.H., Michalik, M., Huddy, T.F., Meyer, E.E., Shuster, S.A., Aguayo, A., Hill, E.M*., et al.* (2014). Dopamine receptor 1 neurons in the dorsal striatum regulate food anticipatory circadian activity rhythms in mice. Elife *3*, e03781.

Gallego, M., and Virshup, D.M. (2007). Post-translational modifications regulate the ticking of the circadian clock. Nat Rev Mol Cell Biol *8*, 139-148.

Girault, J.A. (2012). Integrating neurotransmission in striatal medium spiny neurons. Adv Exp Med Biol *970*, 407-429.

Gordon, H.W. (2019). Differential Effects of Addictive Drugs on Sleep and Sleep Stages. J Addict Res (OPAST Group) *3*.

Grandori, C., Gomez-Roman, N., Felton-Edkins, Z.A., Ngouenet, C., Galloway, D.A., Eisenman, R.N., and White, R.J. (2005). c-Myc binds to human ribosomal DNA and stimulates transcription of rRNA genes by RNA polymerase I. Nat Cell Biol *7*, 311-318.

Green, C.B., Takahashi, J.S., and Bass, J. (2008). The meter of metabolism. Cell *134*, 728-742.

Grozdanov, P., Georgiev, O., and Karagyozov, L. (2003). Complete sequence of the 45-kb mouse ribosomal DNA repeat: analysis of the intergenic spacer. Genomics *82*, 637-643.

Grummt, I. (2003). Life on a planet of its own: regulation of RNA polymerase I transcription in the nucleolus. Genes Dev *17*, 1691-1702.

Grummt, I., and Ladurner, A.G. (2008). A metabolic throttle regulates the epigenetic state of rDNA. Cell *133*, 577-580.

Hasler, B.P., Smith, L.J., Cousins, J.C., and Bootzin, R.R. (2012). Circadian rhythms, sleep, and substance abuse. Sleep Med Rev *16*, 67-81.

Hatori, M., Vollmers, C., Zarrinpar, A., Ditacchio, L., Bushong, E.A., Gill, S., Leblanc, M., Chaix, A., Joens, M., Fitzpatrick, J.A., *et al.* (2012). Time-Restricted Feeding without Reducing Caloric Intake Prevents Metabolic Diseases in Mice Fed a High-Fat Diet. Cell Metab *15*, 848-860.

Henras, A.K., Plisson-Chastang, C., O'Donohue, M.F., Chakraborty, A., and Gleizes, P.E. (2015). An overview of pre-ribosomal RNA processing in eukaryotes. Wiley Interdiscip Rev RNA *6*, 225-242.

Hikida, T., Kimura, K., Wada, N., Funabiki, K., and Nakanishi, S. (2010). Distinct roles of synaptic transmission in direct and indirect striatal pathways to reward and aversive behavior. Neuron *66*, 896-907.

Hirano, A., Fu, Y.H., and Ptacek, L.J. (2016). The intricate dance of post-translational modifications in the rhythm of life. Nat Struct Mol Biol *23*, 1053-1060.

Hirayama, J., Sahar, S., Grimaldi, B., Tamaru, T., Takamatsu, K., Nakahata, Y., and Sassone-Corsi, P. (2007). CLOCK-mediated acetylation of BMAL1 controls circadian function. Nature *450*, 1086-1090.

Hood, S., Cassidy, P., Cossette, M.P., Weigl, Y., Verwey, M., Robinson, B., Stewart, J., and Amir, S. (2010). Endogenous dopamine regulates the rhythm of expression of the clock protein PER2 in the rat dorsal striatum via daily activation of D2 dopamine receptors. J Neurosci *30*, 14046-14058.

Huang da, W., Sherman, B.T., and Lempicki, R.A. (2009). Systematic and integrative analysis of large gene lists using DAVID bioinformatics resources. Nat Protoc *4*, 44-57.

Huang, N., Chelliah, Y., Shan, Y., Taylor, C.A., Yoo, S.H., Partch, C., Green, C.B., Zhang, H., and Takahashi, J.S. (2012). Crystal structure of the heterodimeric CLOCK:BMAL1 transcriptional activator complex. Science *337*, 189-194.

Hughes, M.E., Hogenesch, J.B., and Kornacker, K. (2010). JTK_CYCLE: an efficient nonparametric algorithm for detecting rhythmic components in genome-scale data sets. J Biol Rhythms *25*, 372-380.

Huttenhofer, A., Kiefmann, M., Meier-Ewert, S., O'Brien, J., Lehrach, H., Bachellerie, J.P., and Brosius, J. (2001). RNomics: an experimental approach that identifies 201 candidates for novel, small, non-messenger RNAs in mouse. EMBO J *20*, 2943-2953.

Iijima, M., Nikaido, T., Akiyama, M., Moriya, T., and Shibata, S. (2002). Methamphetamine-induced, suprachiasmatic nucleus-independent circadian rhythms of activity and mPer gene expression in the striatum of the mouse. Eur J Neurosci *16*, 921-929.

Imbesi, M., Yildiz, S., Dirim Arslan, A., Sharma, R., Manev, H., and Uz, T. (2009). Dopamine receptor-mediated regulation of neuronal "clock" gene expression. Neuroscience *158*, 537-544.

Iyer-Bierhoff, A., Krogh, N., Tessarz, P., Ruppert, T., Nielsen, H., and Grummt, I. (2018). SIRT7-Dependent Deacetylation of Fibrillarin Controls Histone H2A Methylation and rRNA Synthesis during the Cell Cycle. Cell reports *25*, 2946-2954 e2945.

Jiang, Q., Heneka, M., and Landreth, G.E. (2008). The role of peroxisome proliferator-activated receptor-gamma (PPARgamma) in Alzheimer's disease: therapeutic implications. CNS Drugs *22*, 1-14.

Jouffe, C., Cretenet, G., Symul, L., Martin, E., Atger, F., Naef, F., and Gachon, F. (2013). The circadian clock coordinates ribosome biogenesis. PLoS biology *11*, e1001455.

Kanterman, R.Y., Mahan, L.C., Briley, E.M., Monsma, F.J., Jr., Sibley, D.R., Axelrod, J., and Felder, C.C. (1991). Transfected D2 dopamine receptors mediate the potentiation of arachidonic acid release in Chinese hamster ovary cells. Mol Pharmacol *39*, 364-369.

Kass, S., Tyc, K., Steitz, J.A., and Sollner-Webb, B. (1990). The U3 small nucleolar ribonucleoprotein functions in the first step of preribosomal RNA processing. Cell *60*, 897-908.

Kelz, M.B., Chen, J., Carlezon, W.A., Jr., Whisler, K., Gilden, L., Beckmann, A.M., Steffen, C., Zhang, Y.J., Marotti, L., Self, D.W.*, et al.* (1999). Expression of the transcription factor deltaFosB in the brain controls sensitivity to cocaine. Nature *401*, 272-276.

Khan, M.A., Alam, Q., Haque, A., Ashafaq, M., Khan, M.J., Ashraf, G.M., and Ahmad, M. (2019). Current Progress on Peroxisome Proliferator-activated Receptor Gamma Agonist as an Emerging Therapeutic Approach for the Treatment of Alzheimer's Disease: An Update. Curr Neuropharmacol *17*, 232-246.

Kharkwal, G., Radl, D., Lewis, R., and Borrelli, E. (2016). Dopamine D2 receptors in striatal output neurons enable the psychomotor effects of cocaine. Proc Natl Acad Sci U S A *113*, 11609-11614.

Kieffer-Kwon, P., Martianov, I., and Davidson, I. (2004). Cell-specific nucleolar localization of TBP-related factor 2. Molecular biology of the cell *15*, 4356-4368.

Kinouchi, K., Magnan, C., Ceglia, N., Liu, Y., Cervantes, M., Pastore, N., Huynh, T., Ballabio, A., Baldi, P., Masri, S.*, et al.* (2018). Fasting Imparts a Switch to Alternative Daily Pathways in Liver and Muscle. Cell reports *25*, 3299-3314 e3296.

Kiyota, Y., Kondo, T., Maeshiba, Y., Hashimoto, A., Yamashita, K., Yoshimura, Y., Motohashi, M., and Tanayama, S. (1997). Studies on the metabolism of the new antidiabetic agent pioglitazone. Identification of metabolites in rats and dogs. Arzneimittelforschung *47*, 22-28.

Kliewer, S.A., Forman, B.M., Blumberg, B., Ong, E.S., Borgmeyer, U., Mangelsdorf, D.J., Umesono, K., and Evans, R.M. (1994). Differential expression and activation of a family of murine peroxisome proliferator-activated receptors. Proc Natl Acad Sci U S A *91*, 7355-7359.

Kohsaka, A., Laposky, A.D., Ramsey, K.M., Estrada, C., Joshu, C., Kobayashi, Y., Turek, F.W., and Bass, J. (2007). High-fat diet disrupts behavioral and molecular circadian rhythms in mice. Cell Metab *6*, 414-421.

Kojima, S., Shingle, D.L., and Green, C.B. (2011). Post-transcriptional control of circadian rhythms. J Cell Sci *124*, 311-320.

Kondratov, R.V., Chernov, M.V., Kondratova, A.A., Gorbacheva, V.Y., Gudkov, A.V., and Antoch, M.P. (2003). BMAL1-dependent circadian oscillation of nuclear CLOCK: posttranslational events induced by dimerization of transcriptional activators of the mammalian clock system. Genes Dev *17*, 1921-1932.

Koressaar, T., and Remm, M. (2007). Enhancements and modifications of primer design program Primer3. Bioinformatics *23*, 1289-1291.

Korpi, E.R., den Hollander, B., Farooq, U., Vashchinkina, E., Rajkumar, R., Nutt, D.J., Hyytia, P., and Dawe, G.S. (2015). Mechanisms of Action and Persistent Neuroplasticity by Drugs of Abuse. Pharmacol Rev *67*, 872-1004.

Korshunov, K.S., Blakemore, L.J., and Trombley, P.Q. (2017). Dopamine: A Modulator of Circadian Rhythms in the Central Nervous System. Front Cell Neurosci *11*, 91.

Kuehl, F.A., Jr., and Egan, R.W. (1980). Prostaglandins, arachidonic acid, and inflammation. Science *210*, 978-984.

Lamia, K.A., Sachdeva, U.M., DiTacchio, L., Williams, E.C., Alvarez, J.G., Egan, D.F., Vasquez, D.S., Juguilon, H., Panda, S., Shaw, R.J.*, et al.* (2009). AMPK regulates the circadian clock by cryptochrome phosphorylation and degradation. Science *326*, 437-440.

Lapik, Y.R., Fernandes, C.J., Lau, L.F., and Pestov, D.G. (2004). Physical and functional interaction between Pes1 and Bop1 in mammalian ribosome biogenesis. Molecular cell *15*, 17-29.

Lee, C.H., Olson, P., and Evans, R.M. (2003). Minireview: lipid metabolism, metabolic diseases, and peroxisome proliferator-activated receptors. Endocrinology *144*, 2201-2207.

Lestrade, L., and Weber, M.J. (2006). snoRNA-LBME-db, a comprehensive database of human H/ACA and C/D box snoRNAs. Nucleic acids research *34*, D158-162.

Lewis, R.G., Serra, M., Radl, D., Gori, M., Tran, C., Michalak, S.E., Vanderwal, C.D., and Borrelli, E. (2020). Dopaminergic Control of Striatal Cholinergic Interneurons Underlies Cocaine-Induced Psychostimulation. Cell reports *31*, 107527.

Lipton, J.O., Yuan, E.D., Boyle, L.M., Ebrahimi-Fakhari, D., Kwiatkowski, E., Nathan, A., Guttler, T., Davis, F., Asara, J.M., and Sahin, M. (2015). The Circadian Protein BMAL1 Regulates Translation in Response to S6K1-Mediated Phosphorylation. Cell *161*, 1138-1151.

Liu, J.L., Lee, L.F., Ye, Y., Qian, Z., and Kung, H.J. (1997). Nucleolar and nuclear localization properties of a herpesvirus bZIP oncoprotein, MEQ. J Virol *71*, 3188-3196.

Lobo, M.K., and Nestler, E.J. (2011). The striatal balancing act in drug addiction: distinct roles of direct and indirect pathway medium spiny neurons. Front Neuroanat *5*, 41.

Logan, R.W., Parekh, P.K., Kaplan, G.N., Becker-Krail, D.D., Williams, W.P., 3rd, Yamaguchi, S., Yoshino, J., Shelton, M.A., Zhu, X., Zhang, H.*, et al.* (2019). NAD+ cellular redox and SIRT1 regulate the diurnal rhythms of tyrosine hydroxylase and conditioned cocaine reward. Mol Psychiatry *24*, 1668-1684.

Logan, R.W., Williams, W.P., 3rd, and McClung, C.A. (2014). Circadian rhythms and addiction: mechanistic insights and future directions. Behav Neurosci *128*, 387-412.

Longo, V.D., and Panda, S. (2016). Fasting, Circadian Rhythms, and Time-Restricted Feeding in Healthy Lifespan. Cell Metab *23*, 1048-1059.

Luscher, C., and Bellone, C. (2008). Cocaine-evoked synaptic plasticity: a key to addiction? Nat Neurosci *11*, 737-738.

Luscher, C., and Malenka, R.C. (2011). Drug-evoked synaptic plasticity in addiction: from molecular changes to circuit remodeling. Neuron *69*, 650-663.

Mangelsdorf, D.J., Thummel, C., Beato, M., Herrlich, P., Schutz, G., Umesono, K., Blumberg, B., Kastner, P., Mark, M., Chambon, P.*, et al.* (1995). The nuclear receptor superfamily: the second decade. Cell *83*, 835-839.

Masri, S., Cervantes, M., and Sassone-Corsi, P. (2013a). The circadian clock and cell cycle: interconnected biological circuits. Current opinion in cell biology *25*, 730-734.

Masri, S., Patel, V.R., Eckel-Mahan, K.L., Peleg, S., Forne, I., Ladurner, A.G., Baldi, P., Imhof, A., and Sassone-Corsi, P. (2013b). Circadian acetylome reveals regulation of mitochondrial metabolic pathways. Proceedings of the National Academy of Sciences of the United States of America *110*, 3339-3344.

Masri, S., and Sassone-Corsi, P. (2010). Plasticity and specificity of the circadian epigenome. Nat Neurosci *13*, 1324-1329.

McClung, C.A., Sidiropoulou, K., Vitaterna, M., Takahashi, J.S., White, F.J., Cooper, D.C., and Nestler, E.J. (2005). Regulation of dopaminergic transmission and cocaine reward by the Clock gene. Proc Natl Acad Sci U S A *102*, 9377-9381.

Meskauskas, A., Baxter, J.L., Carr, E.A., Yasenchak, J., Gallagher, J.E., Baserga, S.J., and Dinman, J.D. (2003). Delayed rRNA processing results in significant ribosome biogenesis and functional defects. Mol Cell Biol *23*, 1602-1613.

Miller, W.R., Fox, R.G., Stutz, S.J., Lane, S.D., Denner, L., Cunningham, K.A., and Dineley, K.T. (2018). PPARgamma agonism attenuates cocaine cue reactivity. Addict Biol *23*, 55-68.

Moffat, J., Grueneberg, D.A., Yang, X., Kim, S.Y., Kloepfer, A.M., Hinkle, G., Piqani, B., Eisenhaure, T.M., Luo, B., Grenier, J.K*., et al.* (2006). A lentiviral RNAi library for human and mouse genes applied to an arrayed viral high-content screen. Cell *124*, 1283-1298.

Mohawk, J.A., Green, C.B., and Takahashi, J.S. (2012). Central and peripheral circadian clocks in mammals. Annu Rev Neurosci *35*, 445-462.

Muller, C., Bremer, A., Schreiber, S., Eichwald, S., and Calkhoven, C.F. (2010). Nucleolar retention of a translational C/EBPalpha isoform stimulates rDNA transcription and cell size. EMBO J *29*, 897-909.

Murakami, M., Tognini, P., Liu, Y., Eckel-Mahan, K.L., Baldi, P., and Sassone-Corsi, P. (2016). Gut microbiota directs PPARgamma-driven reprogramming of the liver circadian clock by nutritional challenge. EMBO Rep *17*, 1292-1303.

Nader, M.A., Morgan, D., Gage, H.D., Nader, S.H., Calhoun, T.L., Buchheimer, N., Ehrenkaufer, R., and Mach, R.H. (2006). PET imaging of dopamine D2 receptors during chronic cocaine self-administration in monkeys. Nat Neurosci *9*, 1050-1056.

Nazar, R.N. (2004). Ribosomal RNA processing and ribosome biogenesis in eukaryotes. IUBMB life *56*, 457-465.

Nemeth, A., and Grummt, I. (2018). Dynamic regulation of nucleolar architecture. Current opinion in cell biology *52*, 105-111.

Nestler, E.J. (2005). The neurobiology of cocaine addiction. Sci Pract Perspect *3*, 4-10.

Neve, K.A., Seamans, J.K., and Trantham-Davidson, H. (2004). Dopamine receptor signaling. J Recept Signal Transduct Res *24*, 165-205.

Nosjean, O., and Boutin, J.A. (2002). Natural ligands of PPARgamma: are prostaglandin J(2) derivatives really playing the part? Cell Signal *14*, 573-583.

Ozburn, A.R., Kern, J., Parekh, P.K., Logan, R.W., Liu, Z., Falcon, E., Becker-Krail, D., Purohit, K., Edgar, N.M., Huang, Y*., et al.* (2017). NPAS2 Regulation of Anxiety-Like Behavior and GABAA Receptors. Front Mol Neurosci *10*, 360.

Panda, S. (2016). Circadian physiology of metabolism. Science *354*, 1008-1015.

Parekh, P.K., Logan, R.W., Ketchesin, K.D., Becker-Krail, D., Shelton, M.A., Hildebrand, M.A., Barko, K., Huang, Y.H., and McClung, C.A. (2019). Cell-Type-Specific Regulation of Nucleus Accumbens Synaptic Plasticity and Cocaine Reward Sensitivity by the Circadian Protein, NPAS2. J Neurosci *39*, 4657-4667.

Partch, C.L., Green, C.B., and Takahashi, J.S. (2014). Molecular architecture of the mammalian circadian clock. Trends Cell Biol *24*, 90-99.

Patel, V.R., Eckel-Mahan, K., Sassone-Corsi, P., and Baldi, P. (2012). CircadiOmics: integrating circadian genomics, transcriptomics, proteomics and metabolomics. Nat Methods *9*, 772-773.

Peculis, B.A. (1997). The sequence of the 5' end of the U8 small nucleolar RNA is critical for 5.8S and 28S rRNA maturation. Mol Cell Biol *17*, 3702-3713.

Piomelli, D., Pilon, C., Giros, B., Sokoloff, P., Martres, M.P., and Schwartz, J.C. (1991). Dopamine activation of the arachidonic acid cascade as a basis for D1/D2 receptor synergism. Nature *353*, 164-167.

Ponti, D., Bellenchi, G.C., Puca, R., Bastianelli, D., Maroder, M., Ragona, G., Roussel, P., Thiry, M., Mercola, D., and Calogero, A. (2014). The transcription factor EGR1 localizes to the nucleolus and is linked to suppression of ribosomal precursor synthesis. PLoS One *9*, e96037.

Poortinga, G., Wall, M., Sanij, E., Siwicki, K., Ellul, J., Brown, D., Holloway, T.P., Hannan, R.D., and McArthur, G.A. (2011). c-MYC coordinately regulates ribosomal gene chromatin remodeling and Pol I availability during granulocyte differentiation. Nucleic acids research *39*, 3267-3281.

Radl, D., Chiacchiaretta, M., Lewis, R.G., Brami-Cherrier, K., Arcuri, L., and Borrelli, E. (2018). Differential regulation of striatal motor behavior and related cellular responses by dopamine D2L and D2S isoforms. Proc Natl Acad Sci U S A *115*, 198-203.

Reuveni, S., Ehrenberg, M., and Paulsson, J. (2017). Ribosomes are optimized for autocatalytic production. Nature *547*, 293-297.

Ribas-Latre, A., and Eckel-Mahan, K. (2016). Interdependence of nutrient metabolism and the circadian clock system: Importance for metabolic health. Mol Metab *5*, 133-152.

Ripperger, J.A., and Schibler, U. (2006). Rhythmic CLOCK-BMAL1 binding to multiple E-box motifs drives circadian Dbp transcription and chromatin transitions. Nature genetics *38*, 369-374.

Robles, M.S., Humphrey, S.J., and Mann, M. (2017). Phosphorylation Is a Central Mechanism for Circadian Control of Metabolism and Physiology. Cell Metab *25*, 118-127.

Rudic, R.D., McNamara, P., Curtis, A.M., Boston, R.C., Panda, S., Hogenesch, J.B., and Fitzgerald, G.A. (2004). BMAL1 and CLOCK, two essential components of the circadian clock, are involved in glucose homeostasis. PLoS biology *2*, e377.

Sahar, S., Masubuchi, S., Eckel-Mahan, K., Vollmer, S., Galla, L., Ceglia, N., Masri, S., Barth, T.K., Grimaldi, B., Oluyemi, O.*, et al.* (2014). Circadian control of fatty acid elongation by SIRT1

protein-mediated deacetylation of acetyl-coenzyme A synthetase 1. The Journal of biological chemistry *289*, 6091-6097.

Sahar, S., and Sassone-Corsi, P. (2009). Metabolism and cancer: the circadian clock connection. Nature reviews Cancer *9*, 886-896.

Sahar, S., and Sassone-Corsi, P. (2012). Regulation of metabolism: the circadian clock dictates the time. Trends Endocrinol Metab *23*, 1-8.

Samikkannu, T., Rao, K.V., Ding, H., Agudelo, M., Raymond, A.D., Yoo, C., and Nair, M.P. (2014). Immunopathogenesis of HIV infection in cocaine users: role of arachidonic acid. PLoS One *9*, e106348.

Schade, R., Vick, K., Ott, T., Sohr, R., Pfister, C., Bellach, J., Golor, G., and Lemmer, B. (1995). Circadian rhythms of dopamine and cholecystokinin in nucleus accumbens and striatum of rats--influence on dopaminergic stimulation. Chronobiol Int *12*, 87-99.

Scheer, U., and Hock, R. (1999). Structure and function of the nucleolus. Current opinion in cell biology *11*, 385-390.

Scheiermann, C., Kunisaki, Y., and Frenette, P.S. (2013). Circadian control of the immune system. Nat Rev Immunol *13*, 190-198.

Scher, J.U., and Pillinger, M.H. (2005). 15d-PGJ2: the anti-inflammatory prostaglandin? Clin Immunol *114*, 100-109.

Schibler, U., and Sassone-Corsi, P. (2002). A web of circadian pacemakers. Cell *111*, 919-922.

Schinelli, S., Paolillo, M., and Corona, G.L. (1994). Opposing actions of D1- and D2-dopamine receptors on arachidonic acid release and cyclic AMP production in striatal neurons. J Neurochem *62*, 944-949.

Shim, H.S., Kim, H., Lee, J., Son, G.H., Cho, S., Oh, T.H., Kang, S.H., Seen, D.S., Lee, K.H., and Kim, K. (2007). Rapid activation of CLOCK by Ca2+-dependent protein kinase C mediates resetting of the mammalian circadian clock. EMBO reports *8*, 366-371.

Shumay, E., Fowler, J.S., Wang, G.J., Logan, J., Alia-Klein, N., Goldstein, R.Z., Maloney, T., Wong, C., and Volkow, N.D. (2012). Repeat variation in the human PER2 gene as a new genetic marker associated with cocaine addiction and brain dopamine D2 receptor availability. Transl Psychiatry *2*, e86.

Sidiropoulos, K., Viteri, G., Sevilla, C., Jupe, S., Webber, M., Orlic-Milacic, M., Jassal, B., May, B., Shamovsky, V., Duenas, C.*, et al.* (2017). Reactome enhanced pathway visualization. Bioinformatics *33*, 3461-3467.

Sinturel, F., Gerber, A., Mauvoisin, D., Wang, J., Gatfield, D., Stubblefield, J.J., Green, C.B., Gachon, F., and Schibler, U. (2017). Diurnal Oscillations in Liver Mass and Cell Size Accompany Ribosome Assembly Cycles. Cell *169*, 651-663 e614.

Sirri, V., Grob, A., Berthelet, J., Jourdan, N., and Roussel, P. (2019). Sirtuin 7 promotes 45S pre-rRNA cleavage at site 2 and determines the processing pathway. J Cell Sci *132*.

Sloan, K.E., Warda, A.S., Sharma, S., Entian, K.D., Lafontaine, D.L.J., and Bohnsack, M.T. (2017). Tuning the ribosome: The influence of rRNA modification on eukaryotic ribosome biogenesis and function. RNA Biol *14*, 1138-1152.

Soccio, R.E., Chen, E.R., Rajapurkar, S.R., Safabakhsh, P., Marinis, J.M., Dispirito, J.R., Emmett, M.J., Briggs, E.R., Fang, B., Everett, L.J.*, et al.* (2015). Genetic Variation Determines PPARgamma Function and Anti-diabetic Drug Response In Vivo. Cell *162*, 33-44.

Stratmann, M., and Schibler, U. (2006). Properties, entrainment, and physiological functions of mammalian peripheral oscillators. J Biol Rhythms *21*, 494-506.

Swanson, C.R., Joers, V., Bondarenko, V., Brunner, K., Simmons, H.A., Ziegler, T.E., Kemnitz, J.W., Johnson, J.A., and Emborg, M.E. (2011). The PPAR-gamma agonist pioglitazone modulates inflammation and induces neuroprotection in parkinsonian monkeys. J Neuroinflammation *8*, 91.

Takahashi, J.S. (2015). Molecular components of the circadian clock in mammals. Diabetes Obes Metab *17 Suppl 1*, 6-11.

Tamaru, T., Isojima, Y., van der Horst, G.T., Takei, K., Nagai, K., and Takamatsu, K. (2003). Nucleocytoplasmic shuttling and phosphorylation of BMAL1 are regulated by circadian clock in cultured fibroblasts. Genes Cells *8*, 973-983.

Tiku, V., and Antebi, A. (2018). Nucleolar Function in Lifespan Regulation. Trends Cell Biol *28*, 662-672.

Torrano, V., Navascues, J., Docquier, F., Zhang, R., Burke, L.J., Chernukhin, I., Farrar, D., Leon, J., Berciano, M.T., Renkawitz, R.*, et al.* (2006). Targeting of CTCF to the nucleolus inhibits nucleolar transcription through a poly(ADP-ribosyl)ation-dependent mechanism. J Cell Sci *119*, 1746-1759.

Trapnell, C., Hendrickson, D.G., Sauvageau, M., Goff, L., Rinn, J.L., and Pachter, L. (2013). Differential analysis of gene regulation at transcript resolution with RNA-seq. Nat Biotechnol *31*, 46-53.

Travnickova-Bendova, Z., Cermakian, N., Reppert, S.M., and Sassone-Corsi, P. (2002). Bimodal regulation of mPeriod promoters by CREB-dependent signaling and CLOCK/BMAL1 activity. Proceedings of the National Academy of Sciences of the United States of America *99*, 7728-7733.

Turek, F.W., Joshu, C., Kohsaka, A., Lin, E., Ivanova, G., McDearmon, E., Laposky, A., Losee-Olson, S., Easton, A., Jensen, D.R.*, et al.* (2005). Obesity and metabolic syndrome in circadian Clock mutant mice. Science *308*, 1043-1045.

Untergasser, A., Cutcutache, I., Koressaar, T., Ye, J., Faircloth, B.C., Remm, M., and Rozen, S.G. (2012). Primer3--new capabilities and interfaces. Nucleic acids research *40*, e115.

Vallone, D., Picetti, R., and Borrelli, E. (2000). Structure and function of dopamine receptors. Neurosci Biobehav Rev *24*, 125-132.

Verheggen, C., Lafontaine, D.L., Samarsky, D., Mouaikel, J., Blanchard, J.M., Bordonne, R., and Bertrand, E. (2002). Mammalian and yeast U3 snoRNPs are matured in specific and related nuclear compartments. EMBO J *21*, 2736-2745.

Volkow, N.D., Chang, L., Wang, G.J., Fowler, J.S., Ding, Y.S., Sedler, M., Logan, J., Franceschi, D., Gatley, J., Hitzemann, R.*, et al.* (2001). Low level of brain dopamine D2 receptors in methamphetamine abusers: association with metabolism in the orbitofrontal cortex. Am J Psychiatry *158*, 2015-2021.

Walker, D.M., Cates, H.M., Loh, Y.E., Purushothaman, I., Ramakrishnan, A., Cahill, K.M., Lardner, C.K., Godino, A., Kronman, H.G., Rabkin, J.*, et al.* (2018). Cocaine Self-administration Alters Transcriptome-wide Responses in the Brain's Reward Circuitry. Biol Psychiatry *84*, 867-880.

Wang, J., Mauvoisin, D., Martin, E., Atger, F., Galindo, A.N., Dayon, L., Sizzano, F., Palini, A., Kussmann, M., Waridel, P.*, et al.* (2017). Nuclear Proteomics Uncovers Diurnal Regulatory Landscapes in Mouse Liver. Cell metabolism *25*, 102-117.

Wang, M., Anikin, L., and Pestov, D.G. (2014). Two orthogonal cleavages separate subunit RNAs in mouse ribosome biogenesis. Nucleic acids research *42*, 11180-11191.

Watkins, N.J., and Bohnsack, M.T. (2012). The box C/D and H/ACA snoRNPs: key players in the modification, processing and the dynamic folding of ribosomal RNA. Wiley Interdiscip Rev RNA *3*, 397-414.

Welsh, D.K., Takahashi, J.S., and Kay, S.A. (2010). Suprachiasmatic nucleus: cell autonomy and network properties. Annu Rev Physiol *72*, 551-577.

Welter, M., Vallone, D., Samad, T.A., Meziane, H., Usiello, A., and Borrelli, E. (2007). Absence of dopamine D2 receptors unmasks an inhibitory control over the brain circuitries activated by cocaine. Proc Natl Acad Sci U S A *104*, 6840-6845.

Woolford, J.L., Jr., and Baserga, S.J. (2013). Ribosome biogenesis in the yeast Saccharomyces cerevisiae. Genetics *195*, 643-681.

Yager, L.M., Garcia, A.F., Wunsch, A.M., and Ferguson, S.M. (2015). The ins and outs of the striatum: role in drug addiction. Neuroscience *301*, 529-541.

Yagita, K., Horie, K., Koinuma, S., Nakamura, W., Yamanaka, I., Urasaki, A., Shigeyoshi, Y., Kawakami, K., Shimada, S., Takeda, J.*, et al.* (2010). Development of the circadian oscillator during differentiation of mouse embryonic stem cells in vitro. Proceedings of the National Academy of Sciences of the United States of America *107*, 3846-3851.

Yoshitane, H., Takao, T., Satomi, Y., Du, N.H., Okano, T., and Fukada, Y. (2009). Roles of CLOCK phosphorylation in suppression of E-box-dependent transcription. Mol Cell Biol *29*, 3675-3686.

Zhang, E.E., and Kay, S.A. (2010). Clocks not winding down: unravelling circadian networks. Nat Rev Mol Cell Biol *11*, 764-776.

Zhang, J., Zhang, L., Jiao, H., Zhang, Q., Zhang, D., Lou, D., Katz, J.L., and Xu, M. (2006). c-Fos facilitates the acquisition and extinction of cocaine-induced persistent changes. J Neurosci *26*, 13287-13296.